

Climate Change Impacts on the Upstream Water Resources of the Amu and Syr Darya River Basins

March 2012

Authors

W.W. Immerzeel

A.F. Lutz

P. Droogers

Client

Asian Development Bank

Report FutureWater: 107



FutureWater

Costerweg 1G
6702 AA Wageningen
The Netherlands

+31 (0)317 460050

info@futurewater.nl

www.futurewater.nl

PREFACE

This report contributes to the Asian Development Bank study TA 7532 “Water and Adaptation Interventions in Central and West Asia” carried out by the Finnish Consulting Group (FCG) in collaboration with FutureWater (Netherlands) and the Finnish Meteorological Institute (FMI).

The relevance of the study is that the regional policy can only be implemented if there is a strong scientific background for investment plans and commitment to international agreements and conventions.

The study focuses on Kyrgyz Republic, Tajikistan, Kazakhstan, Turkmenistan, and Uzbekistan. The approach of the study is to develop hydrological models for the Amu Darya and Syr Darya and include various climate impact scenarios. Results will be used to develop national capacity in each of the participating countries to use these models to prepare climate impact scenarios and develop adaptation strategies.

The Request for Proposal for this study was distributed amongst five consortiums on 1-Dec-2010. Based on a Quality- and Cost-Based Selection (QCBS) the consortium of Finnish Consulting Group (FCG) in collaboration with FutureWater (Netherlands) and the Finnish Meteorological Institute (FMI) was granted to undertake the study (Contract number. 100039-S41593). The study started in Mar-2011 and will be completed in Jun-2012

Since the start of the study in March 2011, the following official documents have been published:

- Inception report, June 2011
- Interim report, November 2011

This FutureWater report describes the impact of climate change based on climate change projections produced by FMI using the hydrological model developed, calibrated and validated for the upstream parts of the Amu Darya and Syr Darya river basins. This report will form the base for a subsequent report describing the impact and the adaptation options for the downstream areas in the two river basins. These reports will be incorporated in the study’s Final Report, to be delivered in May 2012.



Table of contents

1	Introduction	9
2	Review of Climate Change Impact Studies on Water Resources	13
2.1	Impact of climate change on water resources	13
2.2	Impact of climate change for snow and ice	13
2.3	Glacier changes in Central Asia	14
2.4	Modelling the hydrological response to climate change in high mountain regions	17
3	The Upstream Parts of the Amu and Syr Darya River Basins	22
3.1	Topography	22
3.2	Climate	22
3.3	Glaciers and snow	23
3.4	Land use and land cover	25
3.5	Water management and hydrology	26
4	Methodology	27
4.1	Data sources and preprocessing	27
4.2	Model concepts	29
4.2.1	Model structure	29
4.2.2	Cryospheric processes	31
4.2.3	Rain runoff	35
4.2.4	Baseflow	37
4.2.5	Routing	37
4.3	Calibration	38
5	Current Hydrological Regime	39
5.1	Calibration results	39
5.2	The contribution of glacial and snow melt to river runoff	44
6	Future Hydrological Regime	52
6.1	Climate change scenarios	52
6.2	Future glacier cover development	52
6.3	Future changes in generation and composition of runoff	56
6.3.1	Change in total runoff	56
6.3.2	Changes in snow melt	69
6.3.3	Changes in rain runoff	75
6.3.4	Changes in base flow	81
6.3.5	Changes in runoff composition	86
6.4	Simulated inflow to downstream areas	88
7	Conclusions	100
8	References	101



Tables

Table 1: Land cover in the upstream parts of the Amu Darya and Syr Darya river basin.....	25
Table 2: Estimated runoff factors for different types of land use/land cover.....	36
Table 3: Calibrated parameters in the Aral Mountain model.....	39
Table 4: Correlation parameters observed and simulated inflow 2001-2010.....	43
Table 5: Average annual inflow (observed and simulated) 2001-2010.....	43
Table 6: Simulated stream flow composition at the major reservoirs.....	50
Table 7: Simulated stream flow composition at the outlet of the upstream hydrological model.....	51
Table 8: Global circulation models used for future climate projections.....	52
Table 9: Absolute and relative decrease in glacier extent for the five GCM forcings and mean decrease in glacier extent.....	56
Table 10: Catchment names Figure 6-42.....	89
Table 11: Simulated average annual inflow into downstream areas (Mm ³) for reference period (2001-2010) and future situations (2021-2030, 2041-2050). Values are mean values for the five GCM outputs.....	96
Table 12: Changes in inflow into downstream areas for future projections (2021-2030, 2041-2050). Ranges indicate maximum and minimum availability change as projected by the five GCMs.....	97
Table 13: Projected average changes in water availability for downstream users Range for five GCMs is shown.....	98

Figures

Figure 1-1: Amu Darya and Syr Darya river basins.....	9
Figure 2-1: Changes in glacier mass balance around the world [Kaser <i>et al.</i> , 2006].....	14
Figure 2-2: The Tien Shan mountains in Kyrgyzstan. Subdivisions of Tien Shan: W, western; N, northern; C, central; I, inner. [Solomina <i>et al.</i> , 2004].....	15
Figure 2-3: Recession of glacier terminus position for Fedchenko glacier 1933-2006.....	16
Figure 2-4: Fedchenko and Murgab meteorological station locations in the Pamir mountains. [Khromova <i>et al.</i> , 2006].....	17
Figure 2-5: Changes in seasonal stream flow assuming 2 °C temperature rise. [Singh and Bengtsson, 2004].....	18
Figure 2-6: Anomalies in glacier ice volume.....	18
Figure 2-7: Total simulated discharge partitioned into rain runoff, glacier runoff, snow runoff and baseflow. [Immerzeel <i>et al.</i> , 2011].....	19
Figure 2-8: Simulated mean upstream discharge for present (2000-2007) and future climate for the A1B SRES scenario. [Immerzeel <i>et al.</i> , 2010a].....	20
Figure 3-1: Upstream topography Amu Darya and Syr Darya river basins.....	22
Figure 3-2: Average air temperature 2001-2010 based on downscaled and interpolated station data.....	23
Figure 3-3: Average annual precipitation 2001-2010 based on the PERSIANN/TRMM dataset.....	23
Figure 3-4: Area covered by glaciers in Amu Darya and Syr Darya river basins.....	24
Figure 3-5: Areas with glaciers in the Amu Darya and Syr Darya river basins.....	24
Figure 3-6: Land cover in the upstream parts of the Amu Darya and Syr Darya river basins [Defourny <i>et al.</i> , 2007].....	25
Figure 3-7: Land cover type in the upstream parts of the Amu Darya and Syr Darya river basin.....	26



Figure 4-1: General project approach	27
Figure 4-2: DEM with major rivers and HydroSheds catchment and subcatchment boundaries.	28
Figure 4-3: Correlation between observed and predicted temperature.	29
Figure 4-4: Spatial distribution of variance of observed and predicted temperature.	29
Figure 4-5: Boundaries of upstream Amu Darya and Syr Darya river basins.	30
Figure 4-6: Schematic model structure AralMountain model.	31
Figure 4-7: Grid cell area covered with clean-ice glaciers and debris-covered glaciers.	32
Figure 4-8: Schematic representation glacier processes in AralMountain model.....	33
Figure 4-9: Schematic representation snow processes in AralMountain model	34
Figure 4-10: Schematic representation of rainfall-runoff modelling in AralMountain model	35
Figure 4-11: Runoff factor per grid cell.....	37
Figure 4-12: Reservoirs used to calibrate the model	38
Figure 5-1: Average annual precipitation 2001-2010	40
Figure 5-2: Average annual rainfall 2001-2010.....	40
Figure 5-3: Average annual snowfall 2001-2010	41
Figure 5-4: Observed and simulated monthly inflow Nurek reservoir 2001-2010.....	41
Figure 5-5: Observed and simulated monthly inflow Toktogul reservoir 2001-2010.....	42
Figure 5-6: Observed and simulated monthly inflow Andijan reservoir 2001-2010	42
Figure 5-7: Average total annual runoff per grid cell 2001-2010.....	44
Figure 5-8: Average annual glacier melt runoff per grid cell 2001-2010	45
Figure 5-9: Average annual snow melt runoff per grid cell 2001-2010	45
Figure 5-10: Average annual rain runoff per grid cell 2001-2010	46
Figure 5-11: Average annual baseflow runoff per grid cell 2001-2010	46
Figure 5-12: Average discharge and relative contribution of glacier melt for major streams 2001- 2010.....	47
Figure 5-13: Average discharge and relative contribution of snow melt for major streams 2001- 2010.....	47
Figure 5-14: Average discharge and relative contribution of rain runoff for major streams 2001- 2010.....	48
Figure 5-15: Simulated contribution of rain, snow melt, glacier melt and baseflow to inflow Nurek reservoir 2001-2010	49
Figure 5-16: Simulated contribution of rain, snow melt, glacier melt and baseflow to inflow Toktogul reservoir 2001-2010	49
Figure 5-17: Simulated contribution of rain, snow melt, glacier melt and baseflow to inflow Andijan reservoir 2001-2010	50
Figure 6-1: Fractional glacier cover 2010.....	53
Figure 6-2: Fractional glacier cover 2050 for CCCMA GCM.....	53
Figure 6-3: Fractional glacier cover 2050 for CCSM3 GCM.	54
Figure 6-4: Fractional glacier cover 2050 for CNRM GCM.	54
Figure 6-5: Fractional glacier cover 2050 for ECHAM GCM.	55
Figure 6-6: Fractional glacier cover 2050 for MIROC GCM.	55
Figure 6-7: Fractional glacier cover 2050, mean of 5 above GCM forced model runs.	56
Figure 6-8: Change in average annual runoff generation per grid cell (mm change with respect to reference period) for 2021-2030 and 2041-2050. Mean of output after forcing model with 5 GCMs.	57
Figure 6-9: Change in average annual runoff generation per grid cell (mm change with respect to reference period) for 2021-2030 and 2041-2050. Output for model forced with MIROC GCM.	58



Figure 6-10: Change in average annual runoff generation per grid cell (mm change with respect to reference period) for 2021-2030 and 2041-2050. Output for model forced with ECHAM GCM.	59
Figure 6-11: Change in average annual runoff generation per grid cell (mm change with respect to reference period) for 2021-2030 and 2041-2050. Output for model forced with CNRM GCM.	60
Figure 6-12: Change in average annual runoff generation per grid cell (mm change with respect to reference period) for 2021-2030 and 2041-2050. Output for model forced with CCSM3 GCM.	61
Figure 6-13: Change in average annual runoff generation per grid cell (mm change with respect to reference period) for 2021-2030 and 2041-2050. Output for model forced with CCCMA GCM.	62
Figure 6-14: Change in average annual runoff generation from glacier melt per grid cell (mm change with respect to reference period) for 2021-2030 and 2041-2050. Mean of output after forcing model with 5 GCMs.	63
Figure 6-15: Change in average annual runoff generation from glacier melt per grid cell (mm change with respect to reference period) for 2021-2030 and 2041-2050. Output for model forced with MIROC GCM.	64
Figure 6-16: Change in average annual runoff generation from glacier melt per grid cell (mm change with respect to reference period) for 2021-2030 and 2041-2050. Output for model forced with ECHAM GCM.	65
Figure 6-17: Change in average annual runoff generation from glacier melt per grid cell (mm change with respect to reference period) for 2021-2030 and 2041-2050. Output for model forced with CNRM GCM.	66
Figure 6-18: Change in average annual runoff generation from glacier melt per grid cell (mm change with respect to reference period) for 2021-2030 and 2041-2050. Output for model forced with CCSM3 GCM.	67
Figure 6-19: Change in average annual runoff generation from glacier melt per grid cell (mm change with respect to reference period) for 2021-2030 and 2041-2050. Output for model forced with CCCMA GCM.	68
Figure 6-20: Change in average annual runoff generation from snow melt per grid cell (mm change with respect to reference period) for 2021-2030 and 2041-2050. Mean of output after forcing model with 5 GCMs.	69
Figure 6-21: Change in average annual runoff generation from snow melt per grid cell (mm change with respect to reference period) for 2021-2030 and 2041-2050. Output for model forced with ECHAM GCM.	70
Figure 6-22: Change in average annual runoff generation from snow melt per grid cell (mm change with respect to reference period) for 2021-2030 and 2041-2050. Output for model forced with CNRM GCM.	71
Figure 6-23: Change in average annual runoff generation from snow melt per grid cell (mm change with respect to reference period) for 2021-2030 and 2041-2050. Output for model forced with CCSM3 GCM.	72
Figure 6-24: Change in average annual runoff generation from snow melt per grid cell (mm change with respect to reference period) for 2021-2030 and 2041-2050. Output for model forced with CCCMA GCM.	73
Figure 6-25: Change in average annual runoff generation from snow melt per grid cell (mm change with respect to reference period) for 2021-2030 and 2041-2050. Output for model forced with MIROC GCM.	74



Figure 6-26: Change in average annual runoff generation from rain per grid cell (mm change with respect to reference period) for 2021-2030 and 2041-2050. Mean of output after forcing model with 5 GCMs.	75
Figure 6-27: Change in average annual runoff generation from rain per grid cell (mm change with respect to reference period) for 2021-2030 and 2041-2050. Output for model forced with MIROC GCM.	76
Figure 6-28: Change in average annual runoff generation from rain per grid cell (mm change with respect to reference period) for 2021-2030 and 2041-2050. Output for model forced with ECHAM GCM.	77
Figure 6-29: Change in average annual runoff generation from rain per grid cell (mm change with respect to reference period) for 2021-2030 and 2041-2050. Output for model forced with CNRM GCM.	78
Figure 6-30: Change in average annual runoff generation from rain per grid cell (mm change with respect to reference period) for 2021-2030 and 2041-2050. Output for model forced with CCSM3 GCM.	79
Figure 6-31: Change in average annual runoff generation from rain per grid cell (mm change with respect to reference period) for 2021-2030 and 2041-2050. Output for model forced with CCCMA GCM.	80
Figure 6-32: Change in average annual base flow generation per grid cell (mm change with respect to reference period) for 2021-2030 and 2041-2050. Mean of output after forcing model with 5 GCMs.	81
Figure 6-33: Change in average annual base flow generation per grid cell (mm change with respect to reference period) for 2021-2030 and 2041-2050. Output for model forced with MIROC GCM.	82
Figure 6-34: Change in average annual base flow generation per grid cell (mm change with respect to reference period) for 2021-2030 and 2041-2050. Output for model forced with ECHAM GCM.	83
Figure 6-35: Change in average annual base flow generation per grid cell (mm change with respect to reference period) for 2021-2030 and 2041-2050. Output for model forced with CNRM GCM.	84
Figure 6-36: Change in average annual base flow generation per grid cell (mm change with respect to reference period) for 2021-2030 and 2041-2050. Output for model forced with CCSM3 GCM.	85
Figure 6-37: Change in average annual base flow generation per grid cell (mm change with respect to reference period) for 2021-2030 and 2041-2050. Output for model forced with CCCMA GCM.	86
Figure 6-38: Projected average annual inflow Toktogul reservoir 2001-2050. Figure shows mean of model output when forced with 5 GCMs and the range of projections when forced by 5 GCMs.	87
Figure 6-39: Projected average annual inflow Nurek reservoir 2001-2050. Figure shows mean of model output when forced with 5 GCMs and the range of projections when forced by 5 GCMs.	87
Figure 6-40: Projected average annual inflow Toktogul reservoir 2001-2050 per runoff component. Figure shows mean of model output when forced with 5 GCMs.	88
Figure 6-41: Projected average annual inflow Nurek reservoir 2001-2050 per runoff component. Figure shows mean of model output when forced with 5 GCMs.	88
Figure 6-42: Upstream catchments used to calculate inflow from upstream to downstream areas. See Table 10 for corresponding catchment names.	89



Figure 6-43: Hydrographs for inflow from upstream into downstream areas showing future projections (2021-2030, 2041-2050) compared to reference period (2001-2010). The range of outputs for the model forced by five GCMs is shown.....	90
Figure 6-44: Hydrographs for inflow from upstream into downstream areas showing future projections (2021-2030, 2041-2050) compared to reference period (2001-2010). The range of outputs for the model forced by five GCMs is shown.....	91
Figure 6-45: Hydrographs for inflow from upstream into downstream areas showing future projections (2021-2030, 2041-2050) compared to reference period (2001-2010). The range of outputs for the model forced by five GCMs is shown.....	92
Figure 6-46: Hydrographs for inflow from upstream into downstream areas showing future projections (2021-2030, 2041-2050) compared to reference period (2001-2010). The range of outputs for the model forced by five GCMs is shown.....	93
Figure 6-47: Hydrographs for inflow from upstream into downstream areas showing future projections (2021-2030, 2041-2050) compared to reference period (2001-2010). The range of outputs for the model forced by five GCMs is shown.....	94
Figure 6-48: Hydrographs for inflow from upstream into downstream areas showing future projections (2021-2030, 2041-2050) compared to reference period (2001-2010). The range of outputs for the model forced by 5 GCMs is shown.	95
Figure 6-49: Average change in monthly inflow into downstream areas for Syr Darya basin in 2041-2050. Range for model forced with five GCMs is shown.	98
Figure 6-50: Average change in monthly inflow into downstream areas for Amu Darya basin in 2041-2050. Range for model forced with five GCMs is shown.	99



1 Introduction

Water resources management in the Central Asia region faces big challenges. The hydrological regimes of the two major rivers in the region, the Syr Darya and the Amu Darya, are complex and vulnerable to climate change. Water diversions to agricultural, industrial and domestic users have reduced flows in downstream regions, resulting in severe ecological damages. The administrative-institutional system is fragmented, with six independent countries sharing control, sometimes with contradicting objectives.

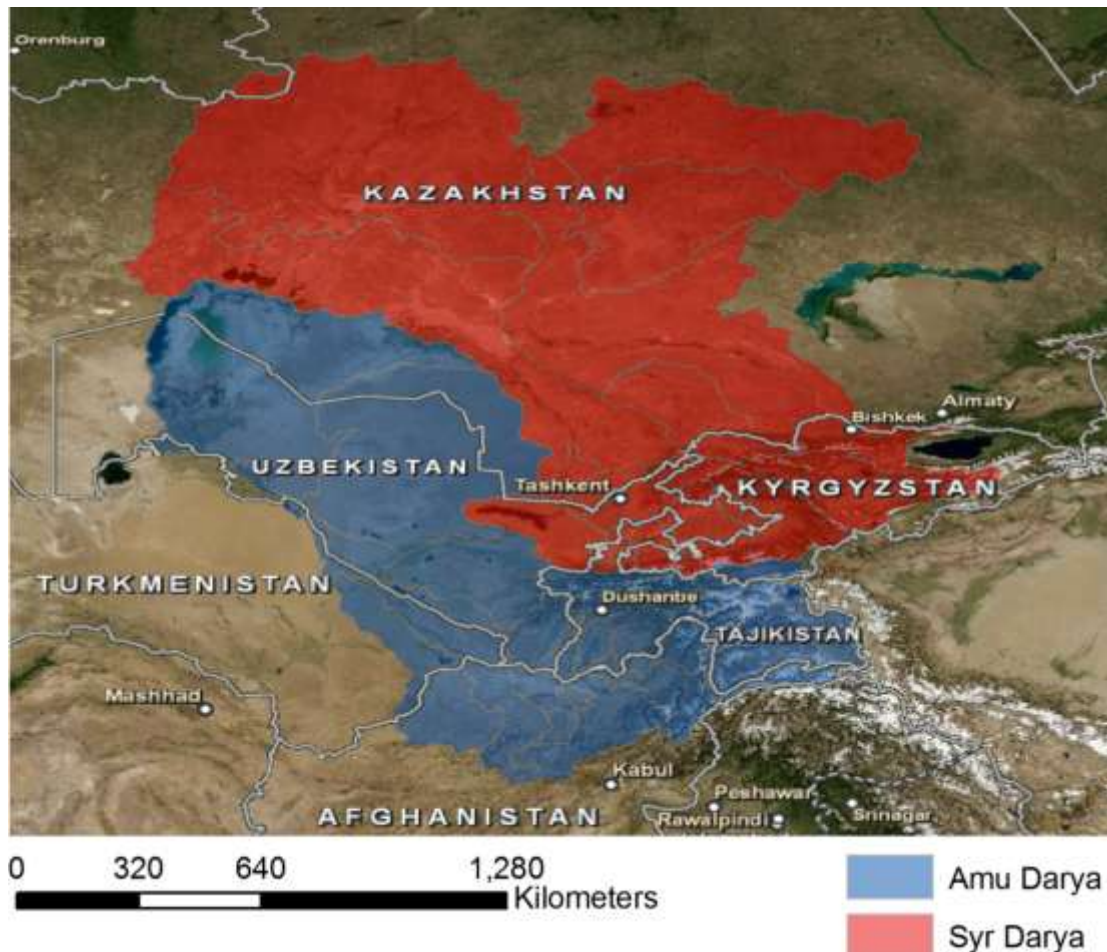


Figure 1-1: Amu Darya and Syr Darya river basins.

In the Central Asian region, water related issues have been prominent since the break-up of the USSR. Major trans-boundary river basins and management agreements in the Aral Sea Basin include 1) 1992 Aral Sea Basin Water Allocation and Management; 2) 1993 Aral Sea Basin Program and 3) 1994 Nukus Declaration on Aral Sea Basin Management; 4) 1998 Framework Agreement on Rational Water and Energy Use; 5) 1999 Revised Mandate of the International Fund for Saving the Aral Sea; and 6) 2003- Revised Aral Sea Basin Program, Phase-2. One of the regional environmental initiatives in Central Asia Countries (CACs) is the International Fund for Saving the Aral Sea (IFAS), established in 1994. IFAS, together with its two commissions, the Interstate Commission on Sustainable Development (ICSD) and the Interstate Commission for Water Coordination (ICWC), is charged with mobilizing funds to implement interstate activities on water resources and land degradation and other social-economic issues, with



financing joint scientific and technical projects, and with participating in international programs and projects directed at the Aral Sea crisis.

UNDP and the Global Water Partnership (2004) have drafted the Integrated Water Resource Management (IWRM) plan that proposed an integrated approach to water management, in which the river basin would be managed holistically, with the participation of water user stakeholders and ensuring environmental sustainability. The regional policy can only be implemented if there is a strong scientific background for investment plans and commitment to international agreements and conventions. It is therefore essential to gain knowledge on the future availability and demand of water resources under of climate change.

The following description of the situation in Central Asia is based on the article 'Water and Energy Conflict in Central Asia' by Tobias Siegfried published in Earth Institute's 'state of the planet' blog.

What once was a basin-wide management approach during the Soviet times has become an uncoordinated management situation with conflicting interests for the upstream countries (Kyrgyzstan, Tajikistan and Afghanistan) and the downstream countries (Uzbekistan, Turkmenistan and Kazakhstan). The hydraulic infrastructure is distributed over various independent countries. As a result, the water resources system is not managed collectively and cooperatively. A mixture of regional, national, and interstate institutions now handles allocation decisions, which used to be centrally administered during Soviet times. As a result, water and energy allocation among the various sectors and users is not efficient. Future water resources development in northern Afghanistan will further add fuel to the water and energy conflict in the region.

In short, the upstream / downstream conflict consists of opposed demand patterns for energy and water resources, in space and in time. Kyrgyzstan and Tajikistan need to release water from a number of large reservoirs during the cold months to generate hydropower for heating. There, hydropower provides the cheapest source of energy with generating costs as low as 0.1 cent/kWh. The winter releases frequently cause flooding in the downstream areas. At the same time and in order to have enough hydropower generating capacity during the cold months, these upstream states spend the warmer summer months saving water in those reservoirs.

That is precisely when the downstream countries have the most pressing need for irrigation water where the degradation of agricultural soils and insufficient flows for ecosystems are issues of growing concern. In the region, cotton is an important cash crop, and, at the same time, wheat is considered essential in order to meet national food security goals. Especially for Uzbekistan, considerations of self-sufficiency have become more important in recent times where food grain prices have increased considerably on the world market.

The original idea in Soviet times was to operate the hydro-infrastructure in irrigation mode. The water resources of Central Asia were managed with the aim to maximize crop production. Part of the hydropower produced during irrigation water-releases in spring and summer was conveniently utilized in the downstream for driving lift irrigation and vertical drainage pumps along the 30,000 kilometers of irrigation channels. In return, the upstream areas received energy supplies in the form of gas and coal to cover winter energy demands.

Future climate change poses additional challenges. The discharge in both the Syr Darya and the Amu Darya rivers is driven mainly by snow and glacial melt. The impact of a warming



climate on these key hydrological processes is not sufficiently understood and no mitigation and adaptation strategies are in place. Whereas changes in precipitation levels are hard to predict for the future, there is a solid consensus that average global temperatures are rising. As a result, more precipitation will fall as rain in the upstream and the ice volume in the Tien Shan and Pamir mountain ranges will likely shrink. The former will impact the seasonality of the runoff whereas the latter will at least temporarily increase average annual flows. Furthermore, changes in sediment loads may pose additional problems. At this point in time, the impacts are not sufficiently quantified and adaptation and mitigation strategies not in place.

The ongoing construction of new dams in Kyrgyzstan and Tajikistan is adding tension to the existing situation. The soviet-era designed hydropower projects Kambarata I and II in Kyrgyzstan and the Rogun dam in Tajikistan are on the table again as a result of an increased access to international donor money with Russia and China investing in these projects. For the downstream countries, these developments have raised concern because this can mean that the upstream states can decouple themselves the necessity to receive energy deliveries in the winter from Kazakhstan, Uzbekistan and Turkmenistan. The upstream countries could lose their will to abide to summer operation rules with severe impacts to irrigated agriculture and the overall economy. From this perspective, it is not surprising that certain tensions between the countries exist. Although the new infrastructure will be effective at damming river flow and in adding management options that are direly needed, measures need to be taken so that further flow impediment does not equal impediment to regional integration.

The unfavorable developments in this geopolitically important and fragile region call for urgent attention of the international community. Interdisciplinary research can critically inform decision making in the region for better risk management and the design of mitigation and adaptation strategies¹.

The upstream hydrology and the contribution of snow and ice to river runoff are crucial to understand the downstream impact of climate change. This report presents a hydrological modelling study assessing the hydrological properties of the Amu Darya and Syr Darya river basin. Using this model, the importance of snow and ice melt to river runoff can be quantified. With the use of climate change scenarios, the impact of climate change for these rivers in the next decades can be estimated. This report presents the state of the art of what is currently known and unknown as far as climate change impacts on the upstream water resources in the Amu Darya and Syr Darya river basins are concerned. Chapter 2 provides a review of available literature discussing the impact of climate change on water resources in the region. In chapter 3, the area is described in terms of topography, climate and factors which are relevant for the hydrological regime in the river basins. The used model, data sources and model calibration process are described in chapter 4. Chapter 5 discusses the current hydrological regime for the river basins as characterized by the model. In chapter 6, the estimated impacts of climate change in the upstream basin for the next decades are described as well as the reliability of the modelling results.

The ultimate objective of this work is to develop national capacity in each of the participating countries (focused on the Kyrgyz Republic, Tajikistan, Kazakhstan, Turkmenistan and Uzbekistan) to use the models to prepare climate impact scenarios and develop adaptation strategies. This will then result in improved national strategies for climate change adaptation.

¹ These sections are partly based on <http://blogs.ei.columbia.edu/2009/08/18/water-and-energy-conflict-in-central-asia/>





2 Review of Climate Change Impact Studies on Water Resources

2.1 Impact of climate change on water resources

Observational records and climate projections provide abundant evidence that freshwater resources are vulnerable and have the potential to be strongly impacted by climate change, with wide-ranging consequences for human societies and ecosystems [Bates *et al.*, 2008]. Observed warming over the last decades has been linked to changes in the hydrological cycle. Examples of changes include changing precipitation patterns, intensity and extremes, changes in snow and ice cover and changes in runoff.

According to the IPCC, climate model simulations for the 21st century are consistent in projecting increased precipitation for high latitudes and parts of the tropics, and decreased precipitation in some subtropical and lower mid-latitude regions [Bates *et al.*, 2008]. Besides a climate change effect on water resources, an increasing population and increasing use of water will put increasing pressure on global water resources: pressures are increasing most rapidly in Africa and parts of southern Asia [Arnell, 1999]. The recent controversy about overestimated melting rates of the Himalayan glaciers, as communicated in the 4th assessment report of the IPCC, shows that the knowledge of high-altitude snow and ice and its response to climate forcing is still very incomplete [Siegfried *et al.*, 2010].

2.2 Impact of climate change for snow and ice

Snow and glacial melt are important hydrologic processes in the area surrounding the Tibetan plateau and adjacent mountain belts [Cruz *et al.*, 2007]. Large amounts of water are stored as snow and ice in the mountains; the third-largest ice mass on earth, after the Antarctic and Greenland ice sheets. Changes in temperature and precipitation are expected to have significant effects on the snow and ice storages [Barnett *et al.*, 2005]. The mountain ranges on earth are located in varying climatic zones, ranging from hot to cold and from wet to dry [Viviroli *et al.*, 2011]. Thus every mountainous region on Earth will be impacted by climate change in a different way. The glacier contribution to water resources is minor in monsoon regimes, moderate in most mid-latitude basins and of high importance in very dry basins, like the Aral Sea basin and Tien Shan mountains [Kaser *et al.*, 2010]. The glacier contribution to water resources differs for the catchments of the Amu Darya and Syr Darya. The percentage of glacierized area of the two catchments differs significantly (2% for the Amu Darya vs. 0.15% for the Syr Darya). This could result in different responses to climate change for the two rivers. In general, the Asian high mountains glaciers are show a negative mass balance as seen in Figure 2-1.



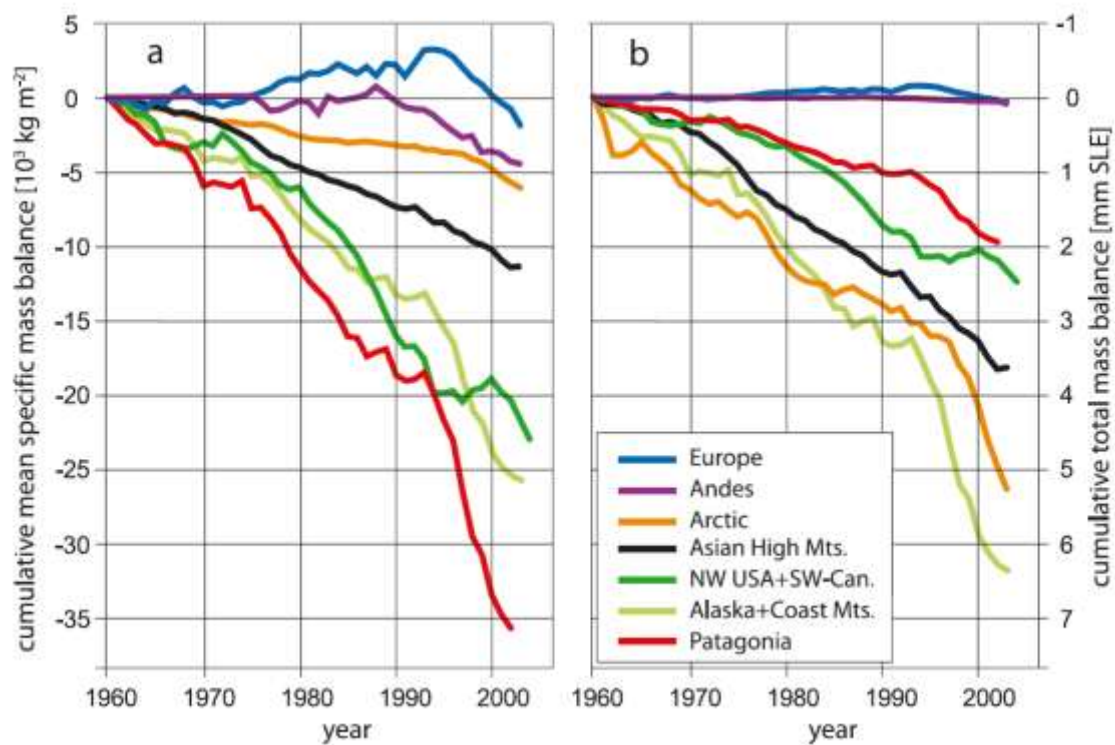


Figure 2-1: Changes in glacier mass balance around the world [Kaser *et al.*, 2006].

The impacts of climate change on hydrology and water management of the Central-Asian mountain environment have a complex geographic and climatologic context. It has been estimated that glaciers in the Syr Darya basin have lost 14% of their total volume over the last 60 years and that 15-40% of the volume will be lost in the coming 40 years [Siegfried *et al.*, 2010]. Over the short/medium term, the warming trend has already increased mean runoff and translated into increased water availability due to significant glacier wastage rates. This may compensate the increasing water demand downstream where climate gets drier and warmer. In the long term water availability may be reduced or the timing may change when the glaciers will be further reduced and the hydrological cycle will be accelerated.

2.3 Glacier changes in Central Asia

Multiple studies were done to estimate glacier changes in the Tien Shan mountains. Figure 2-2 shows the Tien Shan area and its traditional subdivision based on its climatic and orographic properties.



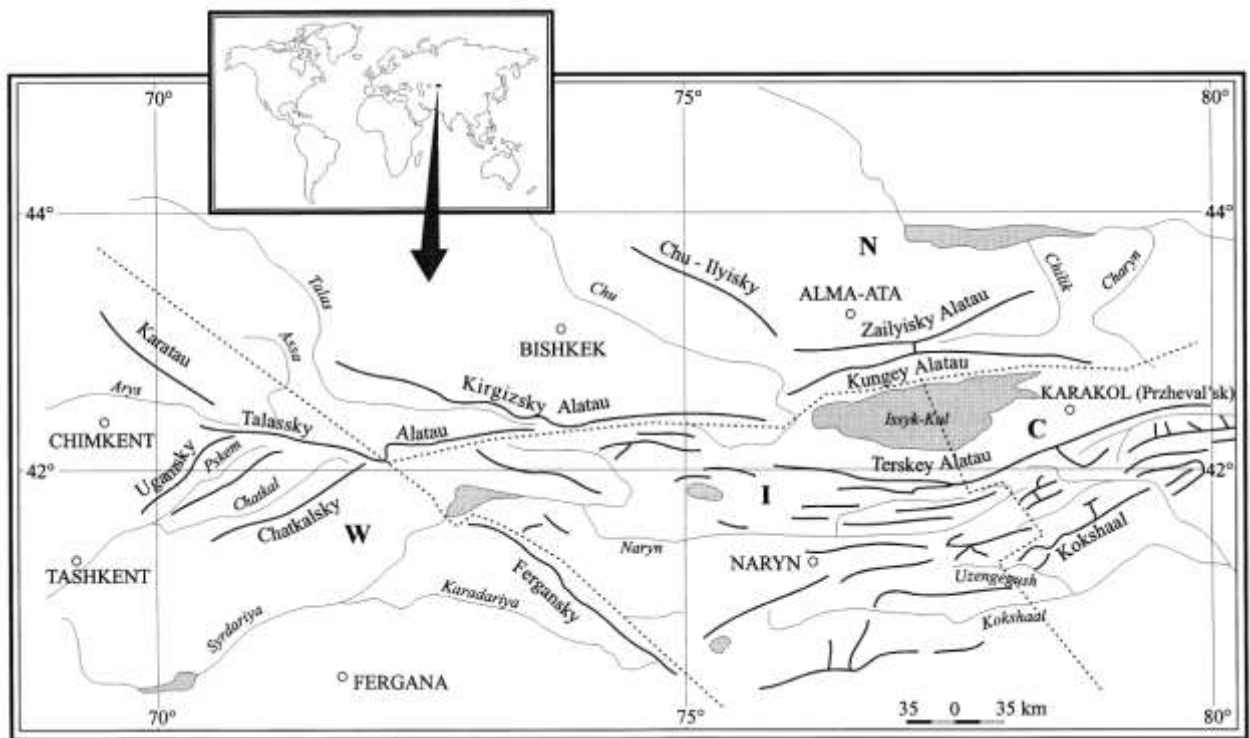


Figure 2-2: The Tien Shan mountains in Kyrgyzstan. Subdivisions of Tien Shan: W, western; N, northern; C, central; I, inner. [Solomina et al., 2004]

For the Akshirak massif in the central Tien Shan and for the Ala Archa glacier basin in the northern Tien Shan glacier changes were estimated using topographic and remote sensing data [Aizen et al., 2007]. Glaciers in the Akshirak massif in the central Tien Shan lost 12.5% of their surface area between 1943 and 2003. The glacier volume for this area was reduced by approximately 29% for the same period. Glacier retreat was accelerated in the second period of observation (after 1977). However, within this area glacier retreat was not uniform. A few glaciers advanced prior to 1977 while the majority retreated. In the Ala Archa basin in the northern Tien Shan, glacier area decreased by 15.7% between 1963 and 2003. Meteorological observations near the Ala Archa basin in the northern Tien Shan show no trends in observed annual precipitation or summer air temperature for 1913-2003. However, air temperature increased during spring and autumn, extending the period of glacier ablation and thus favoring glacier retreat. Near the Akshirak massif in the central Tien Shan no trend in annual precipitation is observed for 1930-2003. Summer air temperature increased for the same period, causing accelerated recession of the glaciers.

Another study conducted at the Akshirak range in the central Tien Shan plateau estimated the glacier changes between 1943 and 2001 using aerial photographs and ASTER images combined with long-term glaciological and meteorological observations [Khromova et al., 2003]. A small retreat between 1943 and 1977 was observed, followed by accelerated reduction between 1977 and 2001. This was caused by a combination of increased summer and annual air temperatures and decreases in annual precipitation. There has been a strong decrease in the summer/winter precipitation ratio. This ratio change implies reduced accumulation, leading to a lower surface albedo and thus increased summer ablation. On the other hand, climatic warming leads also to warming in deeper layers of the glaciers. The glacier velocity can be accelerated by this process, triggering glacier disintegration. Once a glacier disintegrates, it is more subject to incoming radiation and warm air, which accelerates ice degradation. The



authors also state that the role of direct anthropogenic impacts has to be considered. A decrease in surface albedo, through dust deposition originating from gold mining activity, could accelerate summer ablation.

Glacier changes were also studied for the Sokoluk watershed in the northern Tien Shan mountains. The results of this study based on remote sensing and topographic data show a clear trend in glacier retreat between 1963 and 2000 [Niederer *et al.*, 2007]. An overall loss of 28% is observed for this period and degradation accelerated since the 1980's. This acceleration of degradation was strongest for small glaciers. A general increase in the minimum glacier elevation of 78 meters has been observed over the last three decades, corresponding to one third of the total retreat of minimum glacier elevation since the Little Ice Age maximum. The terminus recession of Fedchenko glacier, the largest glacier in the Pamir mountains is indicated in Figure 2-3. According to the researchers, the decrease in glacier area is related to an increase in annual and summer air temperatures combined with a decrease in summer precipitation in Central Asia.



Figure 2-3: Recession of glacier terminus position for Fedchenko glacier 1933-2006.

For the Saukdara and Zulumart Ranges, located in the high-mountain plateau of the eastern Pamir mountains, glacier retreat was quantified using historical surveys and recent satellite imagery [Khromova *et al.*, 2006]. In the studied area, glaciers have retreated around 10% during the last 30 years. Glacier area has declined and recession of glacier termini is observed. Besides, an increase in debris-covered area and the appearance of new lakes is observed. The observed glacier retreat was correlated to two meteorological station records which have very different precipitation cycles despite of their proximity (about 145 km apart) (Figure 2-4). At the 'Fedchenko' station 87% of annual precipitation falls during winter while at 'Murgab' station winter precipitation accounts for only 27% of the total amount. The glaciers in the Zulumart and



Saukdara ranges are located at the boundary of the winter- and summer-dominated precipitation regimes. Glaciers in the more humid part of the Pamir, near 'Fedchenko' station should be losing mass as increases in winter precipitation do not compensate for ablation rate increases. In both regions, with contrasting precipitation regimes, the trend in glacier retreat is similar. This may suggest that air temperature is a more important climatic driver for glacier mass balance than precipitation.

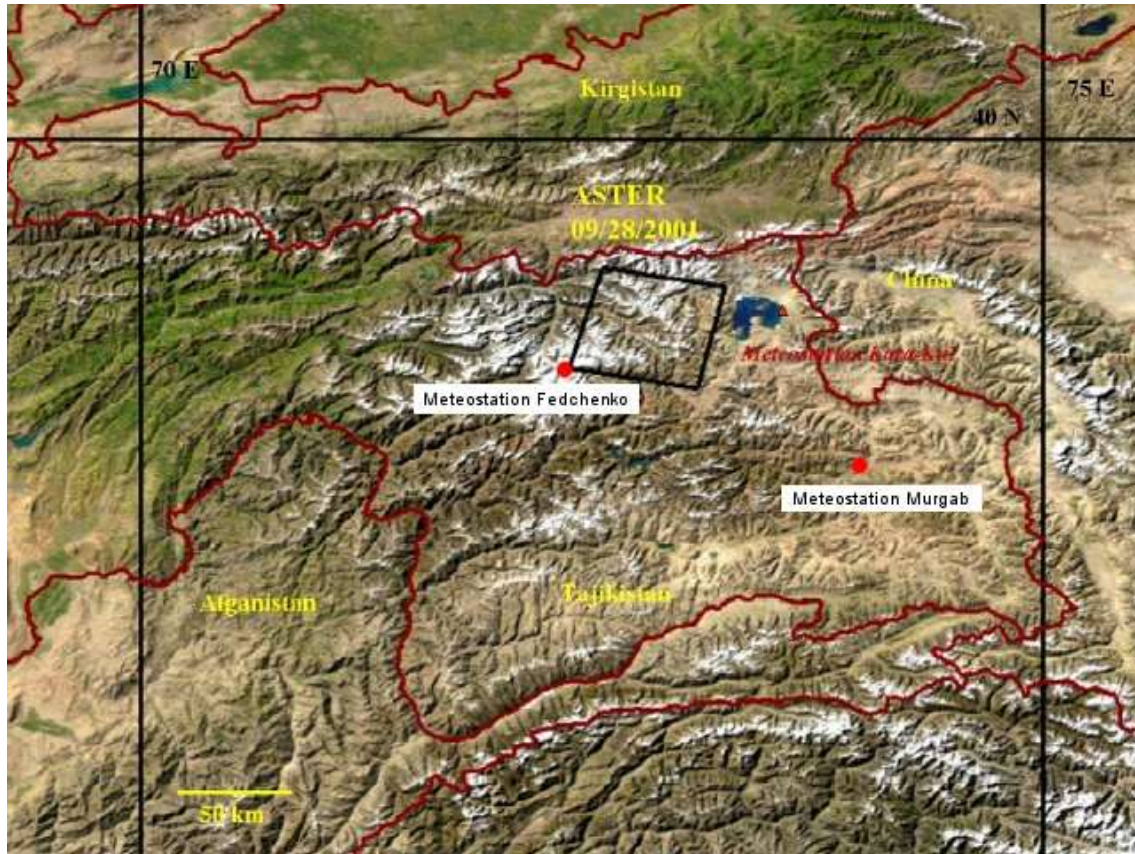


Figure 2-4: Fedchenko and Murgab meteo station locations in the Pamir mountains. [Khromova et al., 2006]

2.4 Modelling the hydrological response to climate change in high mountain regions

Local scale modelling studies quantifying the hydrological response to climate change were done for multiple catchments in the Himalayan area. For example [Singh and Bengtsson, 2004] concluded for the Satluj river basin that the impact of climate change has more effect on the seasonal scale than on the annual water availability (Figure 2-5). Reduction in melt from the lower part was counteracted by the increase of melt from the upper part of the basin, resulting in a decrease in the magnitude of change in annual melt runoff resulting in reduced summer runoff.

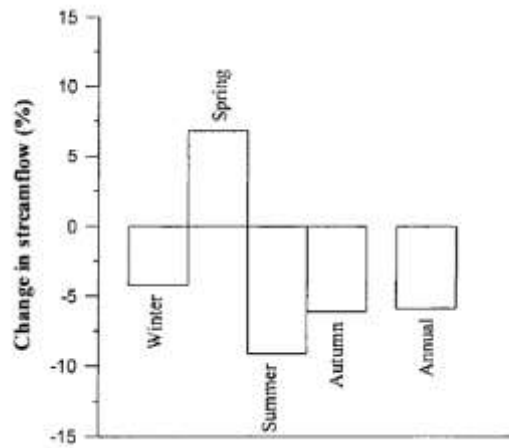


Figure 2-5: Changes in seasonal stream flow assuming 2 °C temperature rise. [Singh and Bengtsson, 2004]

Another study emphasized the regional differences of climatic change impact across the Himalayas [Rees and Collins, 2006]. Two hypothetical catchments were studied: a western catchment in the northeast of Pakistan and an eastern catchment in Nepal. The authors concluded that Himalayan rivers fed by large glaciers descending through considerable elevation range will respond in a broadly similar manner, except that summer snowfall in the east will suppress the rate of initial flow increase, delay peak discharge and postpone eventual disappearance of the ice. Impacts of declining glacier area on river flow will be greater in smaller and more glacierized basins in both the west and east. In the west, where precipitation is scarce, the impact will be important for considerable distances downstream.

[Immerzeel *et al.*, 2011] studied the impacts of climate change for the Langtang catchment in Nepal. A high resolution combined cryospheric hydrological model was developed for the catchment simulating glacier evolution and all major hydrological processes. Parameters related to the glacier modelling are calibrated forcing the model with temperature and precipitation data from 1957-2002 aiming at reproducing the locations of glaciers and permanent snow in 2000, as observed by remote sensing methods. Hydrological parameters were calibrated using 2000-2006 precipitation and temperature data as input and comparing results to observed daily discharges for 2000-2006. The calibrated model is used to estimate glacier changes and discharge changes for 2000-2100 using downscaled data for five different GCM projections. The analysis shows a steady decline in glacier area due to increasing temperature and precipitation (Figure 2-6). The river flow is projected to increase significantly due to the increased ice melt and precipitation (Figure 2-7).

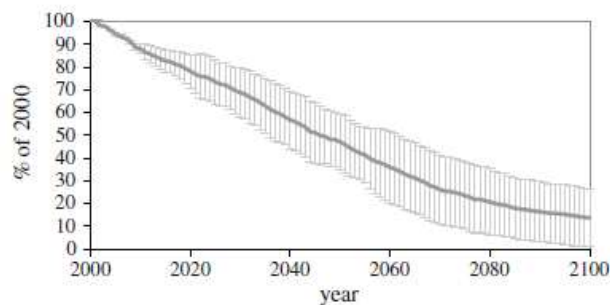


Figure 2-6: Anomalies in glacier ice volume (error bars indicate 1 σ of 5 GCM's) [Immerzeel *et al.*, 2011]



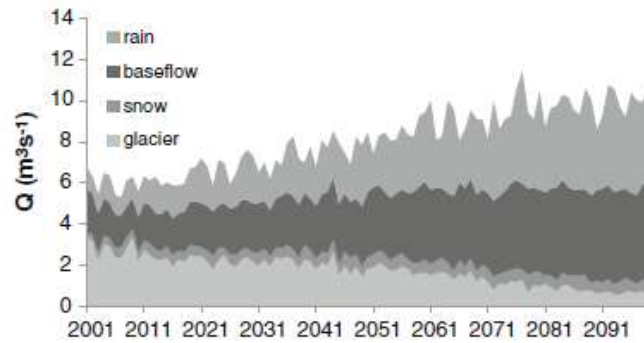


Figure 2-7: Total simulated discharge partitioned into rain runoff, glacier runoff, snow runoff and baseflow. [Immerzeel *et al.*, 2011]

A large scale hydrological modelling study for five large Asian basins originating in the Himalayan mountains gives estimates for the impact of climate change for these basins [Immerzeel *et al.*, 2010b]. The general conclusion is that Asia's water towers are threatened by climate change, but the effects of climate change on water availability and food security in Asia differ significantly among basins and cannot be generalized. The study shows that melt water is extremely important in the Indus basin and important for the Brahmaputra basin but plays just a modest role for the Ganges, Yangtze and Yellow rivers. Regional anomalies in glacier response to climate change are observed in the Himalaya region. Glacial expansion can be observed at high altitude, which may be caused by the presence of supra-glacial debris and possibly an increased orographic precipitation. For the Indus and Brahmaputra basin, the effects are likely to be severe because of the large population and high dependency on melt water. On the contrary, in the Yellow River basin climate change may have positive effects, as the dependence on melt water is low and a projected upstream increase in precipitation could enhance water availability. Figure 2-8 shows the predicted flow for the A1B SRES scenario compared to observed flow in 2000-2007.



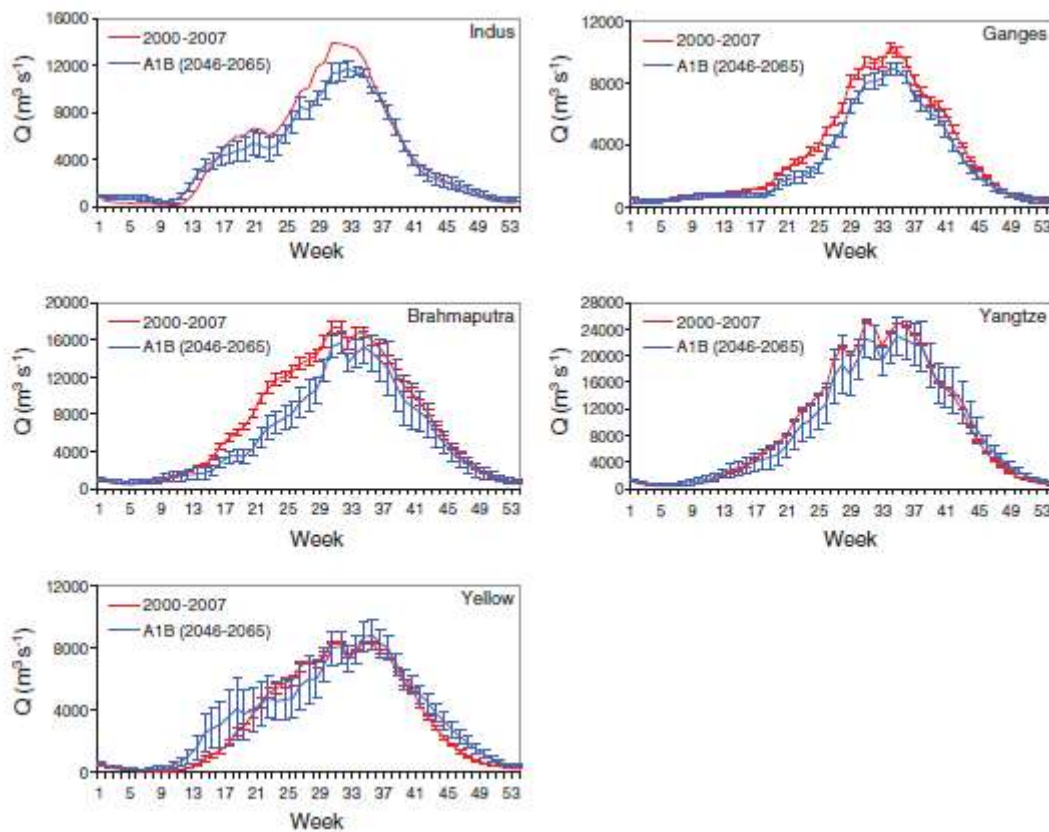


Figure 2-8: Simulated mean upstream discharge for present (2000-2007) and future climate for the A1B SRES scenario. [Immerzeel et al., 2010a]

Recently, a coupled climate-land ice-hydrological model study was conducted for the Syr Darya catchment [Siegfried et al., 2011]. This model was used to project runoff at the basin level and in the subcatchments of the Naryn and Syr Darya until 2050. These projections were made using the mean climatic change derived from five global circulation models (GCMs), providing a mean change in precipitation and temperature for the Syr Darya region. Preliminary results indicate that the contribution of runoff from glacier melt is small at the basin scale, but can be large for some individual sub-catchments of the Syr Darya. Increased glacier melt due to climate change may help to some extent in compensating for decreasing precipitation and growing water demand in some subcatchments. Considering the uncertainties in climate change projections for Central Asia and the low overall contribution of glacier melt to total runoff in the Syr Darya basin, it is unlikely that climate change induced glacier melt will help to sustain water availability in the short to medium term. Climatic warming has consequences on runoff seasonality due to earlier snow melt. Water stress in unregulated catchments will increase because less water will be available for irrigation in the summer months. Threats from natural hazards, mostly glacier lake outbursts are likely to increase as well.

According to a study conducted by the Eurasian Development Bank, changes in air temperature and precipitation in Central Asia has led to a regression in glacier area [Ibatulin et al., 2009]. For example, the total volume of glaciers in the Pamir Mountains of Tadjikistan has shrunk by about ten percent. The decline has been particularly dramatic in basins with large glaciers. In recent years, an increase in air temperature has led to more active surging glaciers. Deglaciation led to a decline in runoff despite the increased contribution to runoff from long-lasting ice reserves.



As a general conclusion, it can be stated that the impact of climate change cannot be generalized. The effects of changes in temperature and precipitation can either result in increased water availability or decreased availability of water. This can also differ on different timescales. Regional differences in expected changes in temperature and precipitation as well as the portion of snow and ice covered area in a catchment lead to high variation in effects of climatic change. For the Amu Darya and Syr Darya basins, knowledge on the effects of climate change on water availability is sparse. Besides, the contribution of glacier melt to total runoff differs significantly for both basins, leading to different responses to climate change. Modelling the hydrological and glacial response to climate change for the mountainous upstream parts of the Syr Darya and Amu Darya river basins will provide important insight in future water availability for the downstream regions of the river basins.



3 The Upstream Parts of the Amu and Syr Darya River Basins

3.1 Topography

The upstream parts of the Amu Darya and Syr Darya river basins are characterized by a high variation in elevation. Figure 3-1 shows main rivers in the upstream parts of the basins and elevation. The elevation ranges from almost 7000 meters above sea level in the southeast to around 170 meters above sea level in the western plains. The Amu Darya and Syr Darya river basins originate in the Tien Shan and Pamir mountain ranges.

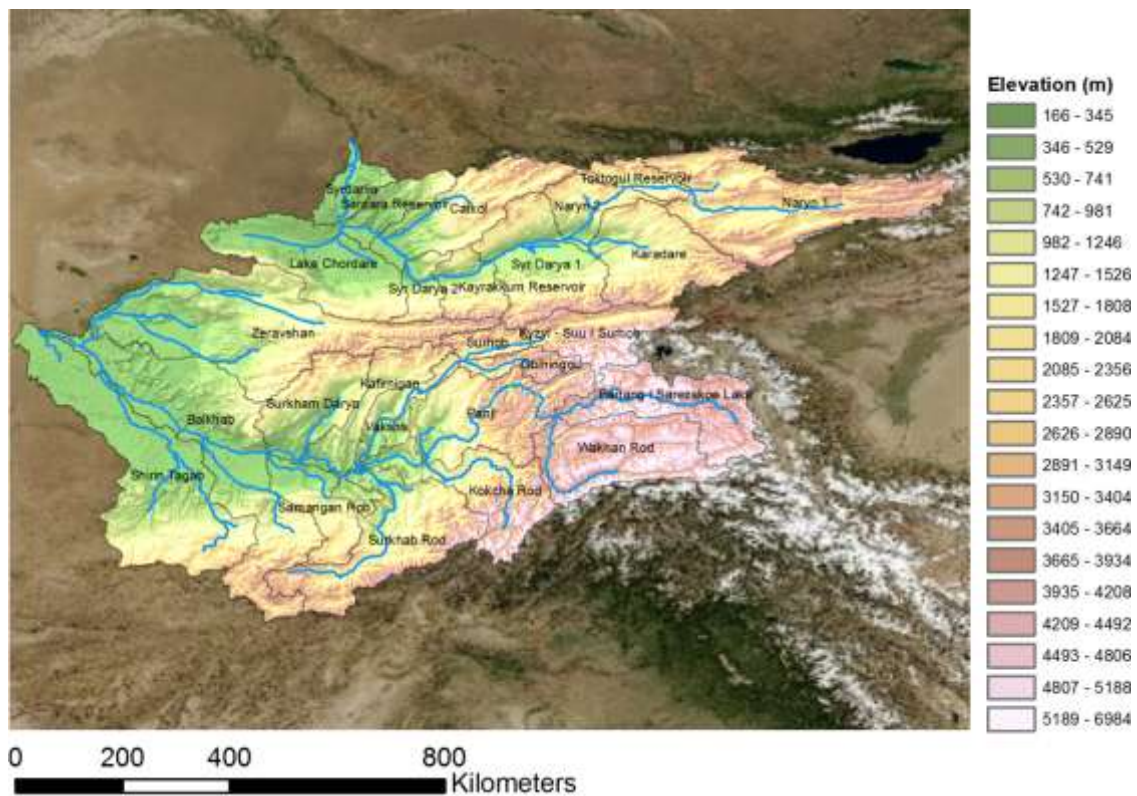


Figure 3-1: Upstream topography Amu Darya and Syr Darya river basins.

3.2 Climate

The climate in the study area is highly continental with extreme variation in summer and winter temperatures [Ibatulin et al., 2009]. Figure 3-2 shows the average air temperature distribution for 2001-2010. The average air temperature for the region differs from around 20 °C in the western plains to around -20 °C in the high mountains. The climate in the lower areas can be described as arid subtropical. The climate in Central Asian high-mountain regions is typically dry and cold. Within the mountain ranges climate differs over short distances. For example, sharp contrasts in climate between the eastern and western Pamir mountains exist. In the west most precipitation falls during winter, while most precipitation in the east falls during summer [Khromova et al., 2006]. In general, the western mountains get more precipitation compared to the eastern mountains, due to orographic effects, as can be seen in Figure 3-3.



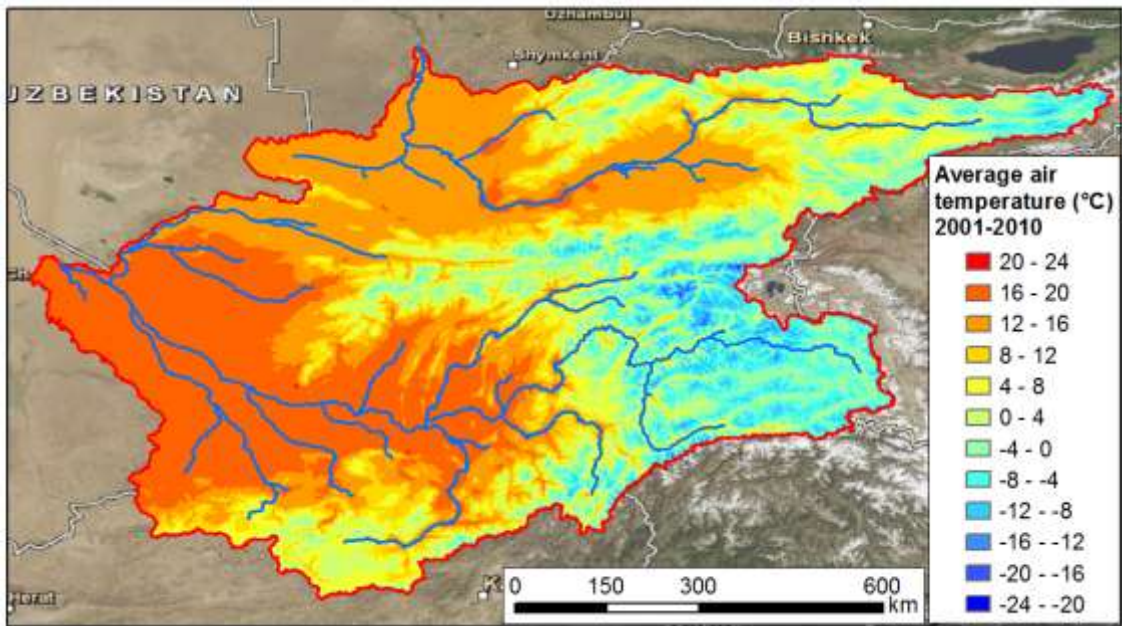


Figure 3-2: Average air temperature 2001-2010 based on downscaled and interpolated station data

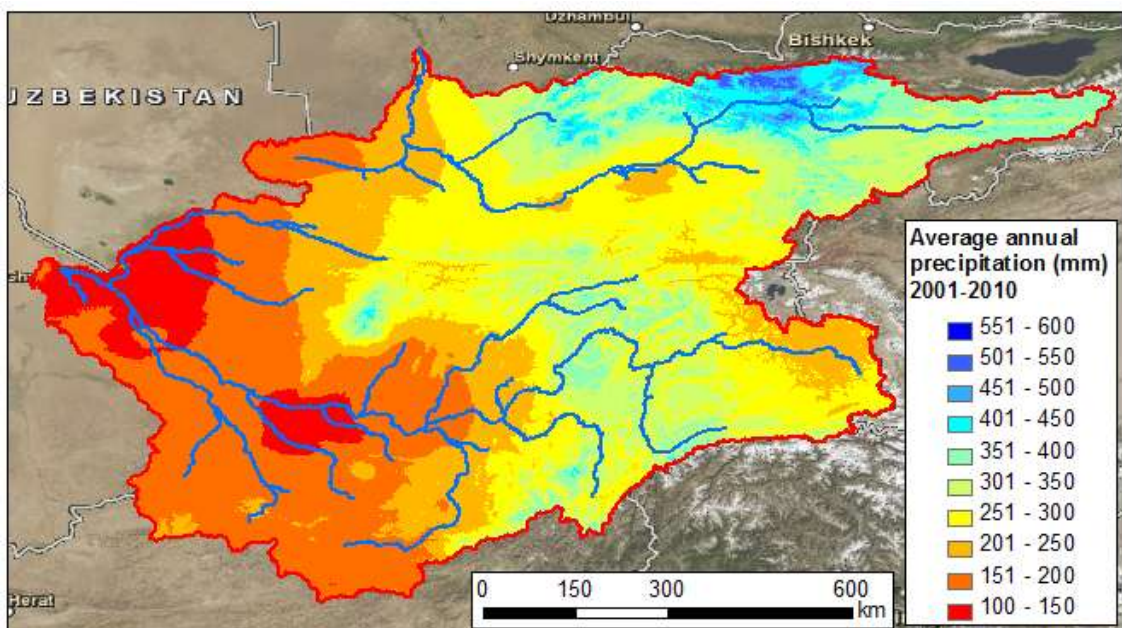


Figure 3-3: Average annual precipitation 2001-2010 based on the PERSIANN/TRMM dataset

The data on current and future climate used in this report is generated and analysed by the Finnish Meteorological institute (FMI), partner in this project. For detailed information on analysis of the climate data see the FMI report on climate change in Central Asia.

3.3 Glaciers and snow

Ice and snow melt are important contributors to runoff in the Himalayan area in general. In the upstream Amu Darya basin, 2% of the total area is covered with ice. For the upstream Syr



Darya basin the glacial cover is 0.15%. The largest glacier present in the area is the Fedchenko glacier in the Pamir mountains covering 77 km in length and covering 650 km² [Aizen *et al.*, 2009]. The glacier is the largest in the world outside the polar regions.

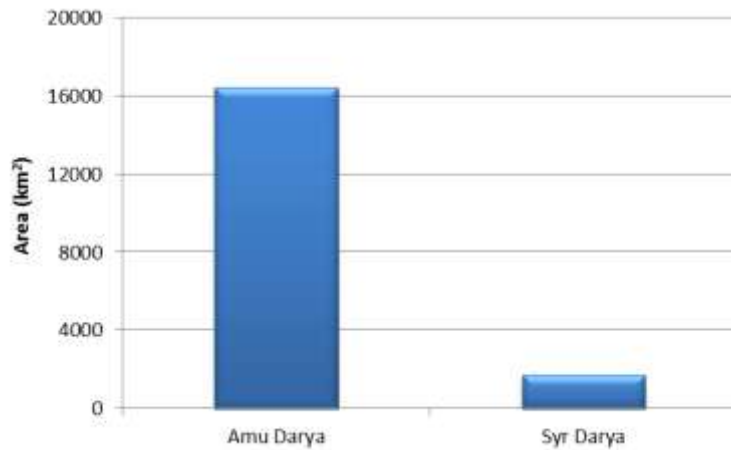


Figure 3-4: Area covered by glaciers in Amu Darya and Syr Darya river basins.

In general, a decline in glacial area is observed in the Himalayas, however regional increases in glacial cover are also observed. A glacier’s response to climate change does not only depend on climate, but also on topography and important regulators such as debris cover. West to East and North to South transitions to wetter and warmer climate exist in the Himalayas, resulting in regional differences in glacier response.

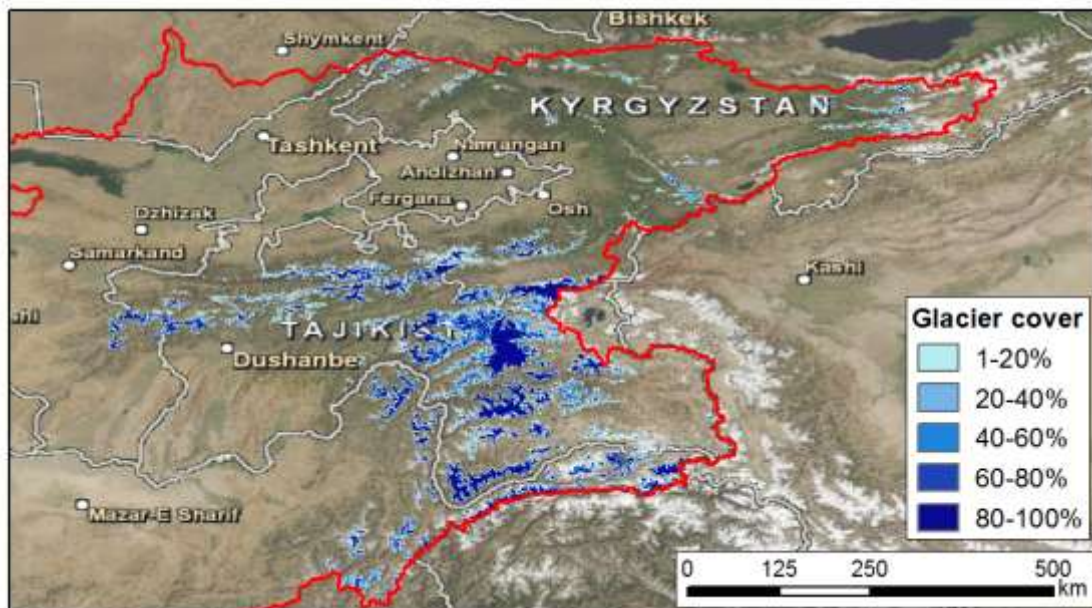


Figure 3-5: Areas with glaciers in the Amu Darya and Syr Darya river basins.

Melting water from glaciers in Tajikistan contributes between 10% and 20% to the runoff in large rivers, and in particularly hot and dry years their contribution may rise to 70% [Ibatulin *et al.*, 2009].



3.4 Land use and land cover

Land use in the Amu Darya and Syr Darya river basins is very variable. The inaccessible mountainous parts at high altitude are characterized by permanent snow and ice and bare areas. At midrange altitudes in the mountains open grasslands dominate while forests are present at low latitudes, especially in the Tien Shan mountains. The Pamir mountains have far less forest land cover. The river valleys downstream are dominated by irrigated croplands, irrigated with water from the Syr Darya and Amu Darya. The downstream areas which are not irrigated are mainly bare areas or areas with sparse vegetation.

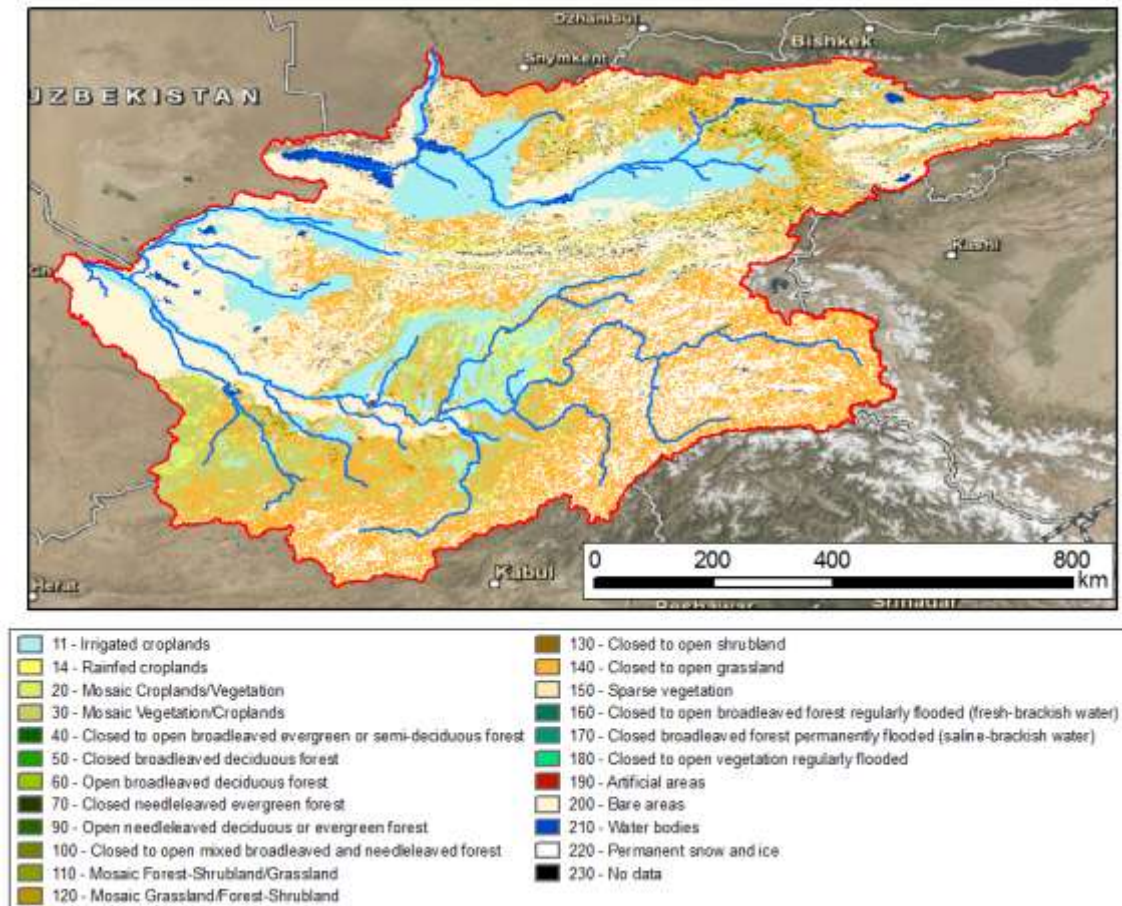


Figure 3-6: Land cover in the upstream parts of the Amu Darya and Syr Darya river basins [Defourny et al., 2007].

Table 1: Land cover in the upstream parts of the Amu Darya and Syr Darya river basin.

Land cover type	Surface area (absolute, km ²)	Surface area (percentage of total)
Bare areas / sparse vegetation	236704	29.6
Grassland	229415	28.7
Croplands	140665	17.6
Croplands / Vegetation	96848	12.1
Permanent snow and ice	78624	9.8
Water bodies	9317	1.2
Forest-Shrubland / Grassland	5011	0.6
Forest	2549	0.3
Artificial areas	125	0.02



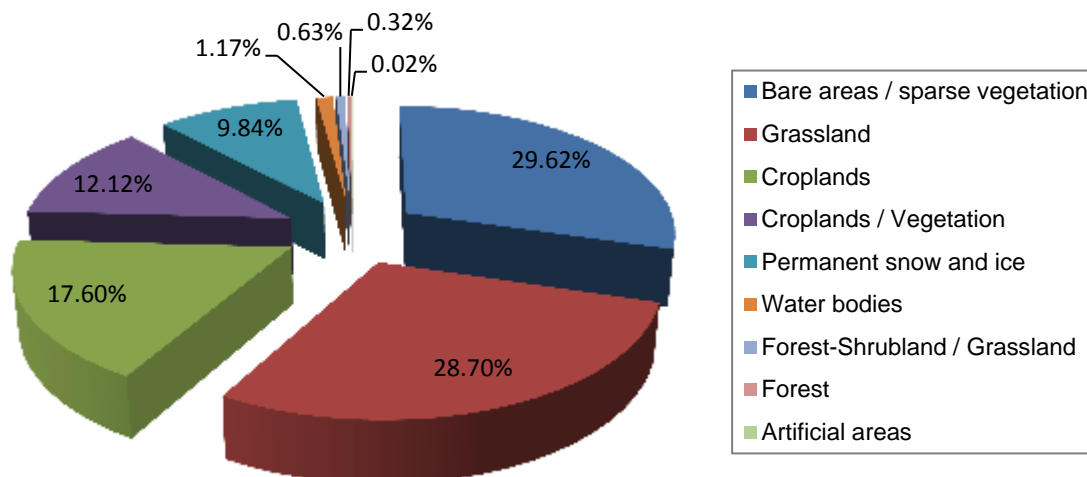


Figure 3-7: Land cover type in the upstream parts of the Amu Darya and Syr Darya river basin.

3.5 Water management and hydrology

Water from the upstream parts of the Amu Darya and Syr Darya is collected in reservoirs to be used for the generation of hydropower and irrigation. The most upstream reservoirs in the Syr Darya basin are the Toktogul and Andijan reservoirs in Kyrgyzstan and the Charvak reservoir in Uzbekistan. The most upstream reservoirs in the Amu Darya basin are the Nurek reservoir in the Vaksh river in Tadjikistan and the Gisarak reservoir in Uzbekistan. These reservoirs form the boundary between the upstream basin and the downstream basin. Downstream of these reservoirs the hydrological properties of the rivers don't correspond to the natural system, which is present upstream of these reservoirs. Upstream of the reservoirs, the influence of human-induced mitigation measures is very small and can be neglected. The upstream system can be approached as a natural system without human interference and this will be studied in the second phase of the project.

Nurek and Toktogul reservoirs have very large catchments with highest observed peak inflows up to 2200 and 1800 m³/s respectively. Andijan and Charvak reservoirs have smaller catchments and peak inflows of 700 to 800 m³/s. Figure 4-12 shows the location of the Nurek, Andijan, Toktogul and Charvak reservoirs.

More information on water management and hydrology and the impact of climate change in the downstream parts of the river basins can be found in a separate report.



4 Methodology

4.1 Data sources and preprocessing

The study takes a unique approach towards the well-known data-scarcity problems in mountain hydrology, by using a mixture of existing data at various spatial and temporal level. Moreover, data from the public domain is combined with data from Remote Sensing as illustrated in Figure 4-1. The modeling framework is used for (i) integration all this information to enable our understanding of the current situation and (ii) projections of the future using downscaled regional climate information.

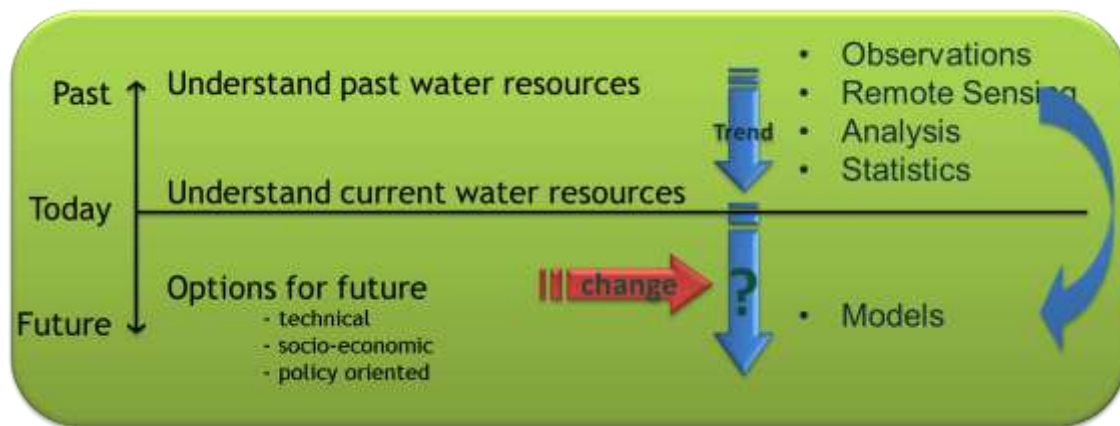


Figure 4-1: General project approach

The data used for the model originates from different sources. All data used is available in the online public domain. The topography for the upstream basins is derived from NGA and NASA's Shuttle Radar Topography Mission (SRTM) dataset. The Digital Elevation Model (DEM) was interpolated from a 15 arc seconds DEM to a 1x1 km cell size grid, to be used for the model (Figure 4-2). Using USGS HydroSheds the catchment boundaries are obtained.¹ HydroSHEDS is a mapping product based on SRTM elevation data, providing hydrographic information for regional and global-scale applications. Using HydroSheds, the boundaries of the modeled area are defined to coincide with the catchments boundaries (Figure 4-2). The locations of rivers in the HydroSheds dataset were used to correct the DEM hydrologically. The DEM surface is lowered a bit at the river's locations to correct for irregularities in the DEM and assure a realistic drainage network.

Data on glacier surface are mainly extracted from the Global Land Ice Measurements from Space (GLIMS) monitoring program.² Where GLIMS data was insufficient, ice cover data was obtained from the Digital Chart of the World dataset (DCW).³

Hydrological measurements for 2001-2010 used for calibration are obtained from the online Central Asian Water portal.⁴

¹ <http://hydrosheds.cr.usgs.gov/>

² www.glims.org

³ www.naturalearthdata.com

⁴ www.cawater-info.net



Data on land use and land cover are obtained from the Globcover regional land cover dataset.¹ This dataset is made with ENVISAT imagery which resulted in a global land cover map according to UN land cover classification. Locations and outlines of lakes positioned in the upstream basins were obtained from the WWF Global lakes and wetlands database.²

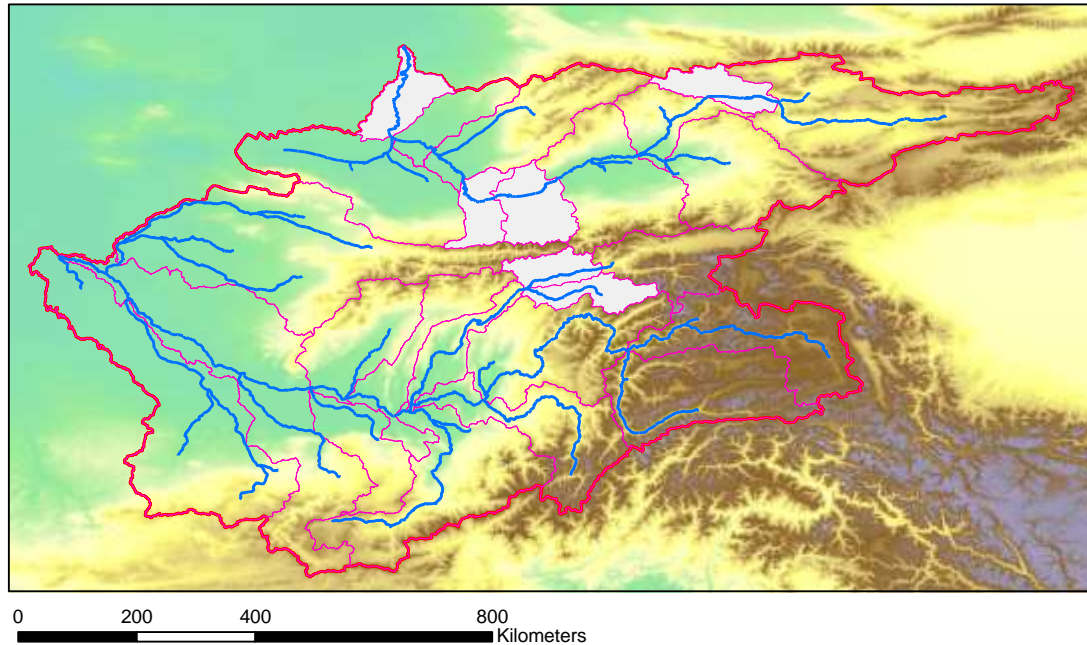


Figure 4-2: DEM with major rivers and HydroSheds catchment and subcatchment boundaries.

For 2001-2010 climate data was gathered from the national meteorological services of Kazakhstan, Uzbekistan, Turkmenistan, Kyrgyzstan and Tadjhikistan. Daily air temperature observations are available for multiple meteorological stations in the basins. Daily maps covering the whole basins were interpolated for air temperature by kriging; a spatial interpolation method, which gives the best linear unbiased predictors of unobserved values. Besides this method can also take into account external forcing, like altitude which is obtained from the DEM combined with a temperature lapse rate. The programming tool applied in this project is the R language and environment that is created for statistical computing and graphics. More precisely R package called “gstat” is applied here. R is available as Free Software under the terms of the Free Software Foundation’s GNU General Public License in source code form and thus the use of this software is free of charge. The spatial variation of temperature can be explained to large extent by surface altitude (Figure 3-2).

The accuracy of the kriging interpolation was checked for each day by calculating the correlation between observed and predicted temperatures.

¹ <http://ionia1.esrin.esa.int/>

² <https://secure.worldwildlife.org/science/data/item1877.html>



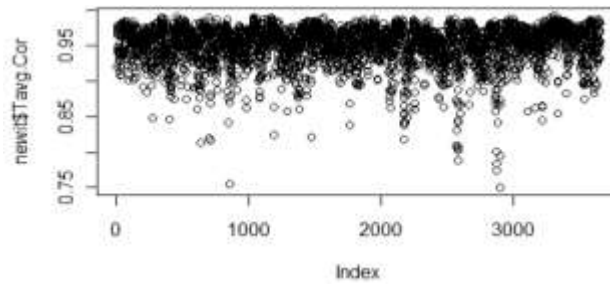


Figure 4-3: Correlation between observed and predicted temperature.

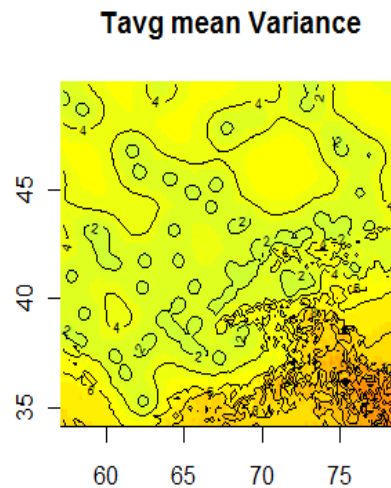


Figure 4-4: Spatial distribution of variance of observed and predicted temperature.

The variance of the predicted values was best near observation stations. The variance in the south-east corner of the kriging area was occasionally large indicating the inaccuracy of the data in the mountain area.

Precipitation data were interpolated bilinearly to $0.2^\circ \times 0.2^\circ$ resolution from the PERSIANN 0.25° daily satellite and neural network based precipitation data (<http://chrs.web.uci.edu/>) [Hsu and Sorooshian, 2009].

More information on the processing of climate data and the generation of climate change scenarios can be found in the FMI report.

4.2 Model concepts

4.2.1 Model structure

The Aral Mountain model is a raster based highly detailed full distributed cryospheric-hydrological model for the upstream part of the Amu Darya and Syr Darya basins. The model is based on commonly accepted standards and the approach has been published in numerous scientific papers. Figure 4 1 shows the areas for the two basins. The model is created in PCRaster environmental modelling software [Karssenberget al., 2001]. PCRaster is a spatio-temporal environmental modelling language developed at Utrecht University, the Netherlands. The model runs at 1×1 km spatial resolution with daily time steps and incorporates all major hydrological processes as well as cryospheric processes.



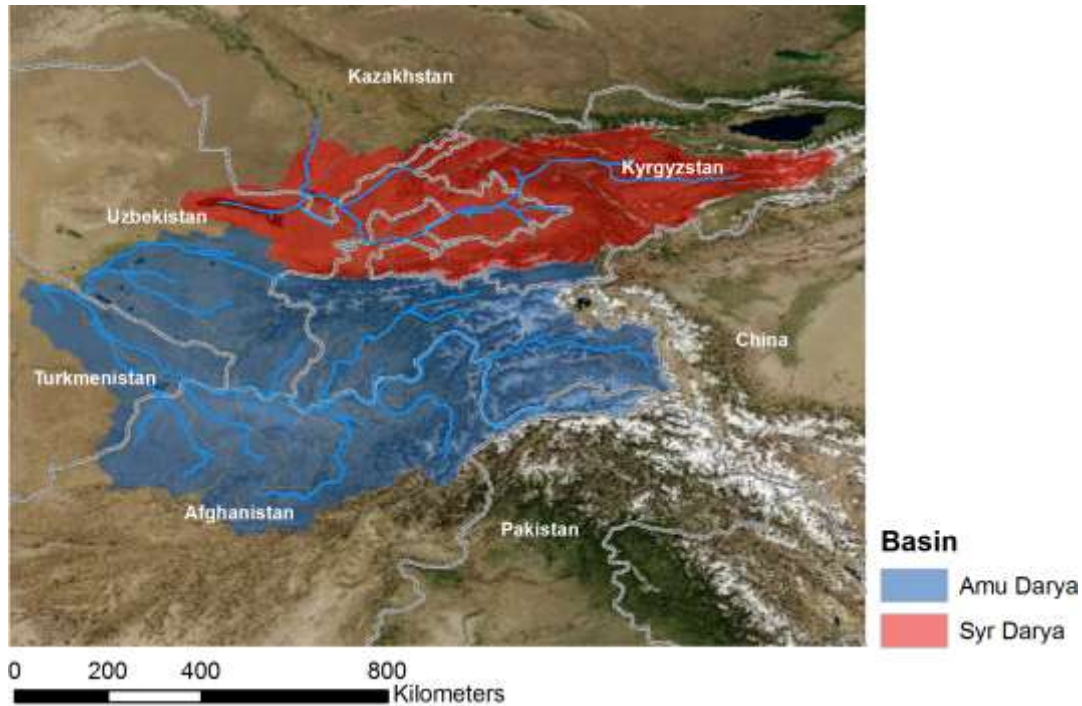


Figure 4-5: Boundaries of upstream Amu Darya and Syr Darya river basins.

The actual runoff which is calculated for each grid cell consists of four contributing factors. These are: runoff originating from rain, runoff originating from snow melt, runoff originating from glacial melt, and baseflow, as visualized in Figure 4-6. With the daily air temperature and daily precipitation per grid cell as input the model evaluates how much precipitation falls and it is disaggregated into either snow or rain based on the air temperature distribution. The model evaluates the amount of snow and glacier melt or accumulation and which part of snow and glacier melt is directly transformed to runoff and which part refreezes. A part of the rainfall is directly transformed to runoff and a part infiltrates and adds to baseflow. Another part is lost to evapotranspiration. The runoff from all contributing components is routed through the system using the DEM.

The model is calibrated for the period 2001-2010 using air temperature and precipitation data for this period as input and comparing output to observed discharges for the same period. In the next step, climatic data based on climate scenarios is then used as input for the calibrated model, providing estimated river discharges for 2010-2050.

The next paragraphs provide detailed information on the modelling steps for the different cryospheric and hydrological processes in the AralMountain model.



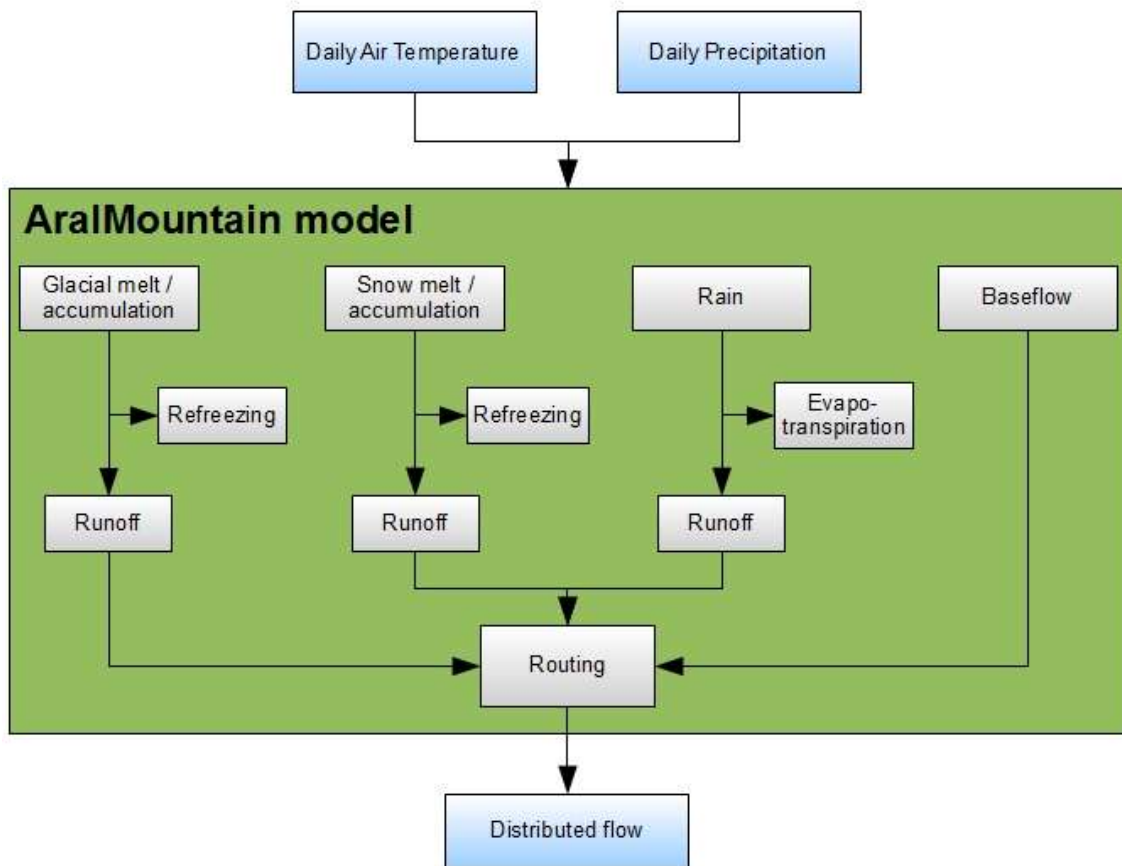


Figure 4-6: Schematic model structure AralMountain model.

4.2.2 Cryospheric processes

The initial glacier cover in the Tien Shan and Pamir mountains is obtained from the GLIMS dataset, replenished with DCW data. With this dataset the glacierized fraction of each grid cell is calculated. Since the model is set up for a 1 x 1 km resolution, the ice cover is described as a fraction varying from 0 (no glacial cover) to 1 (100% glacial cover). In this way, 1 x 1 km grid cells which are partly covered with ice can be simulated. A differentiation is made between clean ice glaciers and debris covered glaciers. This differentiation is made based on elevation and slope. Glaciers at lower altitude tend to have more debris cover because of the cumulative accumulation of debris from higher grounds and glacier parts with a small slope have more debris cover compared to steep-sloped parts of the glacier. In the model, some assumptions were made regarding the occurrence of glaciers and the differentiation between clean ice glaciers and debris covered glaciers. It is assumed that glaciers only occur at elevations above 3100 meters above sea level (Figure 3-4). Debris covered glaciers occur where elevation is between 3100 and 5500 meters and the slope is smaller than 13°. Using these assumptions, the fractions of clean ice and debris covered glaciers were calculated using a DEM with 90 meter spatial resolution to overcome inaccuracy resulting from using the 1 x 1 km DEM used for the modelling. The differentiation between clean ice glaciers and debris covered glaciers is then re-calculated to fractions of the 1 x 1 km grid cells used in the model (Figure 4-7). Summing the fractions of clean ice glacier and clean ice glacier will always result in a total fraction of one.



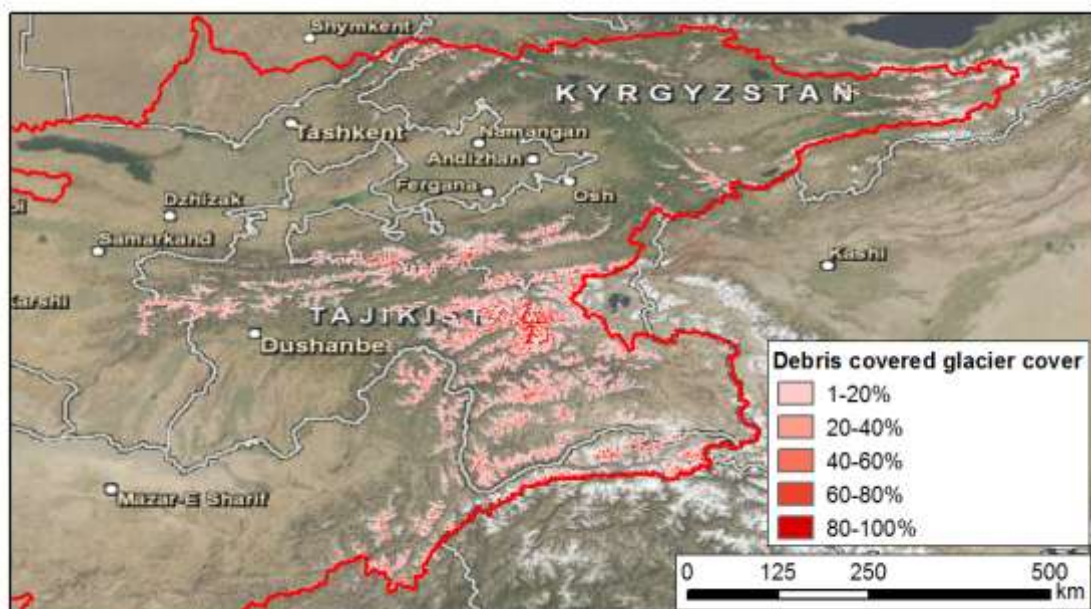
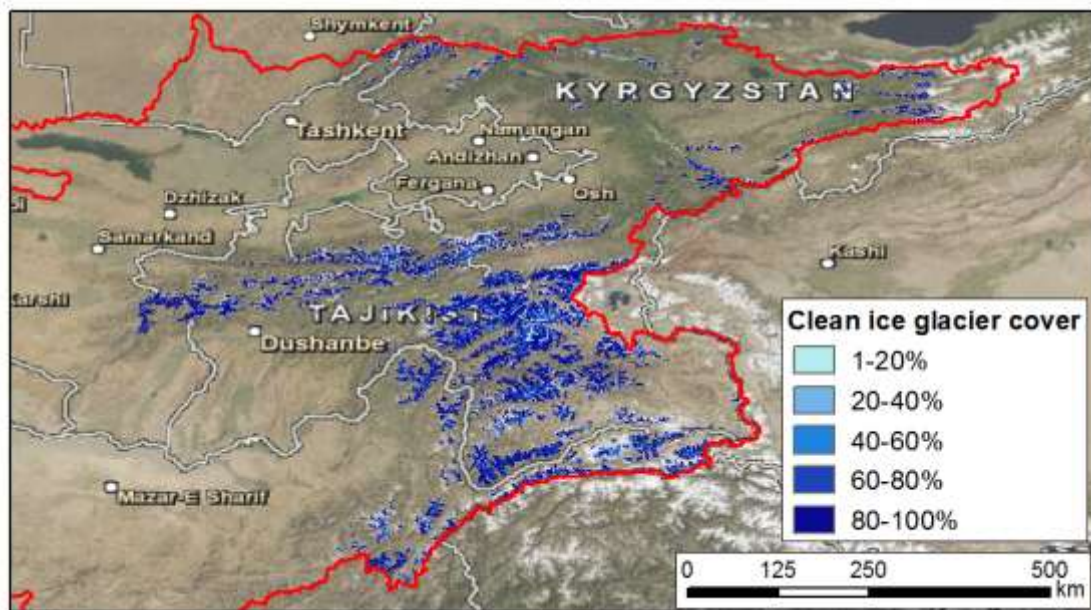


Figure 4-7: Grid cell area covered with clean-ice glaciers and debris-covered glaciers.

Initial conditions for snow cover were obtained directly from the model. A model run was done simulating several years to develop a balanced snow cover. The snow cover at the end of this model run was used as initial snow cover for further model runs.

In the model's calculations, the amounts of ice and snow are described as millimeters water equivalent.

The modelling of processes involving glaciers is described in a schematic way in Figure 4-8. Melt from clean ice glaciers is defined as the air temperature (if above 0 °C) multiplied by the degree day factor for clean ice, multiplied by the clean ice fraction of the glacier cover and the cell fraction with glacier cover.



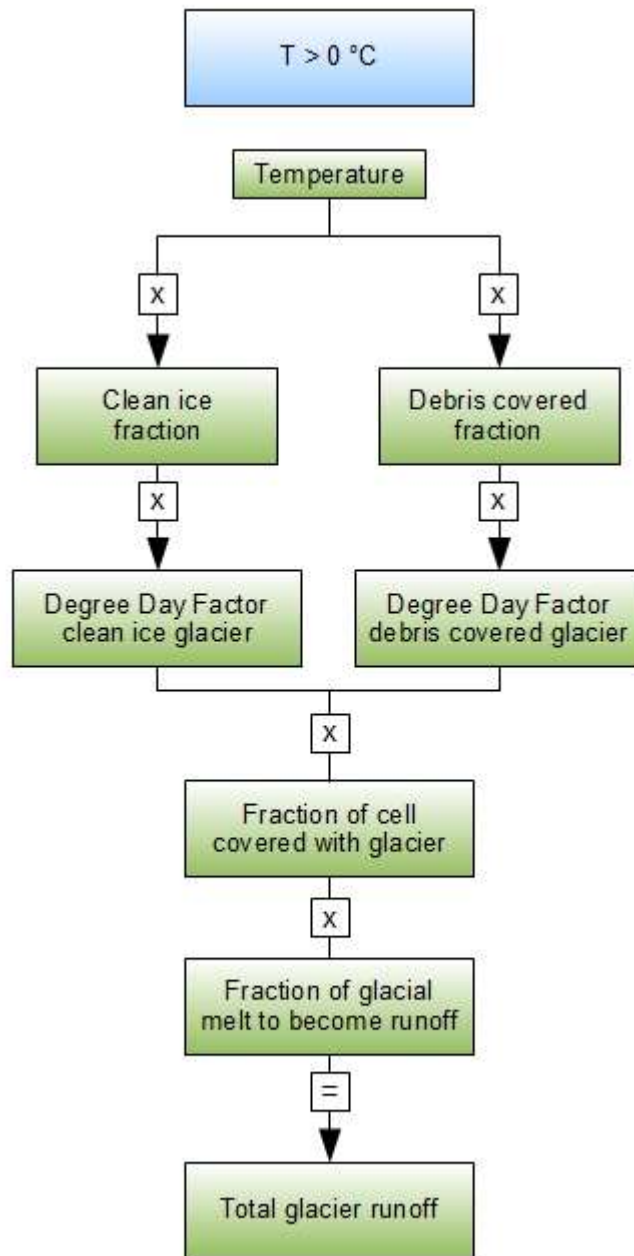


Figure 4-8: Schematic representation glacier processes in AralMountain model

For the melt from debris covered glaciers the calculation is similar, although a different degree day factor for debris covered glaciers is specified. Melt rates for debris covered glaciers are lower, since incoming radiation and other heat flows are blocked by the (thick) debris cover.

Degree Day Factors

The use of temperature index or degree day models is widespread in cryospheric models to estimate ice and snow melt. In these models an empirical relationship between melt and air temperature based on a frequently observed correlation between the two quantities is assumed [Hock, 2005]. Degree-day models are easier to set up compared to energy-balance models, and only require air temperature, which is mostly available and relatively easy to interpolate.



The total glacier melt is then calculated by summing the two components from clean ice glacier melt and debris covered glacier melt. A part of glacial melt also refreezes in the glacier when it percolates the ice. A correction for this process is made by adjusting the glacial melt using a glacial runoff factor.

For each cell the model determines if precipitation falls as snow or rain by comparing the actual air temperature to a critical temperature. When air temperature is below or equal to the critical temperature, precipitation will fall as snow. When air temperature is above the critical temperature, precipitation will fall as rain.

In the model a differentiation is made between the potential snow melt and the actual snow melt (Figure 4-9).

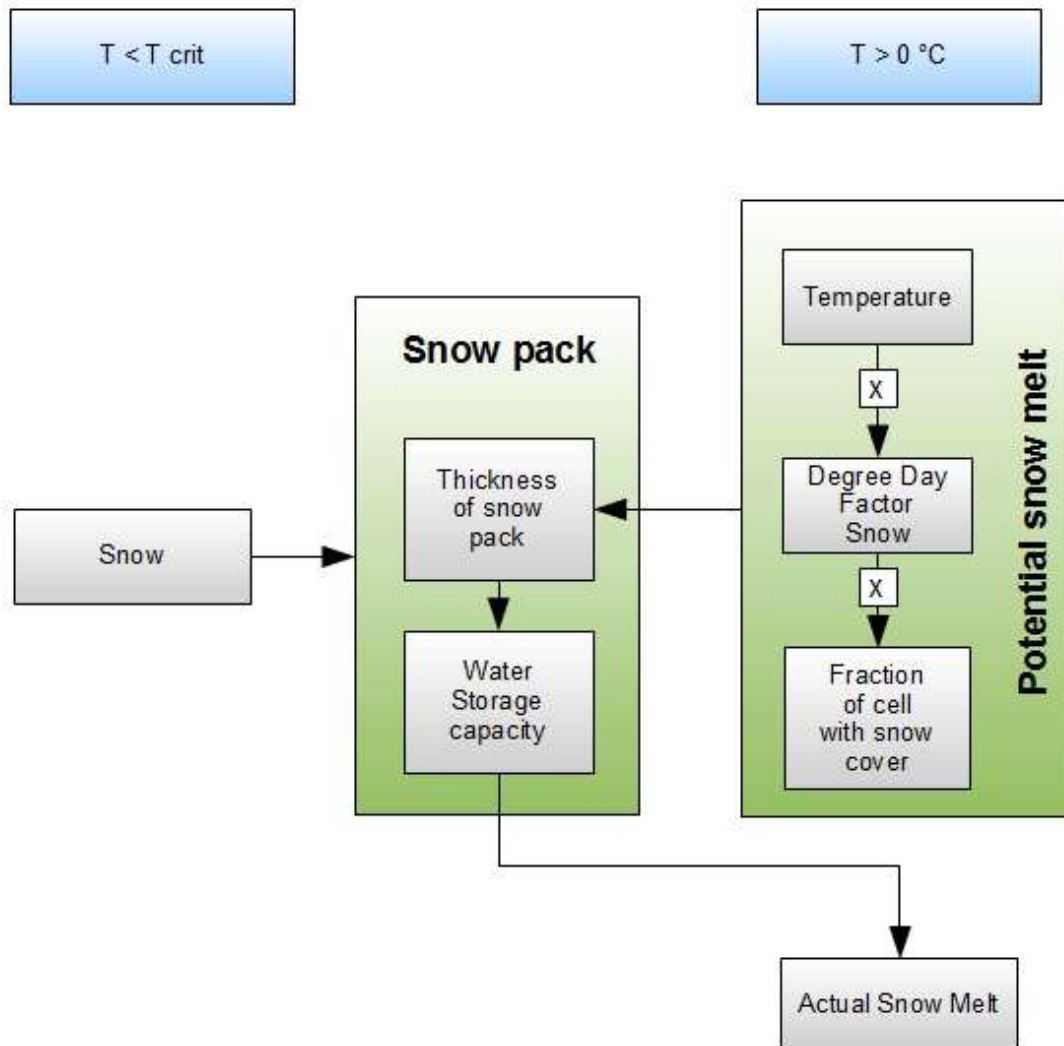


Figure 4-9: Schematic representation snow processes in AralMountain model

The potential snow melt is defined as the air temperature (if above 0 °C) multiplied by a degree day factor for snow multiplied by the cell fraction covered with snow. The actual snow melt however, is limited by the thickness of the snow pack. No more snow can be melted than the amount of snow which is available at the considered time step. The snow storage is then updated, to be used for the next time step. The updated snow storage is the 'old' snow storage with the fresh snow added and the actual snow melt subtracted.



The water resulting from snow melt will partially refreeze as it infiltrates the underlying snow pack. The maximum of water that can refreeze is defined by the water storage capacity of the snow pack which depends on the thickness of the snow pack present and the storage capacity of snow (e.g. the total millimeters of melt water that can refreeze per millimeter of snow). The actual amount of water that is stored in the snow pack is defined as the water stored in the snow pack during the previous time step summed by the actual snow melt. Snow melt will become actual snow melt when the amount of snow melt exceeds the water storage capacity of the snow pack.

4.2.3 Rain runoff

The modelling steps for rainfall in the AralMountain model are represented in Figure 4-10. As mentioned in paragraph 4.2.2, precipitation in the model will fall as rain when the air temperature is above a critical temperature.

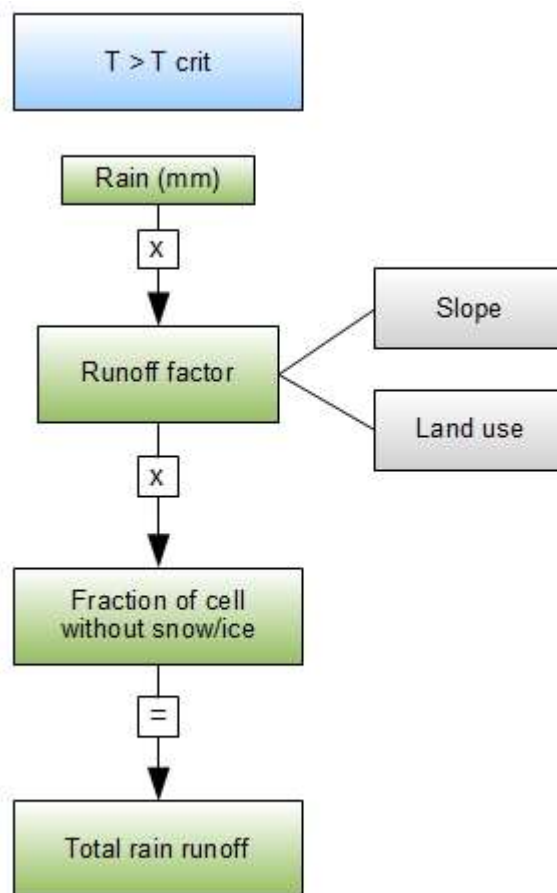


Figure 4-10: Schematic representation of rainfall-runoff modelling in AralMountain model

Differences in land use and land cover (see Figure 3-6) lead to differences in generated runoff because factors like infiltration and evapotranspiration differ per type of land use and land cover. These differences are taken into account by supplying each type of land use/land cover with a specific runoff factor. A runoff factor value 1 means all water comes to runoff. A runoff factor value 0 means all water is 'lost' due to evapotranspiration and infiltration and no water comes to runoff.



Table 2: Estimated runoff factors for different types of land use/land cover.

Type of Land use / land cover	Runoff factor
Post-flooding or irrigated croplands (or aquatic)	1.0
Rainfed croplands	0.8
Mosaic cropland (50-70%) / vegetation (grassland/shrubland/forest) (20-50%)	0.6
Mosaic cropland (50-70%) / grassland or shrubland (20-50%)	0.6
Mosaic vegetation (grassland/shrubland/forest) (50-70%) / cropland (20-50%)	0.6
Closed (>40%) broadleaved deciduous forest (>5m)	0.8
Closed (>40%) needleleaved evergreen forest (>5m)	0.8
Open (15-40%) needleleaved deciduous or evergreen forest (>5m)	0.8
Closed to open (>15%) mixed broadleaved and needleleaved forest (>5m)	0.8
Mosaic forest or shrubland (50-70%) / grassland (20-50%)	0.7
Mosaic grassland (50-70%) / forest or shrubland (20-50%)	0.7
Closed to open (>15%) broadleaved deciduous shrubland (<5m)	0.8
Closed to open (>15%) herbaceous vegetation (grassland, savannas or lichens/mosses)	0.6
Sparse (<15%) vegetation	0.3
Sparse (<15%) grassland	0.3
Sparse (<15%) shrubland	0.3
Closed to open (>15%) grassland or woody vegetation on regularly flooded or waterlogged soil - Fresh, brackish or saline water	0.3
Artificial surfaces and associated areas (Urban areas >50%)	0.2
Bare areas	0.1
Consolidated bare areas (hardpans, gravels, bare rock, stones, boulders)	0.1
Non-consolidated bare areas (sandy desert)	0.1
Salt hardpans	0.1
Water bodies	1.0
Permanent snow and ice	0.2

Besides land use and land cover, the actual runoff also depends on the hill slope. More runoff is generated on steep slopes because less water can infiltrate the soil and less water can evaporate as the water flows with a higher velocity on the surface.

The slope-dependent runoff factor is calculated as a runoff slope factor multiplied by the sinus of the slope. The land use specific runoff factor and the slope specific runoff factor are averaged resulting in a runoff factor per grid cell (Figure 4-11).



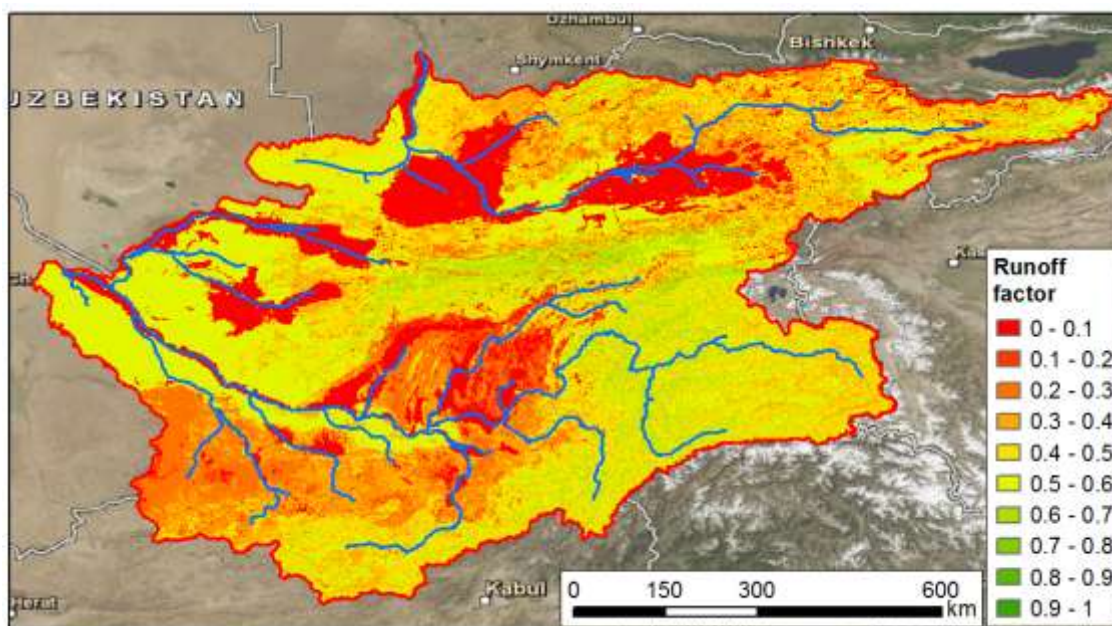


Figure 4-11: Runoff factor per grid cell

The total amount of rain that comes to runoff per grid cell is calculated as the actual rain in millimeters multiplied by the runoff factor and the fraction of the grid cell which is not covered by glacier or snow.

4.2.4 Baseflow

A module calculating baseflow is incorporated in the model. During periods with low runoff the streams are fed by processes such as sustained ground water flow and/or slow throughflow through the soil from earlier precipitation events. This is referred to as baseflow. The baseflow in the model consists of an initial baseflow summed with a certain recharge. The recharge is calculated for the rain fraction, glacial melt fraction, and the snow melt fraction with a recharge factor describing how much rain, glacial melt and snow melt is contributing to the baseflow.

The amount of baseflow is then calculated as an initial baseflow multiplied by the exponential function to the power of the negative of a recession coefficient. This function simulates the delayed effect of the baseflow. The lag time is determined by the recession coefficient parameter. The amount of recharge is multiplied by one minus the exponential function to the power of the negative of a recession coefficient.

4.2.5 Routing

In the model, the generated runoff is routed through the basin according to a flow direction map based on the DEM. For each cell the local drain direction is defined. The runoff generated per grid cell accumulates with runoff generated in downstream grid cells. Using a linear regression with a regression constant, the time needed for water to flow through the reservoir towards the outflow point is simulated.



4.3 Calibration

Model parameters need to be calibrated in order to simulate past river runoff as accurate as possible and after calibration it can be used for assessing future conditions. The model is calibrated for a ten year period (2001-2010). During this period, three inflow observations per month were reported for four upstream reservoirs: Nurek reservoir for the Amu Darya catchment, and Toktogul, Andijan and Charvak reservoirs for the Syr Darya catchment (Figure 4-12).

With these observed inflow data, the AralMountain model is calibrated using the Parameter Estimation software package (PEST). With use of this software, the optimum parameter values were calculated to reproduce the observations for 2001-2010. PEST uses a Gauss-Marquardt-Levenberg algorithm for parameter estimation for nonlinear models. The algorithm runs in an iterative process changing parameter values while trying to constantly reduce the error of simulated values with respect to observed values.

For the calibration phase, the volume and area of glaciers is assumed to be static. No glacier fluctuations are taken into account. Note that glacier fluctuations are taken into account in the future projections with climate change scenarios. Initially, all four reservoirs were used in the calibration process. However, the model performed unsatisfactory for the Charvak reservoir. Simulated inflow was much lower than observed inflow. Why the model doesn't perform well for this area remains unclear. Possible explanations could be underestimation of precipitation data or wrong observed discharge data. There might also be a high inflow from deep groundwater. The Charvak reservoir was not used for further model calibration.

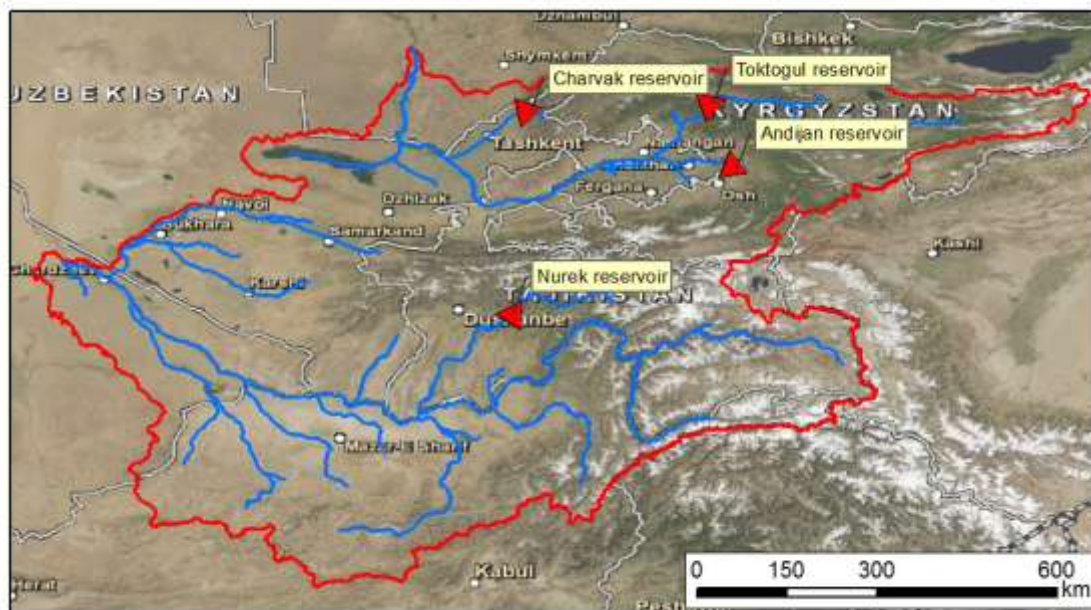


Figure 4-12: Reservoirs used to calibrate the model

Twelve parameters are used in the model. Most of them are mentioned before in previous paragraphs. An important parameter which is not mentioned before is the correction factor for precipitation. The precipitation input data from PERSIANN and TRMM has a high uncertainty. During the calibration processes a correction factor for precipitation is evaluated to improve model performance. Calibration results are presented in paragraph 5.1.



5 Current Hydrological Regime

5.1 Calibration results

The model is calibrated using the Parameter Estimation Software (PEST) package. In total, twelve parameters are used in the model, of which eleven were determined with the PEST software. Calibrating the model produced the optimum parameter configuration to simulate the observed values for the calibration period 2001-2010 for three reservoirs (Figure 4-12). In the calibrated parameters are listed. For every parameter, a range of possible values was provided as boundary conditions in PEST. The estimated parameter values for optimum performance of the model, as obtained by PEST, are listed in the last column. This parameter set is used in the modelled projections for 2011-2050.

Table 3: Calibrated parameters in the AralMountain model

Calibrated parameters			
Abbreviation used in model	Parameter description	Range	Value
TCrit	Critical temperature for precipitation to fall as snow (°C)	fixed	2 °C
DDFG	Degree Day Factor for clean ice glaciers (mm/°C/day)	5.0-10.0	7.95 mm/°C/day
DDFDG	Degree Day Factor for debris covered glaciers (mm/°C/day)	4.0-8.0	3.98 mm/°C/day
DDFS	Degree Day Factor for snow (mm/°C/day)	4.0-7.0	6.36 mm/°C/day
SnowSC	Storage capacity of the snow pack (mm/mm)	0.05-0.2	0.19 mm/mm
GlacF	Fraction of glacial melt to turn into runoff (-)	0.5-0.9	0.9
kx	Recession coefficient used for routing (-)	0.90-0.99	0.967
BaseR	Initial daily baseflow (mm)	0.3-0.4	0.3
RF	Recharge factor (-)	0.01-0.99	0.0988
rc	Recession constant for baseflow (-)	0.001-0.2	0.001
PrecF	Correction factor for precipitation (-)	1.0-3.0	1.23
RunoffSlope	Factor used to estimate slope dependency of runoff factor (-)	0.3-0.9	0.9

For the input data, the precipitation data is provided by the PERSIANN dataset. However, the precipitation values for 2006 and 2007 seemed to be significantly overestimated, and the model simulated discharges much higher than observed discharges. For 2006 and 2007, precipitation input data was replaced with TRMM data, leading to better simulation results. Applying the correction factor for precipitation to the input data yields updated input maps for precipitation (Figure 5-1). Applying the critical temperature to the precipitation input data yields input maps for snowfall and rainfall (Figure 5-2 and Figure 5-3). These maps show averaged values for the calibration period (2001-2010).



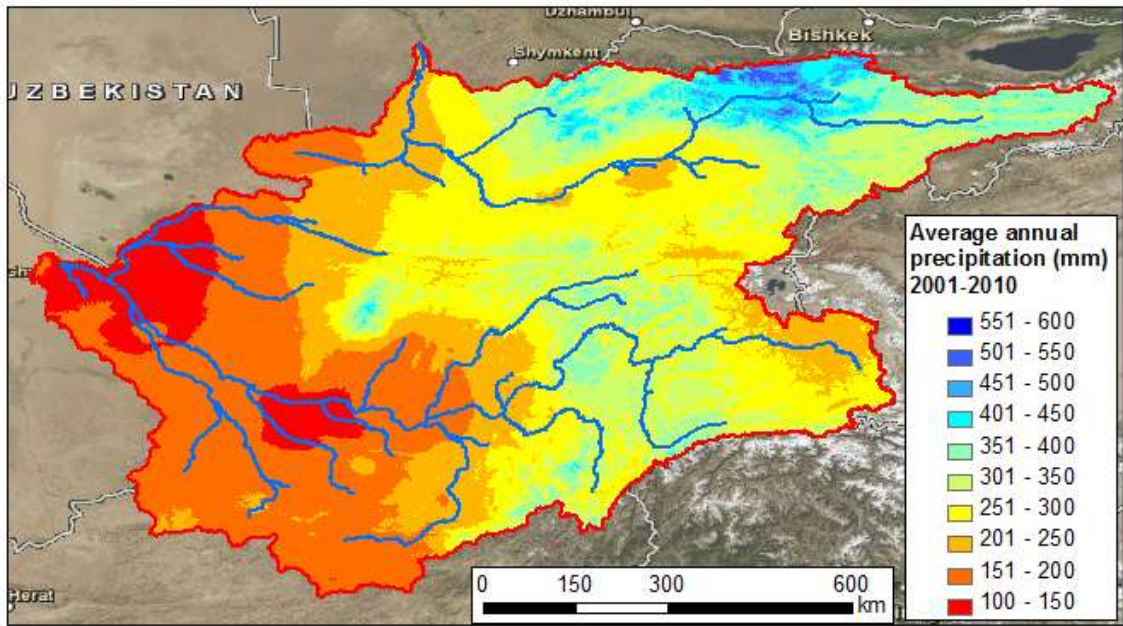


Figure 5-1: Average annual precipitation 2001-2010

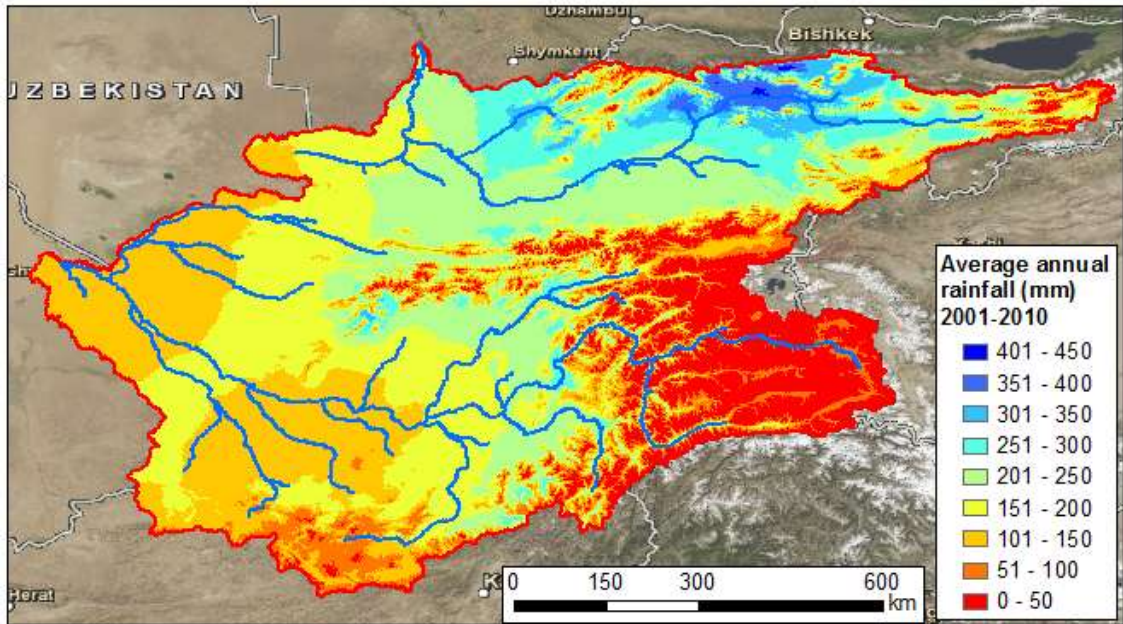


Figure 5-2: Average annual rainfall 2001-2010



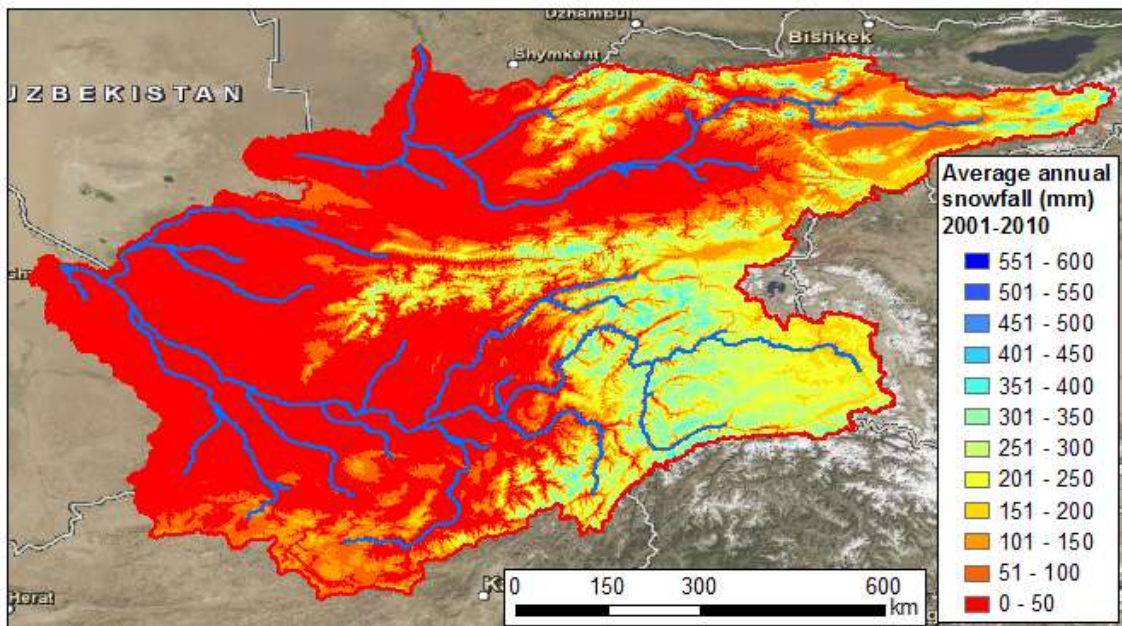


Figure 5-3: Average annual snowfall 2001-2010

The comparison of the simulated values to the observed values during the calibration period for three reservoirs is shown in Figure 5-4 to Figure 5-6.

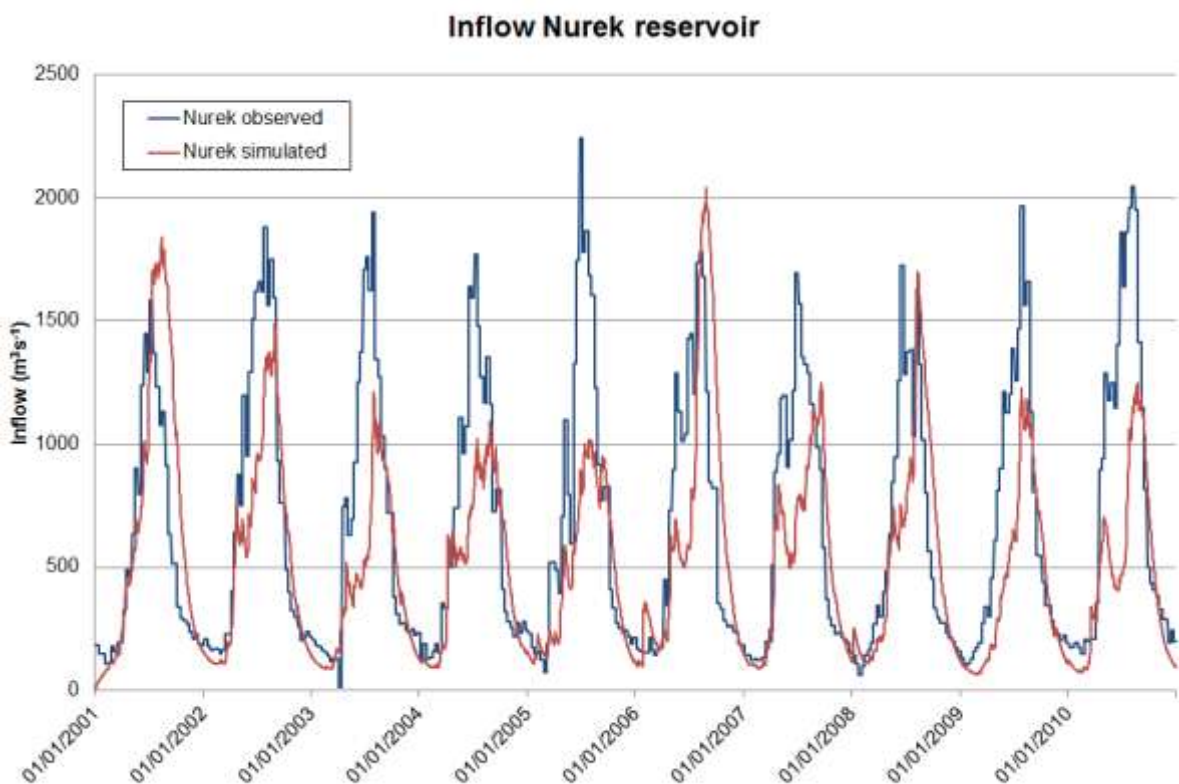


Figure 5-4: Observed and simulated monthly inflow Nurek reservoir 2001-2010



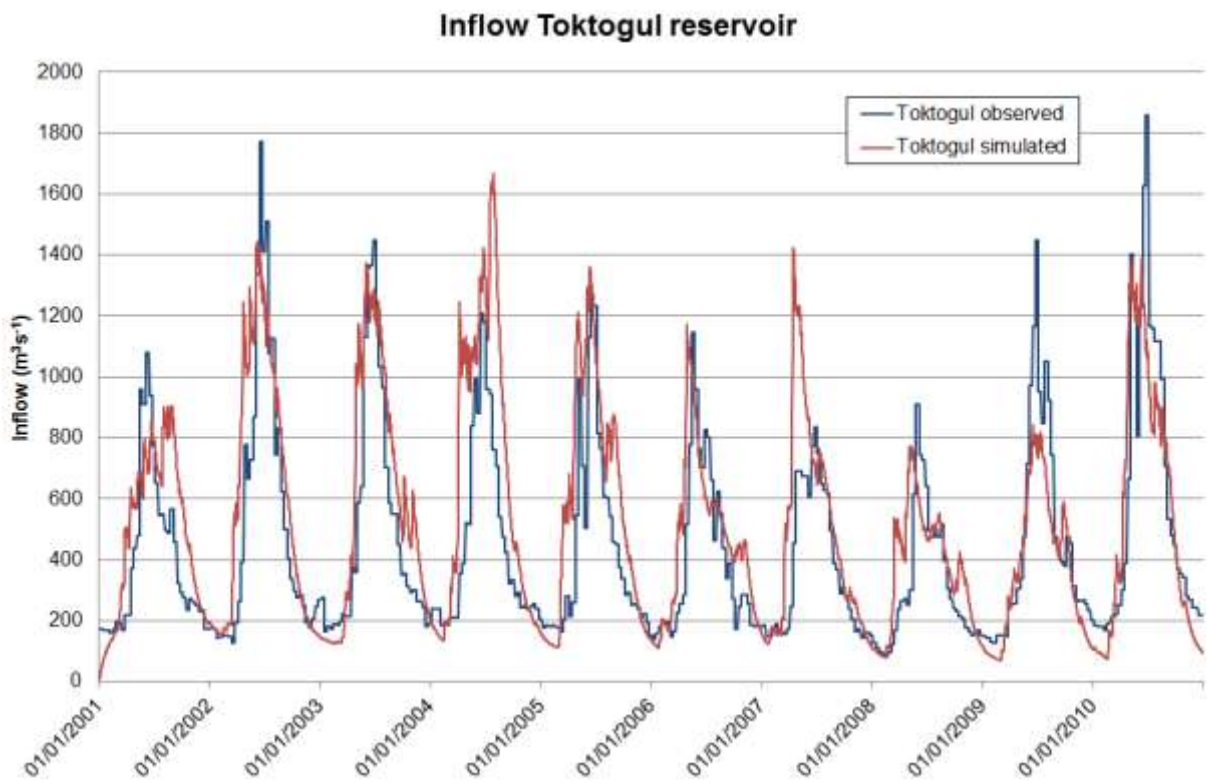


Figure 5-5: Observed and simulated monthly inflow Toktogul reservoir 2001-2010

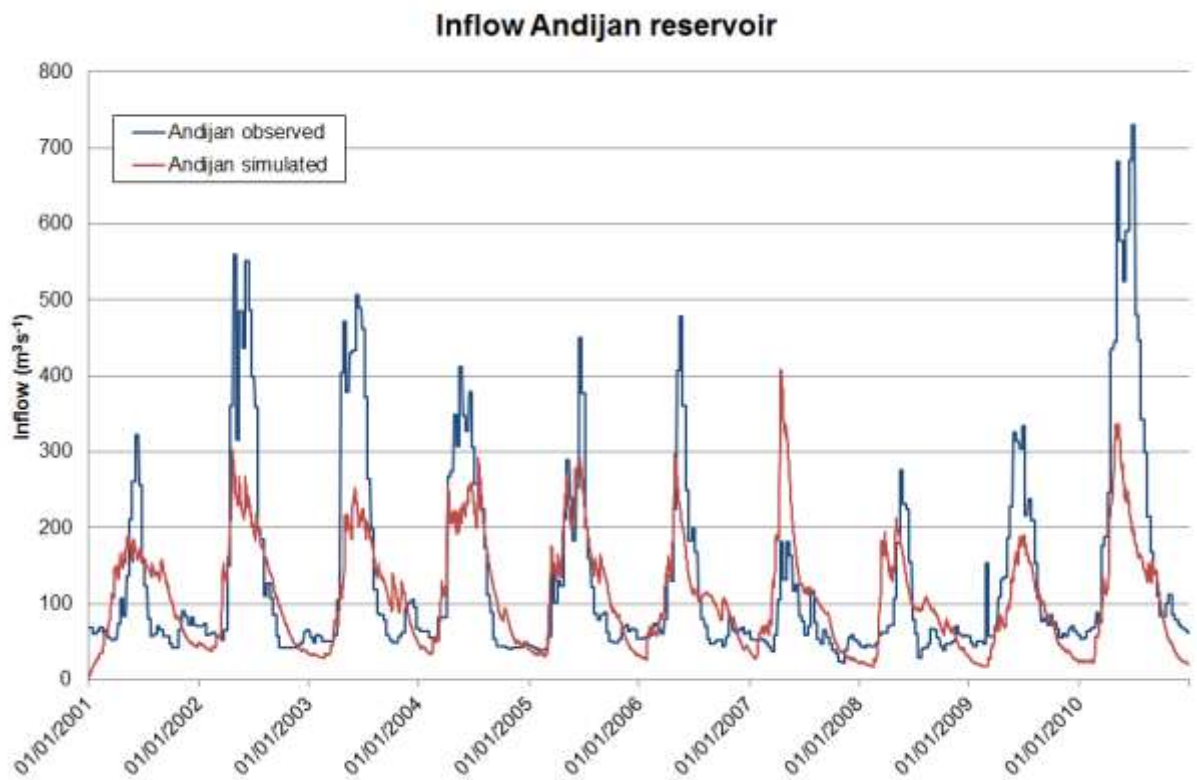


Figure 5-6: Observed and simulated monthly inflow Andijan reservoir 2001-2010



The quality of the model performance can be expressed with different criterions for the correlation between the observed values and the simulated values (Table 4).

Table 4: Correlation parameters observed and simulated inflow 2001-2010

	Pearson's correlation coefficient	Bias	Nash-Sutcliffe model efficiency coefficient
Nurek	0.73	-20.6 %	0.46
Toktogul	0.82	16.8 %	0.56
Andijan	0.74	-17.2 %	0.48

For Pearson's product-moment correlation coefficient, a perfect correlation, where simulated values equal to observed values, would yield a coefficient's value equal to +1 or -1. When no correlation exists, the coefficient's value is equal to 0.

The simulation is unbiased when the bias is equal to 0. A positive value for bias indicates overestimation in the simulation, whereas a negative value for bias indicates underestimation in the simulation. The value for bias is given as percentages.

The Nash-Sutcliffe model efficiency coefficient is used to assess the predictive power of hydrological models. The coefficient's value can range from $-\infty$ to +1. A value of 1 indicates a perfect correlation, where simulated values are equal to observed values. Coefficient value 0 indicates the simulated values are as accurate as the mean of the observed data. For a coefficient value smaller than 0, the mean of the observed data is a better predictor than the model. Another way to provide insight in model performance is to compare observed and simulated average annual inflow (Table 5).

Table 5: Average annual inflow (observed and simulated) 2001-2010

	Average annual inflow (observed Mm ³)	Average annual inflow (simulated Mm ³)
Nurek	8726	6932
Toktogul	5857	6840
Andijan	1751	1450

There are a number of uncertainties in the model, causing impediments in predicting the actual runoff. First, there are uncertainties in the temperature and precipitation input data. Temperature data is based on point measurements, interpolated to spatially cover the entire area. This interpolation comes with uncertainties. Besides, precipitation data is based on PERSIANN and TRMM remotely sensed data, which also have uncertainties. The processes described in the model are simplified with respect to what happens in the real world. Assumptions are made in different stages of the modelling process adding to uncertainty.

Overall we conclude that calibration results are very satisfactory considering the complexity and heterogeneity of mountain hydrology, the large areas that have been modeled and the fact that we have used primarily public domain datasets. Moreover, it has been proven that relative



model accuracy (= difference between current situation and scenario) is always much higher than relative model accuracy (difference between model output and observations) [Droogers *et al.*, 2008]. This is exactly why this modeling activity is undertaken: compare current climate with future climates.

5.2 The contribution of glacial and snow melt to river runoff

With the calibrated model the distribution of runoff generation can be simulated and specified for glacier melt, snow melt, rainfall and baseflow. Figure 5-7 shows the simulated averaged total runoff generation per year per grid cell. The absolute contributions of glacier melt, snow melt rain and baseflow to runoff are shown in Figure 5-8 to Figure 5-11. The values are averaged for the calibration period (2001-2010).

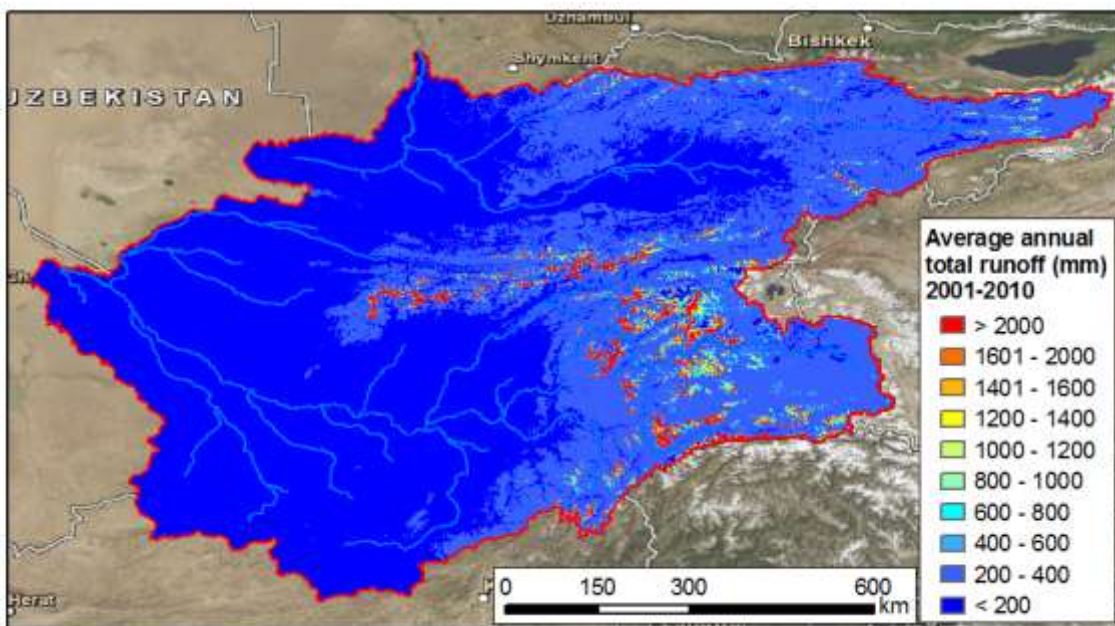


Figure 5-7: Average total annual runoff per grid cell 2001-2010



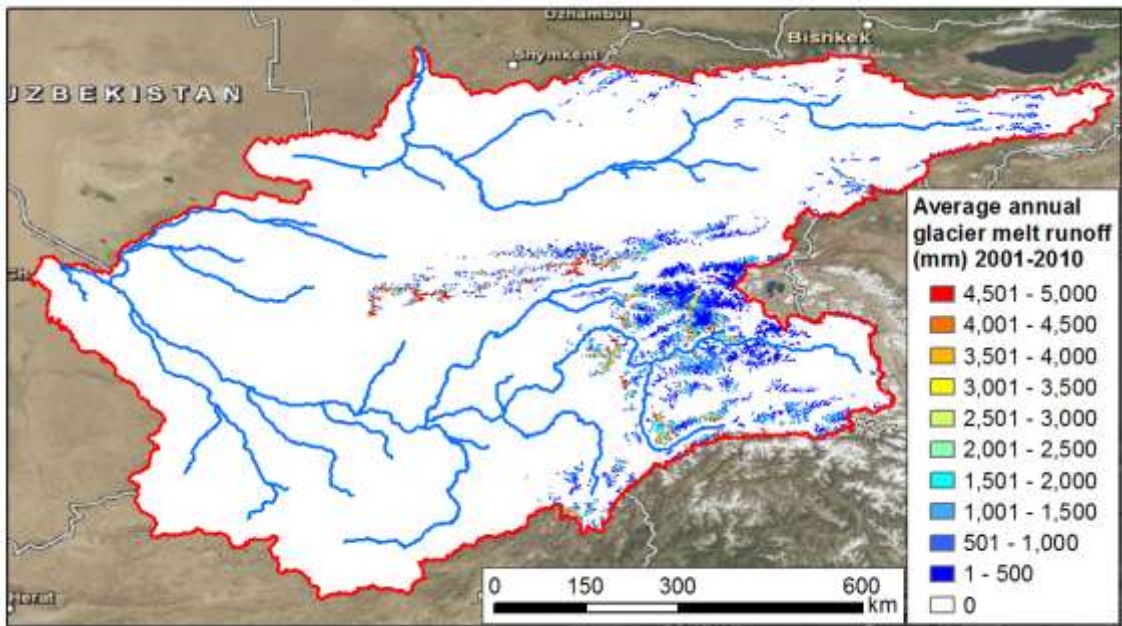


Figure 5-8: Average annual glacier melt runoff per grid cell 2001-2010

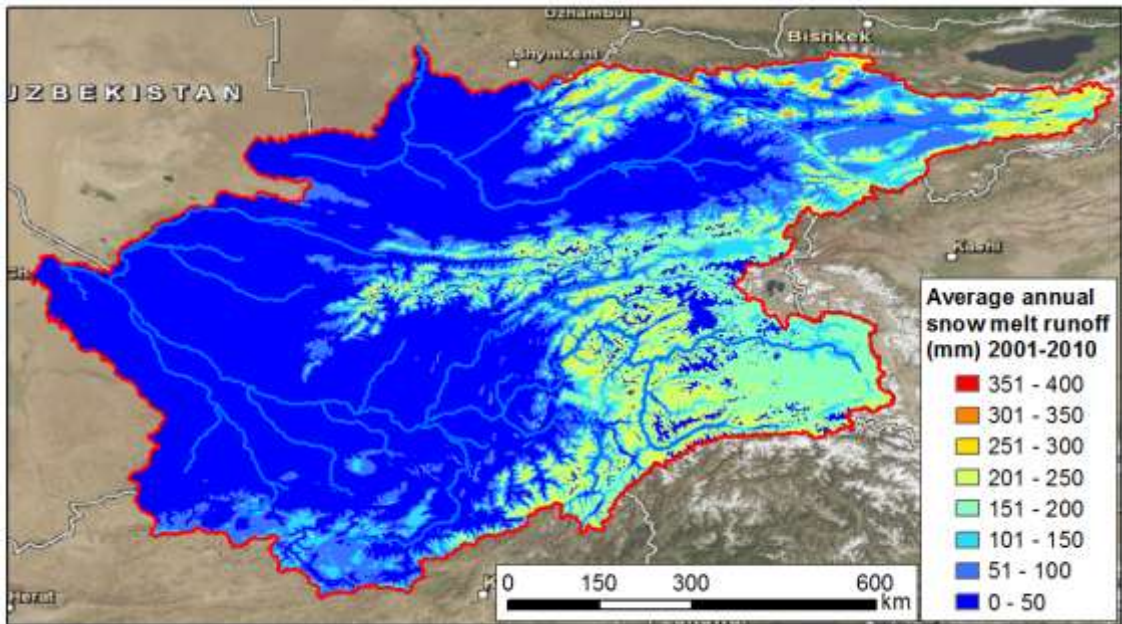


Figure 5-9: Average annual snow melt runoff per grid cell 2001-2010

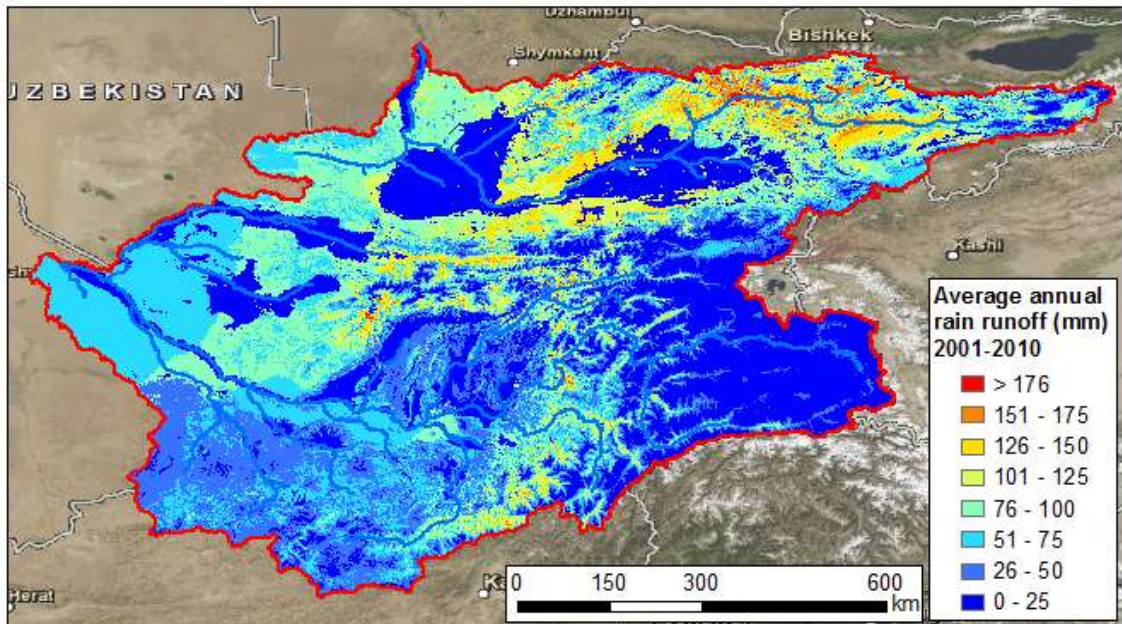


Figure 5-10: Average annual rain runoff per grid cell 2001-2010

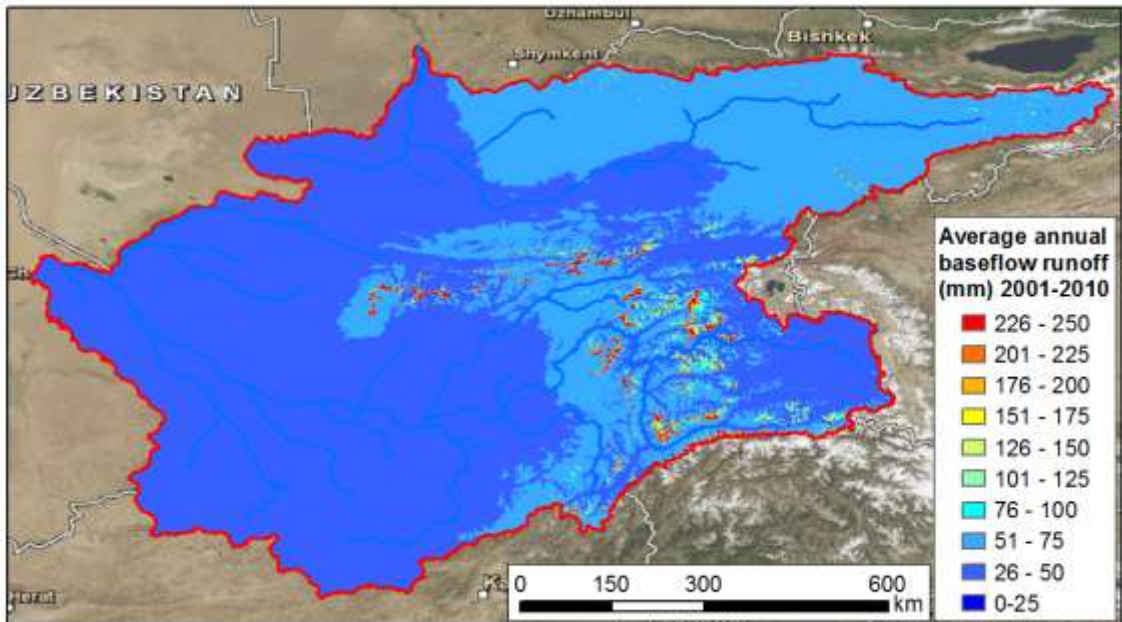


Figure 5-11: Average annual baseflow runoff per grid cell 2001-2010

For each grid cell, the averaged routed flow during the calibration period can be calculated and the contribution of glacier melt, snow melt, and rain to the total runoff can be specified. Figure 5-12 to Figure 5-14 show the relative contributions of these contributors to the average discharge for major streams in the basins for 2001-2010.



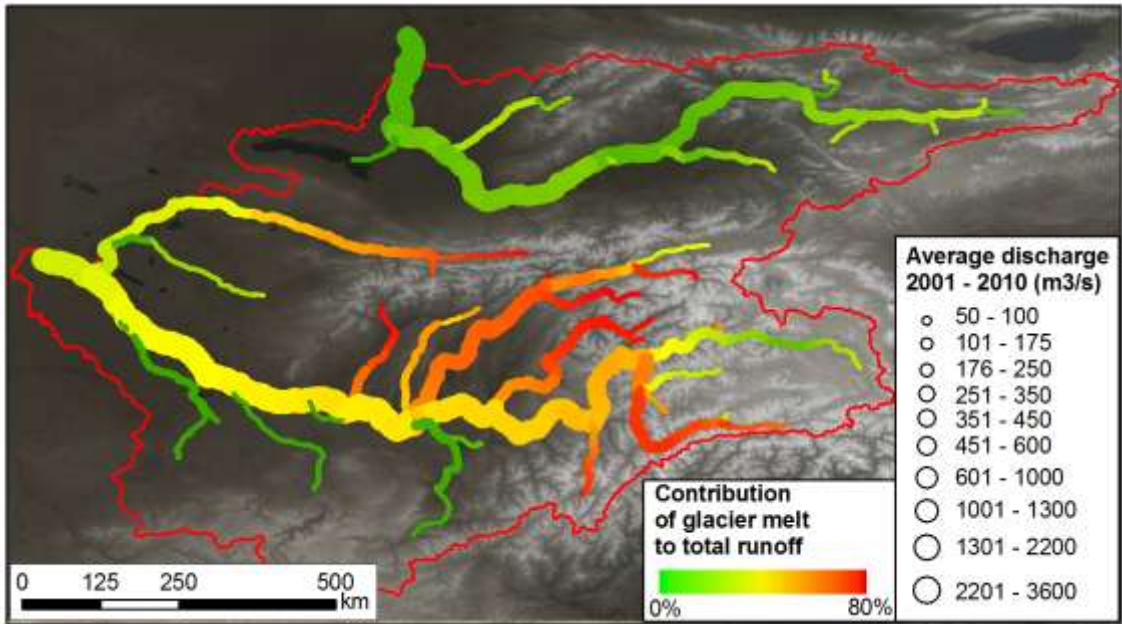


Figure 5-12: Average discharge and relative contribution of glacier melt for major streams 2001-2010

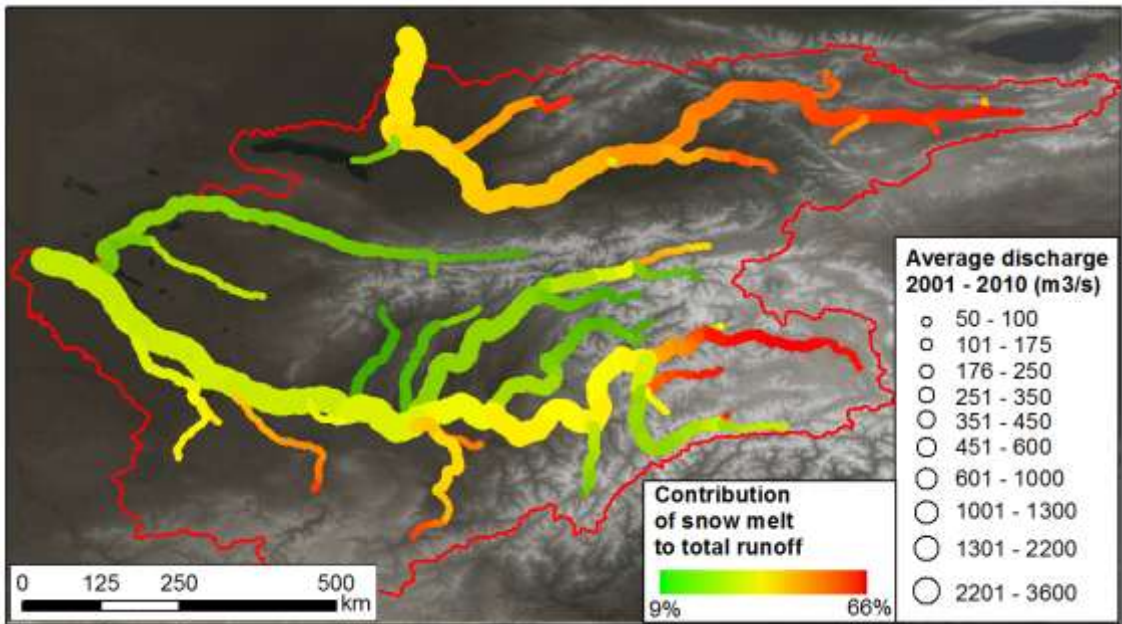


Figure 5-13: Average discharge and relative contribution of snow melt for major streams 2001-2010



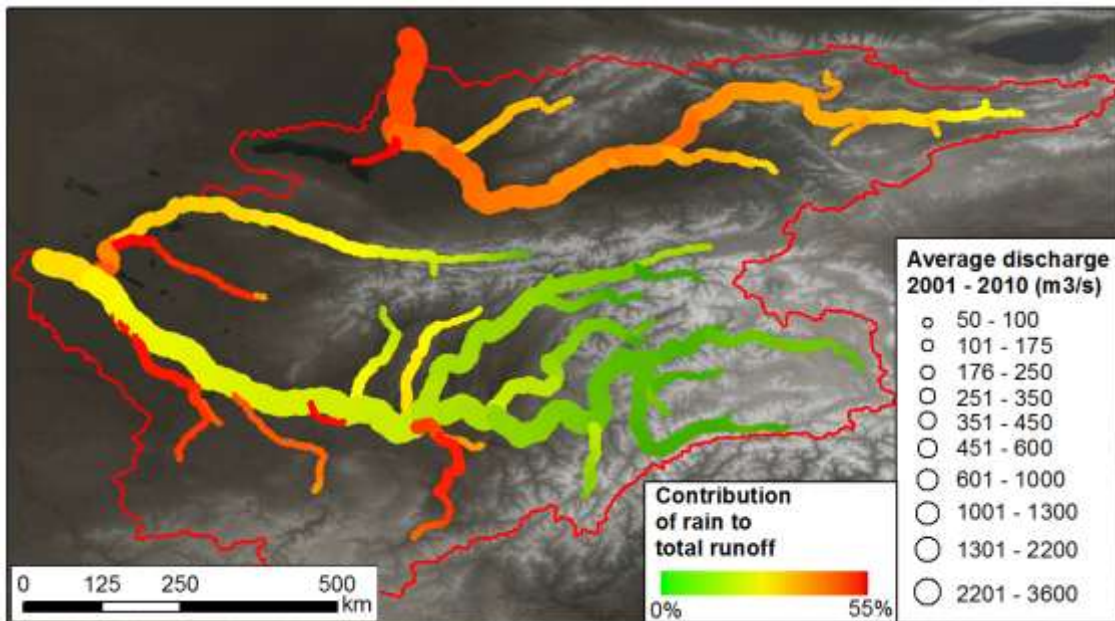


Figure 5-14: Average discharge and relative contribution of rain runoff for major streams 2001-2010

The contribution glacial and snow melt to river runoff differs regionally. In rivers in glaciated areas, the contribution of glacial melt is highest. The contribution of glacial melt is lower downstream, where more snow melt and rain runoff contributes to river discharge. The glacier melt is more important for the Amu Darya than for the Syr Darya as can be clearly seen in Figure 5-12. For the total Amu Darya river basin, the contribution of glaciers is much higher compared to the Syr Darya river basin. The contribution of the different contributors can be simulated per time step for each cell in the model. Results of this simulation are displayed for the reservoirs used in the calibration (Figure 5-15 to Figure 5-17).



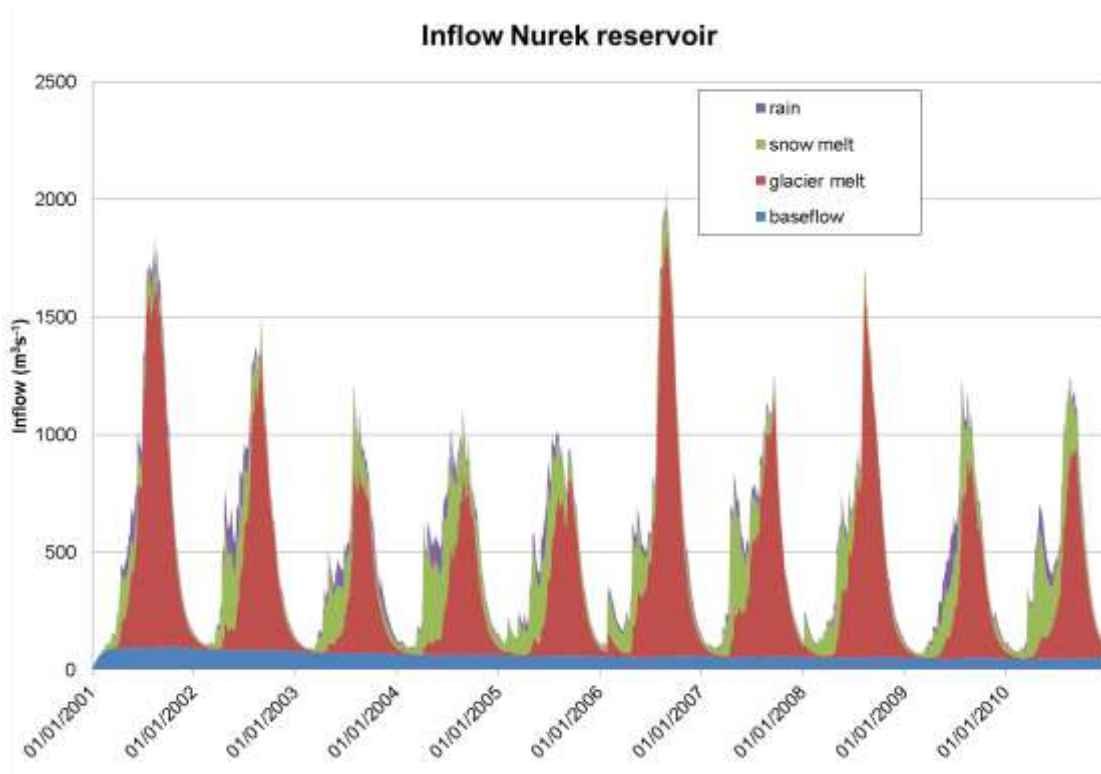


Figure 5-15: Simulated contribution of rain, snow melt, glacier melt and baseflow to inflow Nurek reservoir 2001-2010

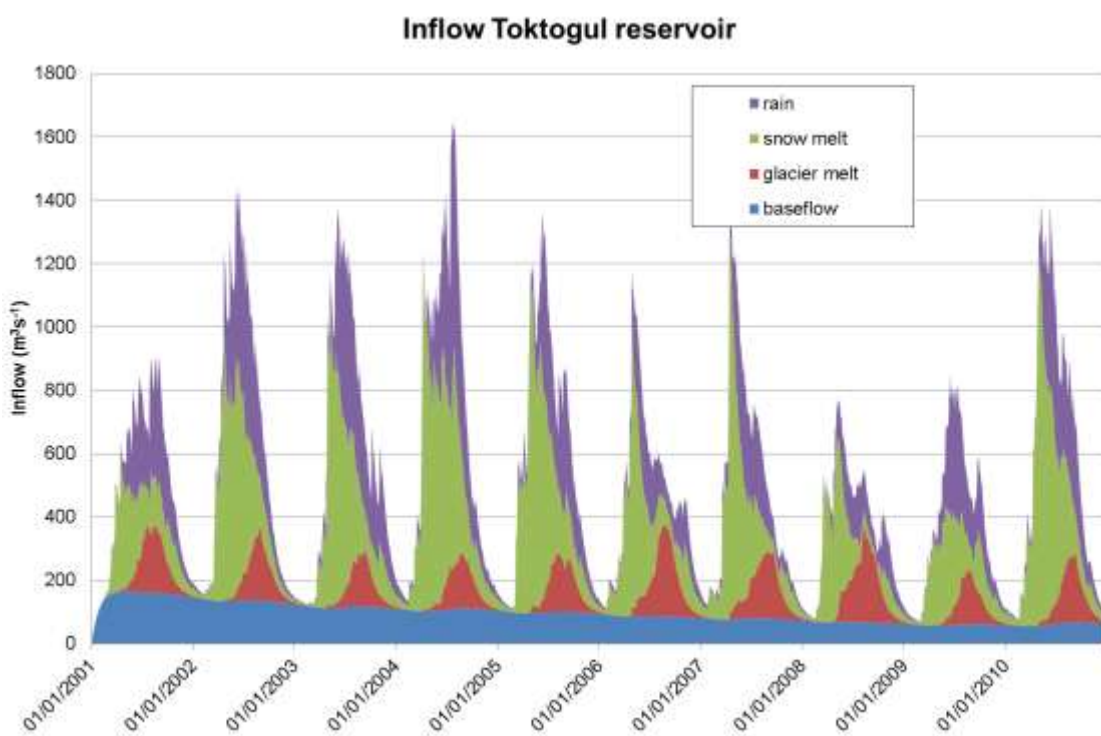


Figure 5-16: Simulated contribution of rain, snow melt, glacier melt and baseflow to inflow Toktogul reservoir 2001-2010



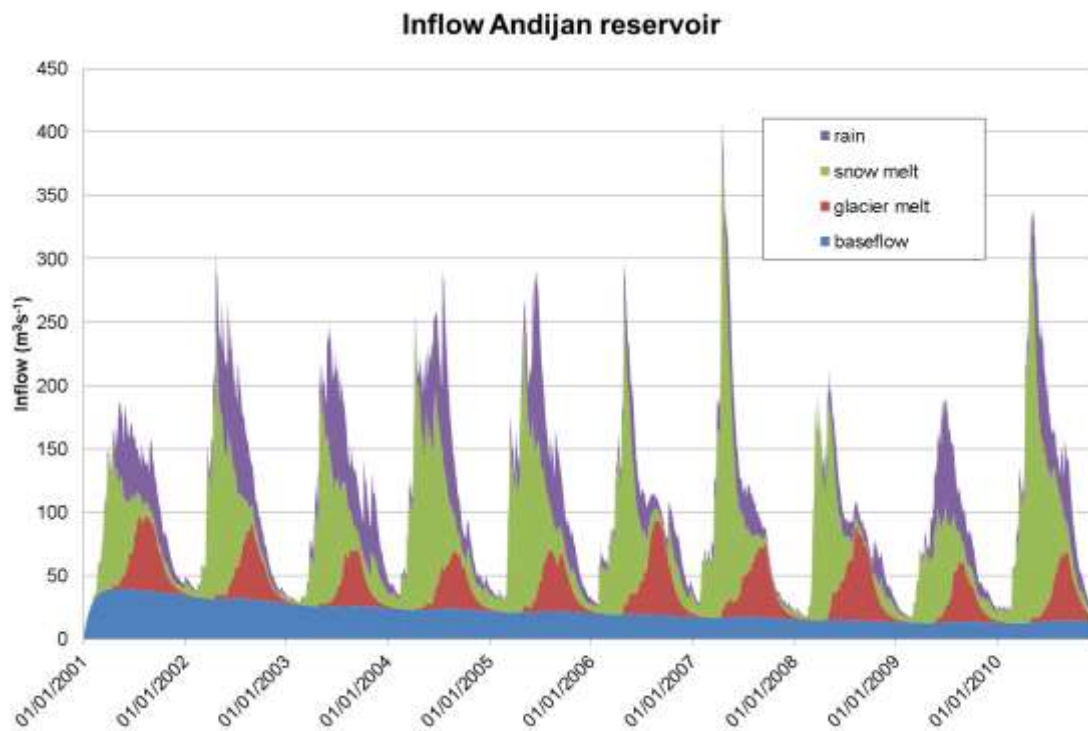


Figure 5-17: Simulated contribution of rain, snow melt, glacier melt and baseflow to inflow Andijan reservoir 2001-2010

For these reservoirs, glacier melt contribution is highest for Nurek reservoir in the Amu Darya basin. Many glaciers are located upstream of this reservoir, contributing to the inflow in the reservoir. For Toktogul reservoir and Andijan reservoir, the contribution of glacial melt is much lower. Snow melt and rain runoff are more important contributors for the inflow into these reservoirs (Table 6). When we consider the stream flow contribution at the outlet of the entire upstream model (Figure 3-1) the difference between Amu Darya and Syr Darya is striking. For Amu Darya 38% of annual stream flow is glacial melt, whereas snow contributed 26.9%. For the Syr Darya the glacial contribution is only 10.7% of the total river flow, whereas snow contribution to melt is estimated at 35.2%. When we consider the entire river basins of the Amu and Syr Darya then the relative melt water contribution will be even lower.

Table 6: Simulated stream flow composition at the major reservoirs.

	Average inflow (m ³ /s)	Contribution of glacier melt	Contribution of snow melt	Contribution of rain	Contribution of baseflow
Nurek	527	59.3 %	22.4 %	6.5 %	11.8%
Toktogul	520	11.7 %	42.2 %	27.6 %	18.5 %
Andijan	110	14.8 %	43.4 %	22.3 %	19.6 %
Charvak	109	22.0 %	40.7 %	21.1 %	16.2 %



Table 7: Simulated stream flow composition at the outlet of the upstream hydrological model

	Average outflow (m ³ /s)	Contribution of glacier melt	Contribution of snow melt	Contribution of rain	Contribution of baseflow
Amu Darya	3549	38.0 %	26.9 %	16.5 %	18.6 %
Syr Darya	1495	10.7 %	35.2 %	31.1 %	23.1 %



6 Future Hydrological Regime

6.1 Climate change scenarios

Five different Global Circulation Models (GCM's) are used to estimate the future changes in climate for the region between 2010 and 2050 (Table 8). From the various existing emission scenarios this study uses the A1B GHG emission scenario. This scenario is chosen because it is widely used and recommended by the IPCC. The A1B scenario is considered as the most likely scenario, because it assumes a world of rapid economic growth, a global population that peaks in mid-century and rapid introduction of new and more efficient technologies. The A1B scenario can be seen as an intermediate between the B1 (with the smallest GHG emissions) and A2 (with the largest GHG emissions) scenario. Moreover, A1B is becoming a de-facto standard in assessment studies.

Detailed information on the used climate models and preprocessing is available in the separate report by the Finnish Meteorological Institute (FMI). We used a delta change approach to make the future climate projection at the subcatchment scale. Temperature and precipitation series for the reference period 2001-2010 are repeated four times (2011-2050). The daily projected change (increase or decrease) in temperature and precipitation is added/subtracted to the corresponding day in the reference period.

Table 8: Global circulation models used for future climate projections.

GCM name	Developing institute	Abbreviation used in report
CGCM3(T63)	Canadian Centre for Climate Modelling and Analysis, Canada	CCCMA
Community Climate System Model 3.0 (NCAR-CCSM3)	Community Earth System Model	CCSM3
CNRM-CM3	Centre National de Recherches Météorologiques, France	CNRM
ECHAM5/MPI-OM	Max Planck Institute for Meteorology, Germany	ECHAM
Model for Interdisciplinary Research On Climate (MIROC3.2 HIRIES)	Atmosphere and Ocean Research Institute, University of Tokyo	MIROC

6.2 Future glacier cover development

As observed in the current hydrological regime, the water supplied by glacier melt has major importance in the river basins (Paragraph 5.2). Therefore it is essential to have a good estimate of future changes in glacier cover to provide good estimates of future inflow into the downstream river basins. For this purpose we developed a glacier development model, which was incorporated in the AralMountain model for 2010-2050. This glacier model was calibrated for 2001-2010 using the observed glacier mass balance in the Pamir mountains [*Khromova et al.*, 2006]. The glacier model estimates glacier surface area and volume change with a monthly time step and for twenty separate glacier size classes between 2010 and 2050. For each model



run the results for the 20 different glacier size classes are integrated to derive an overall relative glacier area depletion curve. The depletion and hypsometric curve are then used to estimate the threshold elevation below which glaciers do not persist. This threshold elevation in combination with the elevation distribution within a 1km grid cell is finally used to derive an updated glacier fraction per grid cell. Figure 6-1 to Figure 6-6 show the projected fractional glacier cover in 2050 when the model is forced with the five different GCMs. Figure 6-7 shows the mean of the five outputs.

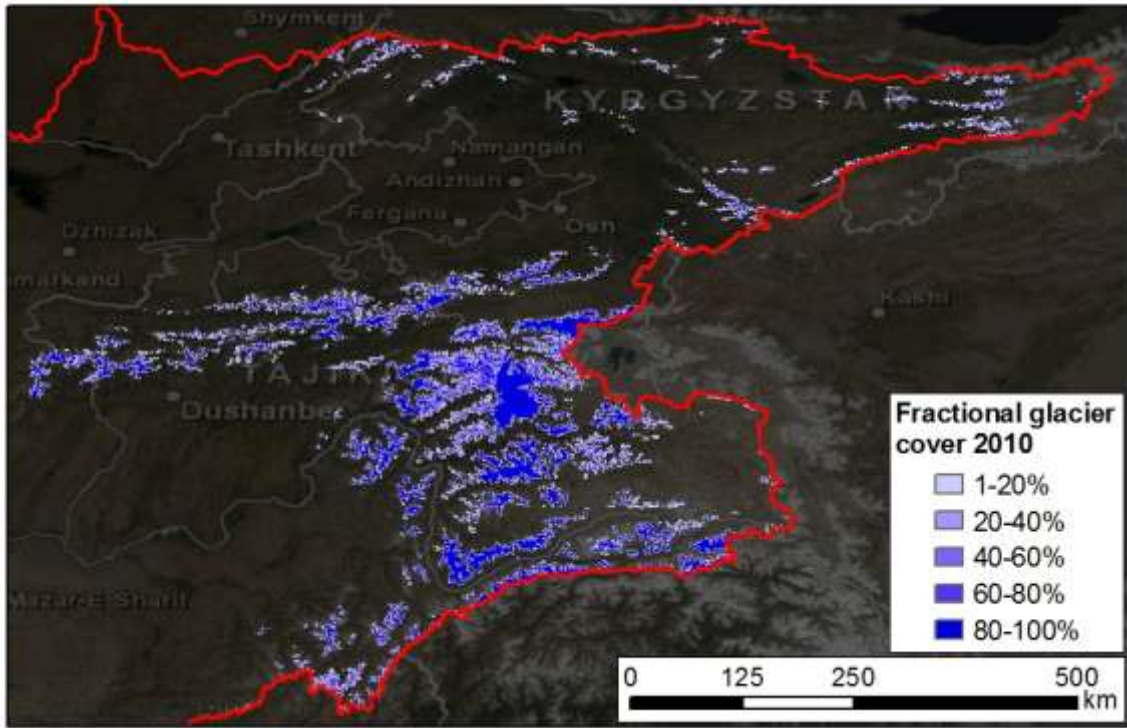


Figure 6-1: Fractional glacier cover 2010.

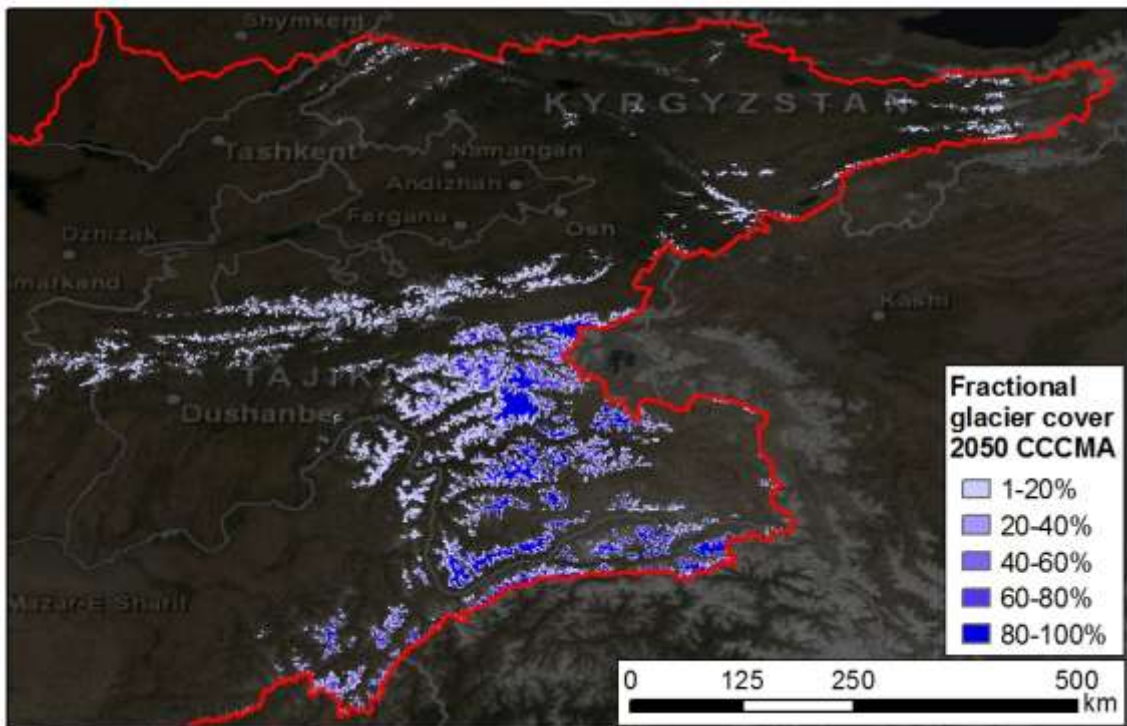


Figure 6-2: Fractional glacier cover 2050 for CCCMA GCM.



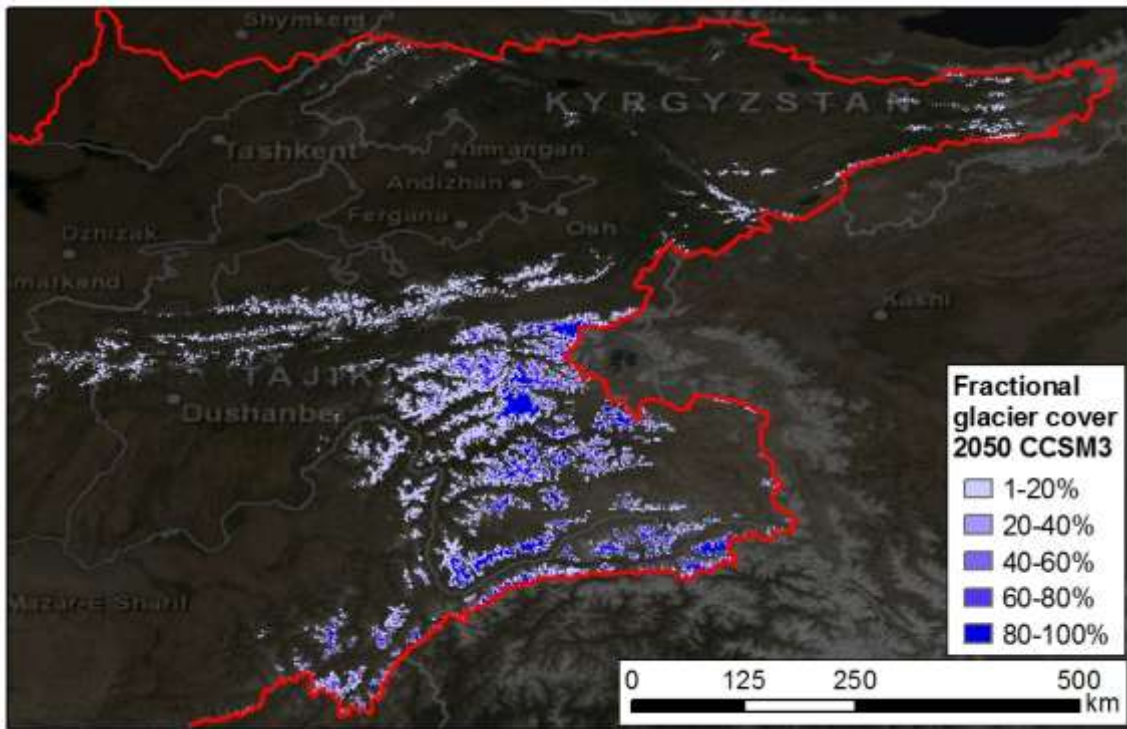


Figure 6-3: Fractional glacier cover 2050 for CCSM3 GCM.

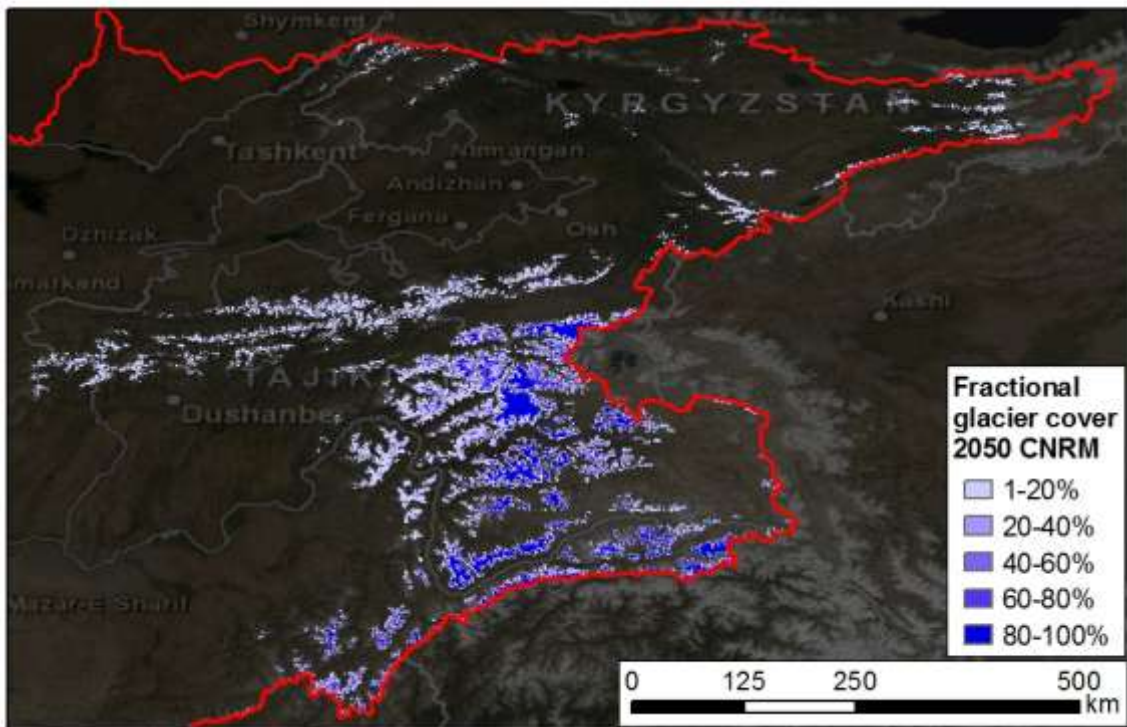


Figure 6-4: Fractional glacier cover 2050 for CNRM GCM.



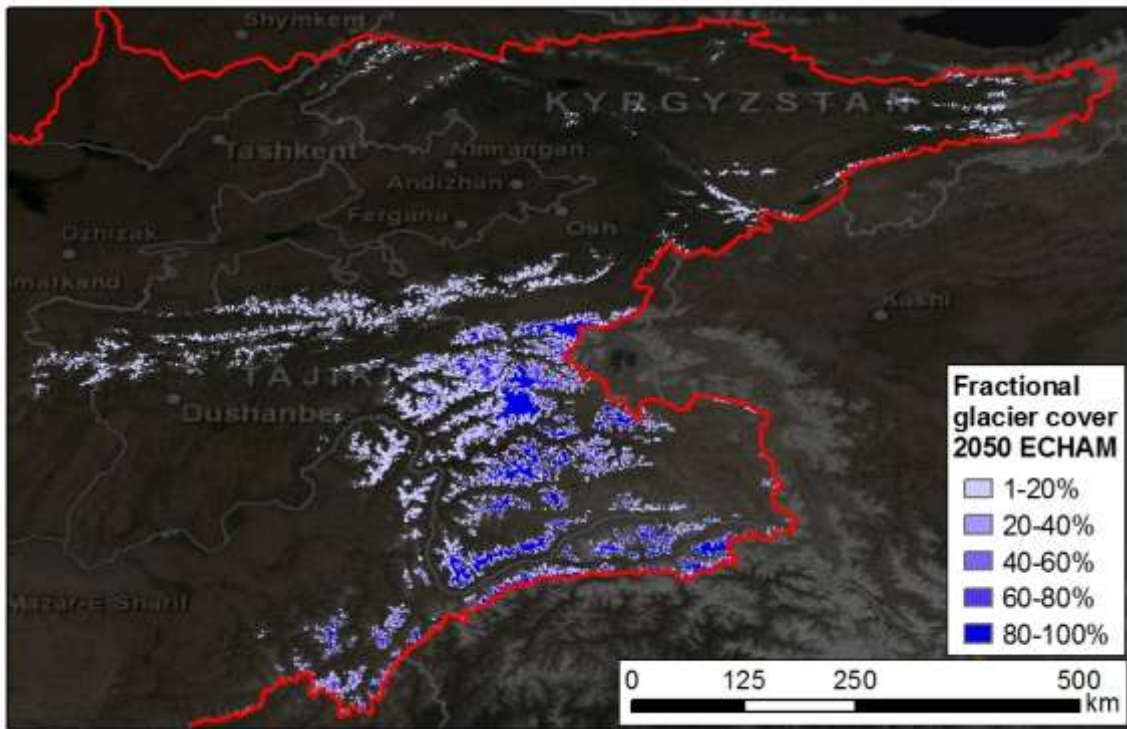


Figure 6-5: Fractional glacier cover 2050 for ECHAM GCM.

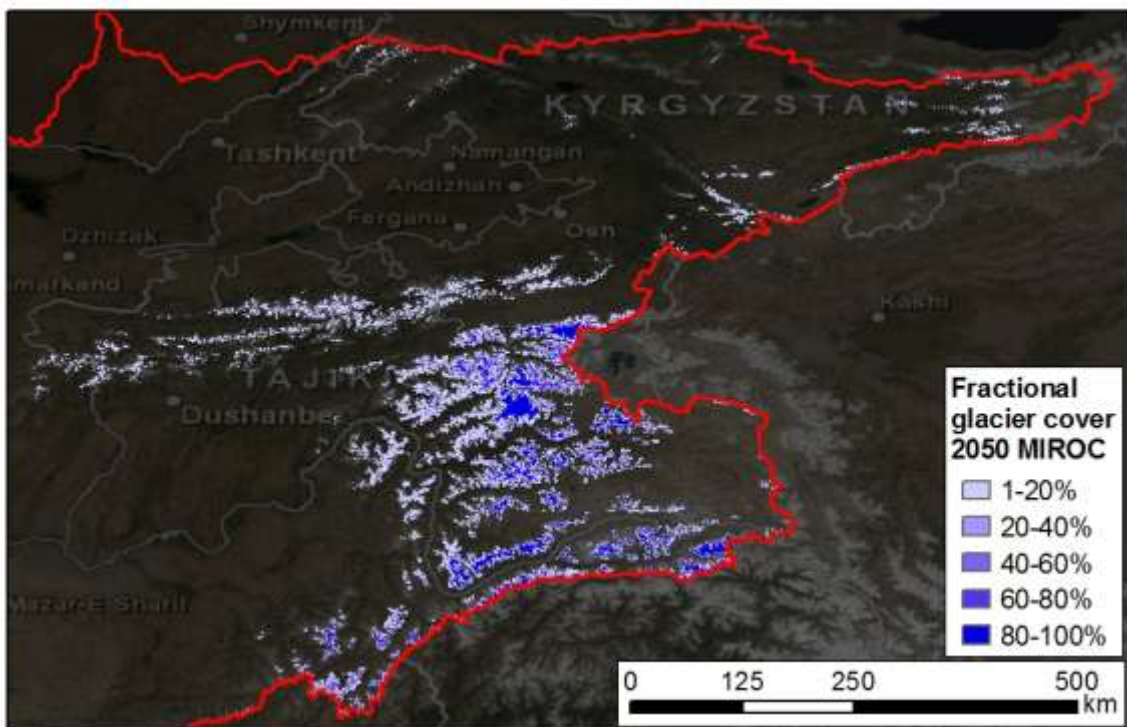


Figure 6-6: Fractional glacier cover 2050 for MIROC GCM.

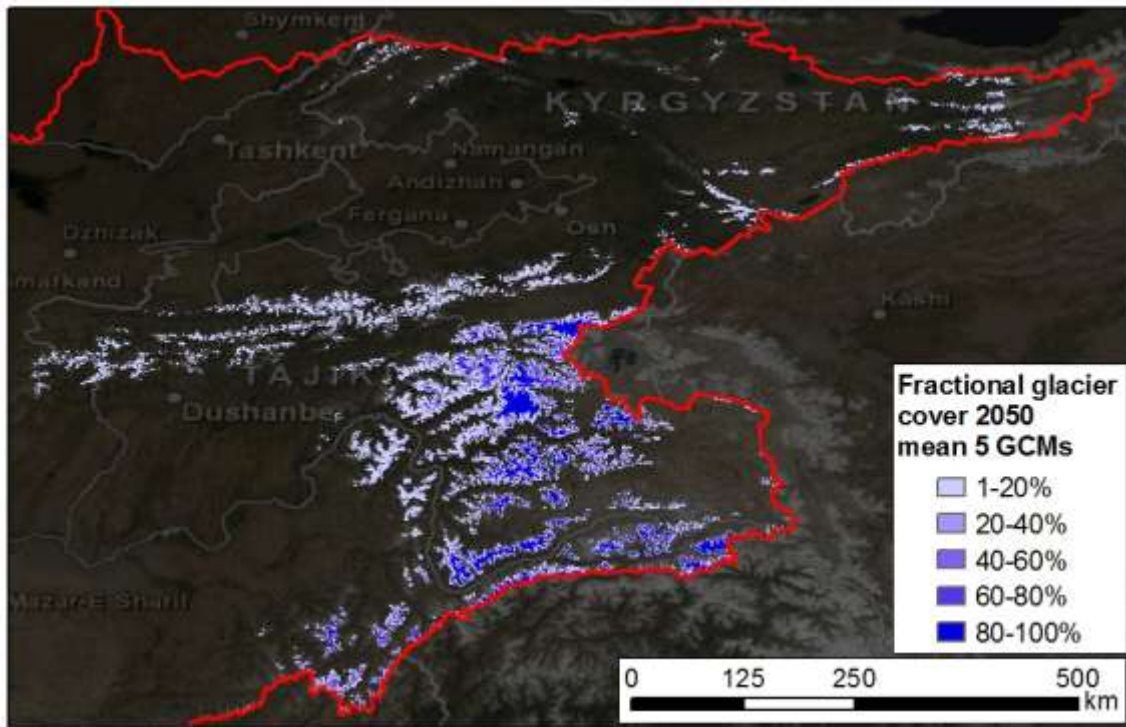


Figure 6-7: Fractional glacier cover 2050, mean of 5 above GCM forced model runs.

The glacier cover decreases significantly more or less independently of the selected GCM. The decrease until 2050 varies from 46.4% for the CNRM GCM to 59.5% for the MIROC GCM (Table 9). It is very likely that glacier extent in 2050 will be just about half of the current extent. Especially small glaciers at low altitudes are affected by the changing climate. This has major impact on the hydrological regime of the Amu Darya and Syr Darya. Contribution of glacier melt to the stream flow changes significantly as described in paragraph 6.3.

Table 9: Absolute and relative decrease in glacier extent for the five GCM forcings and mean decrease in glacier extent.

	Glacier extent 2010 (km ²)	Glacier extent 2050 (km ²)	Decrease in glacier extent (%)
CCCMA	18128.8	9117.6	49.7
CCSM3	18128.8	7395.1	59.2
CNRM	18128.8	9716.1	46.4
ECHAM	18128.8	9017.0	50.3
MIROC	18128.8	7344.0	59.5
<i>Mean</i>	<i>18128.8</i>	<i>8518.0</i>	<i>53.0</i>

6.3 Future changes in generation and composition of runoff

6.3.1 Change in total runoff

As demonstrated in paragraph 5.2 the AralMountain model determines the contribution of glacier melt, snow melt, rain and baseflow to the generated runoff per grid cell. In this paragraph



we show how the average annual runoff generation per component changes for 2021-2030 and 2041-2050 with respect to the reference situation (2001-2010). Figure 6-8 shows the mean change in average annual runoff generation per grid cell for 2021-2030 and 2041-2050 with respect to the reference period (2001-2010). Changes are given in millimeters per year. Figure 6-9 to Figure 6-13 show the changes in runoff generation when the model is forced by the five different GCMs, also in millimeters per year.

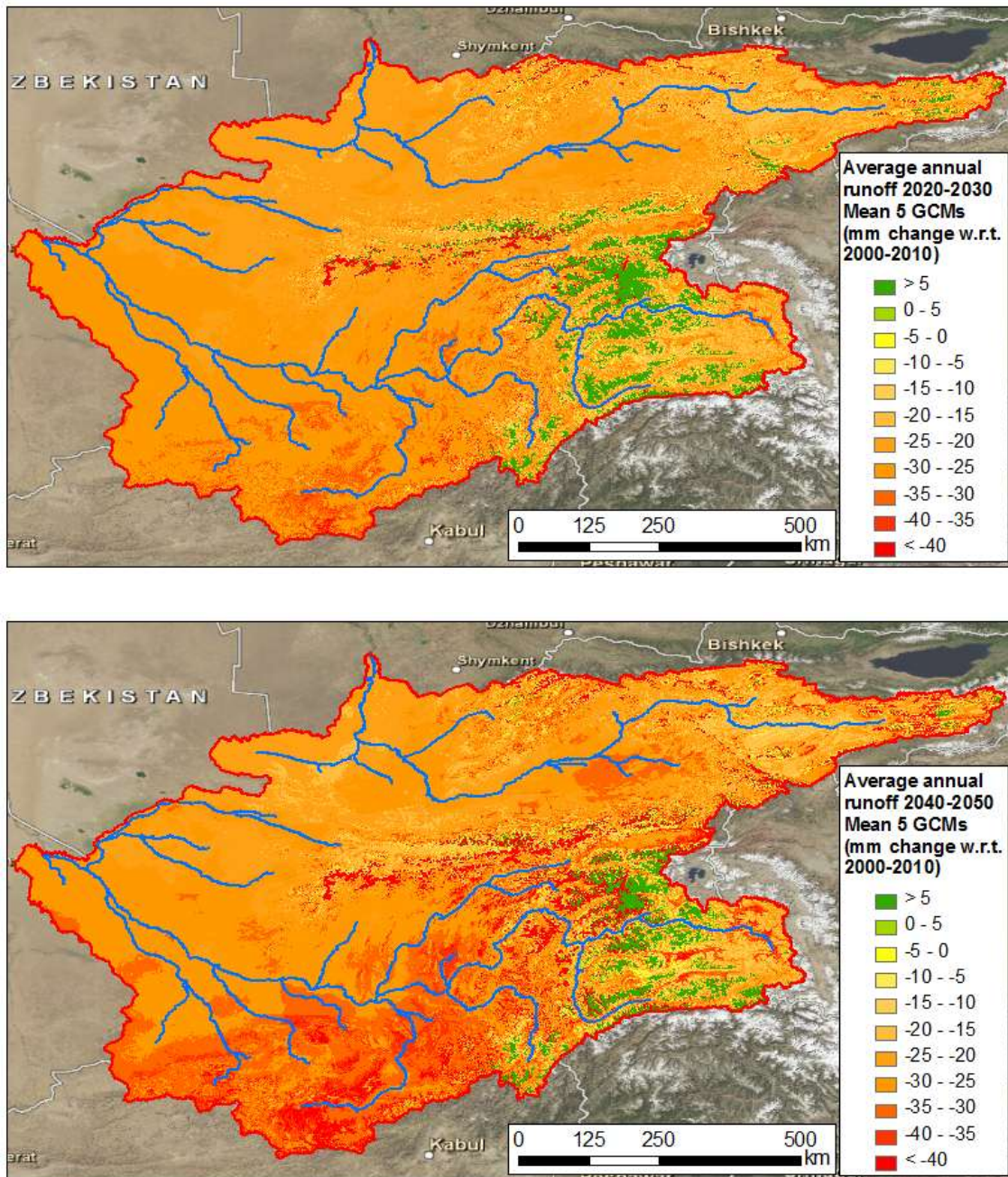


Figure 6-8: Change in average annual runoff generation per grid cell (mm change with respect to reference period) for 2021-2030 and 2041-2050. Mean of output after forcing model with 5 GCMs.



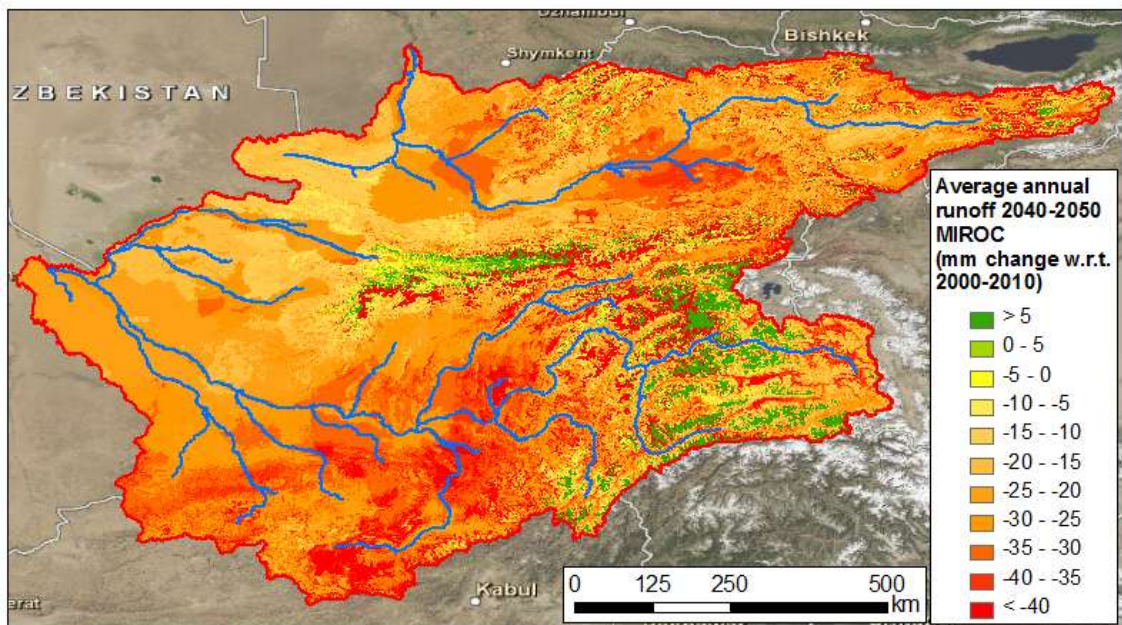
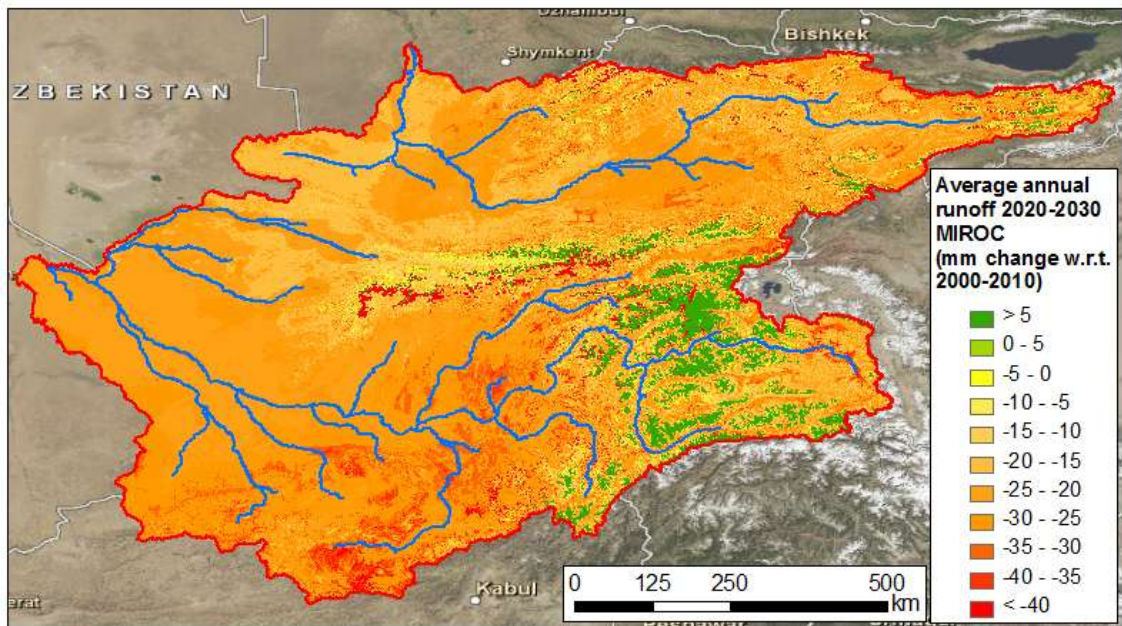


Figure 6-9: Change in average annual runoff generation per grid cell (mm change with respect to reference period) for 2021-2030 and 2041-2050. Output for model forced with MIROC GCM.



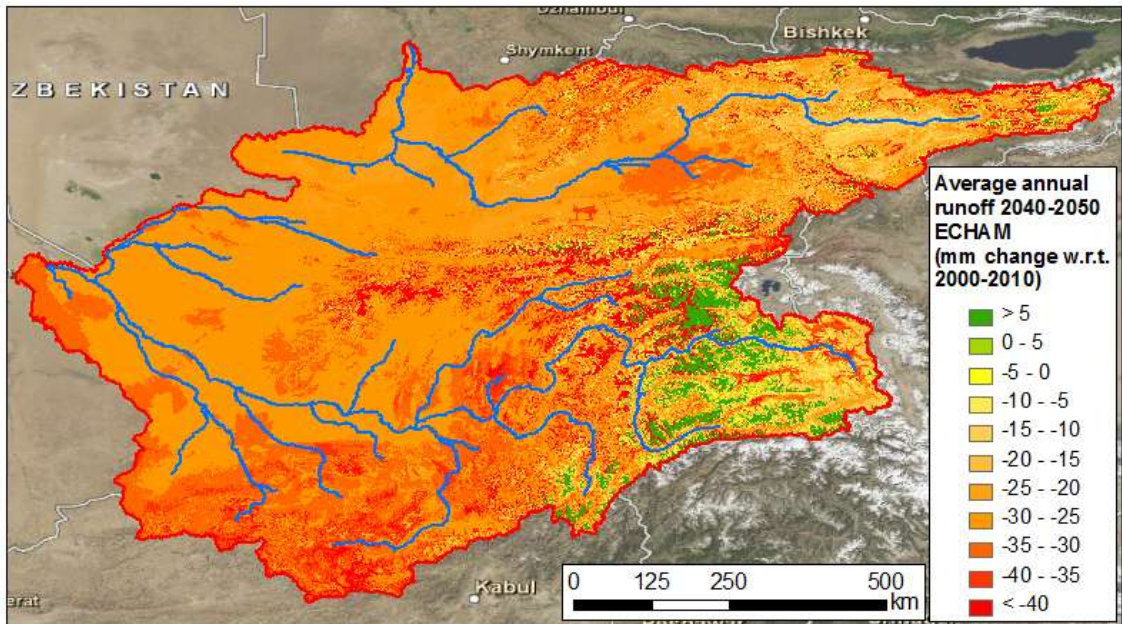
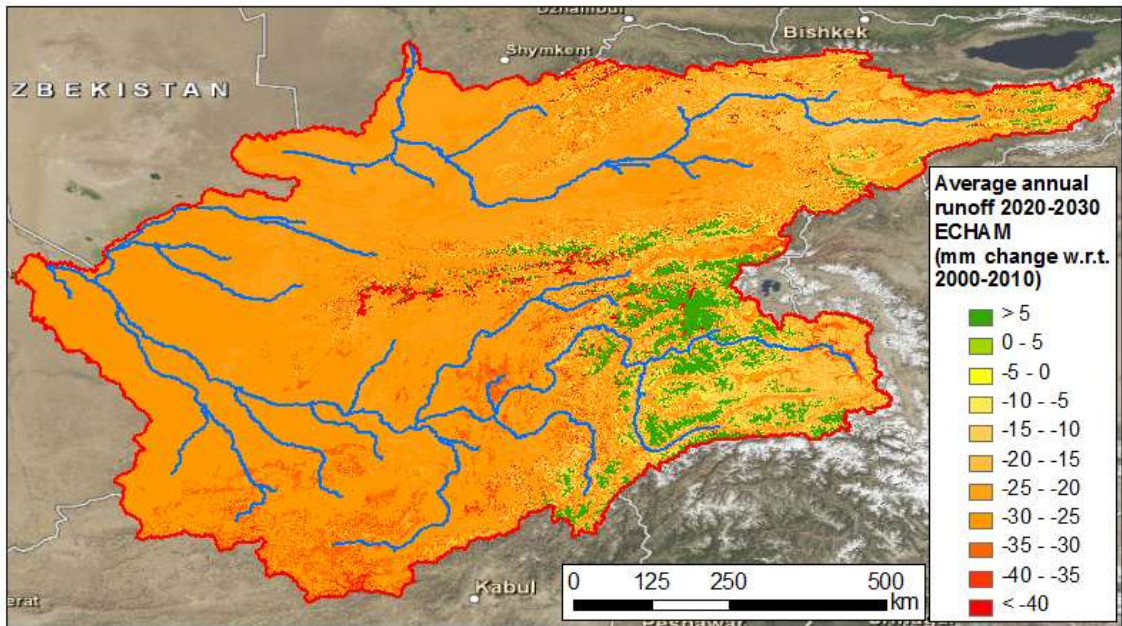


Figure 6-10: Change in average annual runoff generation per grid cell (mm change with respect to reference period) for 2021-2030 and 2041-2050. Output for model forced with ECHAM GCM.



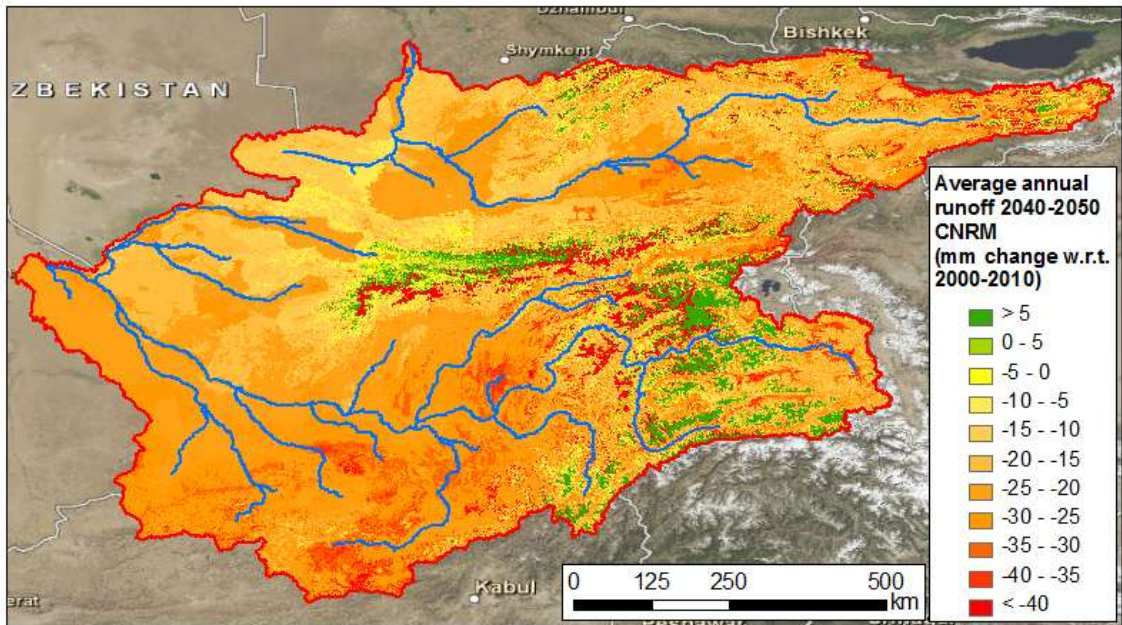
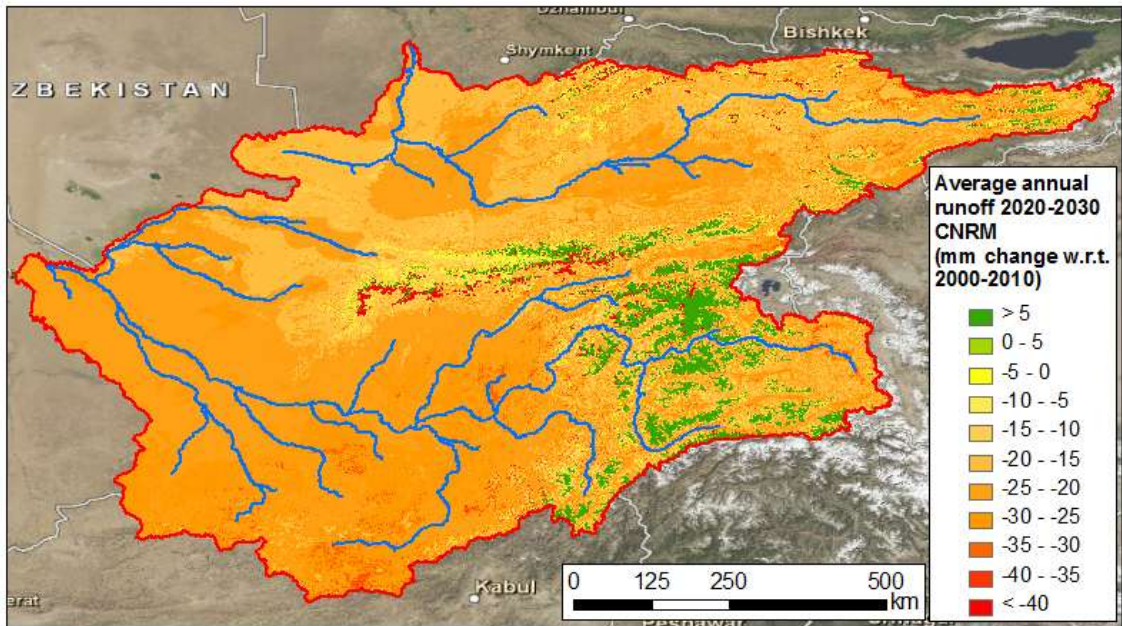


Figure 6-11: Change in average annual runoff generation per grid cell (mm change with respect to reference period) for 2021-2030 and 2041-2050. Output for model forced with CNRM GCM.



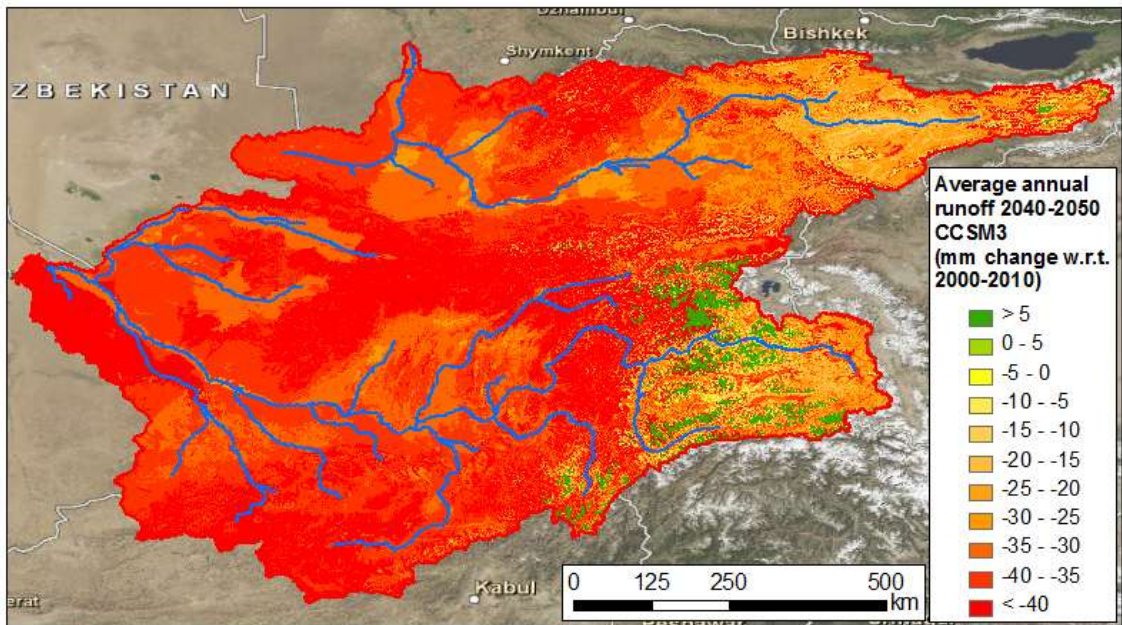
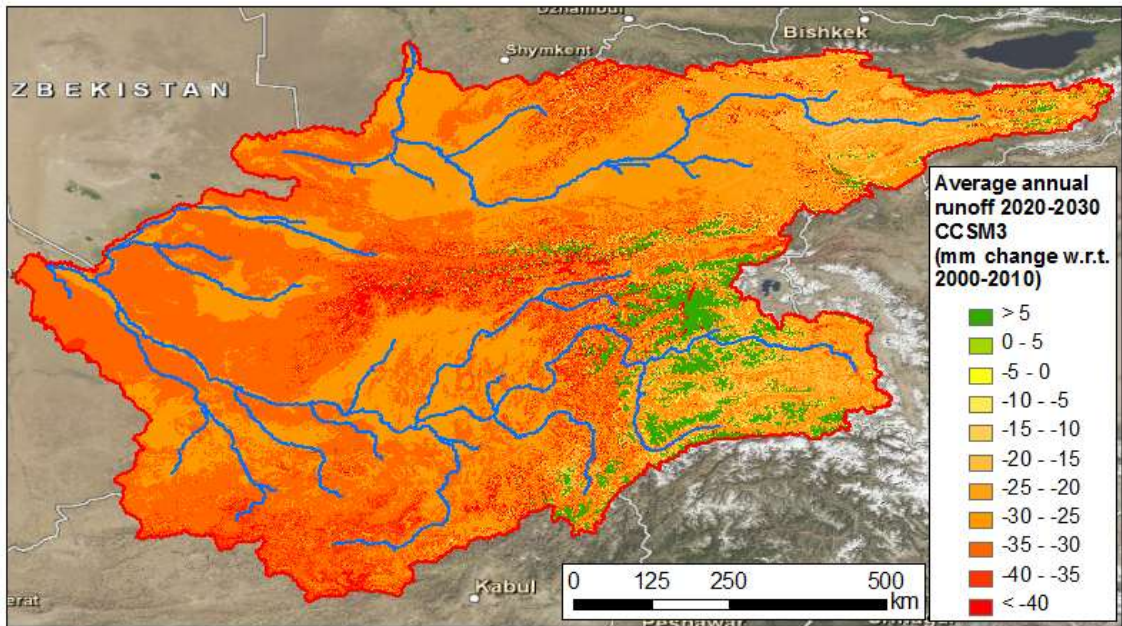


Figure 6-12: Change in average annual runoff generation per grid cell (mm change with respect to reference period) for 2021-2030 and 2041-2050. Output for model forced with CCSM3 GCM.

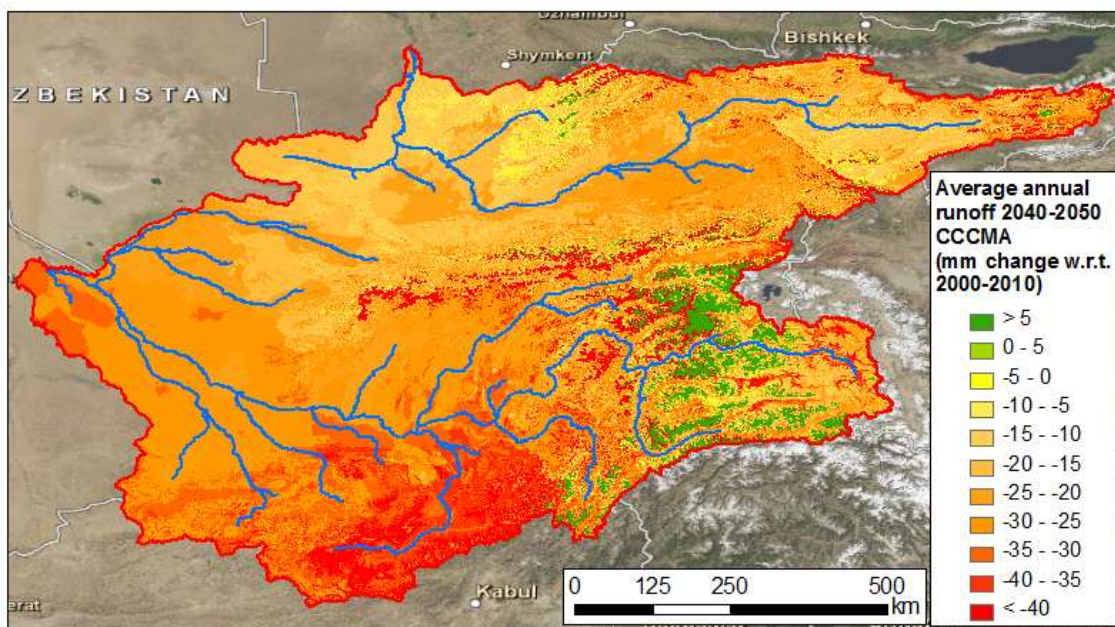
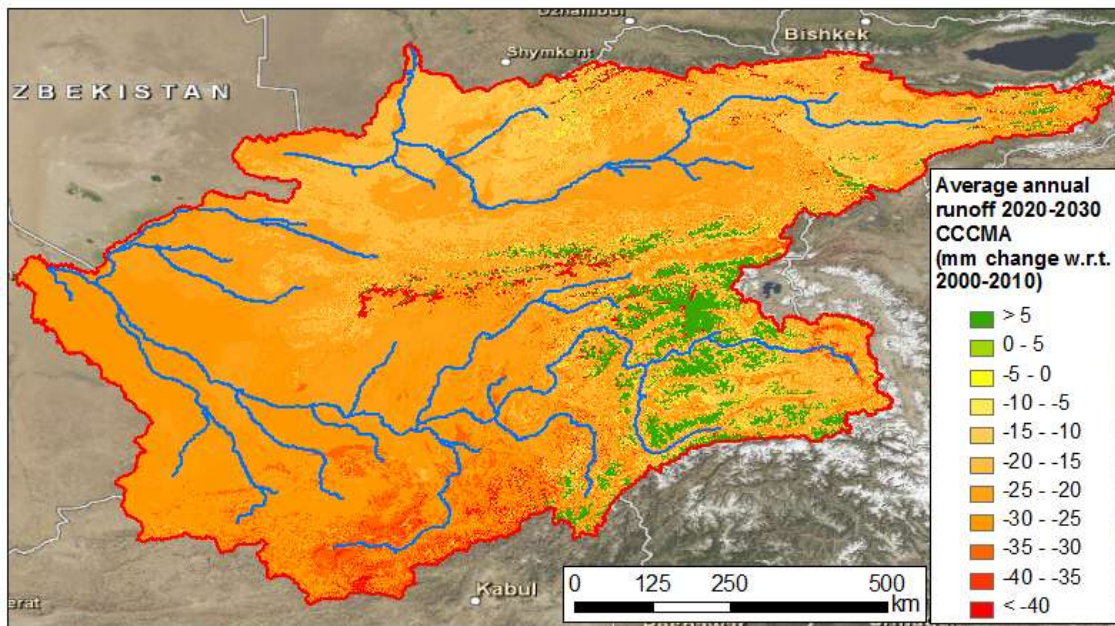


Figure 6-13: Change in average annual runoff generation per grid cell (mm change with respect to reference period) for 2021-2030 and 2041-2050. Output for model forced with CCCMA GCM.

As is obvious from the model output, the generated runoff decreases in general for each of the model outputs forced by the different GCMs. The strongest runoff generation decrease is projected for the CCSM3 scenario. Decreasing runoff is spatially widespread, including the high mountain environment and the lower areas. Increases in runoff are observed for the areas covered with glaciers, since they generate more melt water due to higher temperatures. However, the glaciated area becomes progressively smaller during the period until 2050 reducing the overall generation of glacier melt runoff in the two basins.

Figure 6-14 shows the mean change in annual average runoff generation from glacier melt for each grid cell for 2021-2030 and 2041-2050 with respect to the reference period (2001-2010). Changes are given in millimeters per year. Figure 6-15 to Figure 6-19 show the changes in



runoff generation from glacier melt when the model is forced by the five different GCMs, also in millimeters per year.

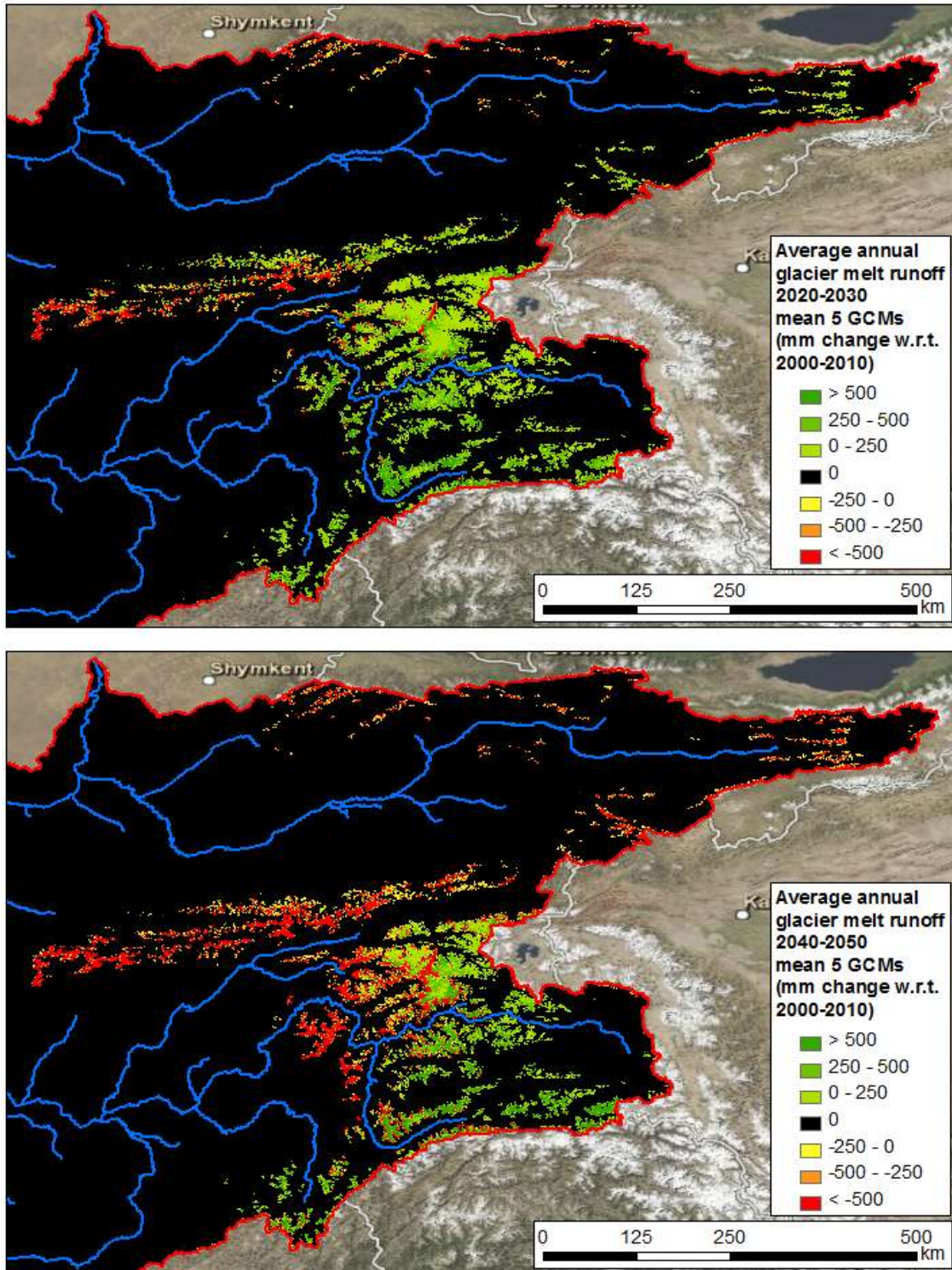


Figure 6-14: Change in average annual runoff generation from glacier melt per grid cell (mm change with respect to reference period) for 2021-2030 and 2041-2050. Mean of output after forcing model with 5 GCMs.



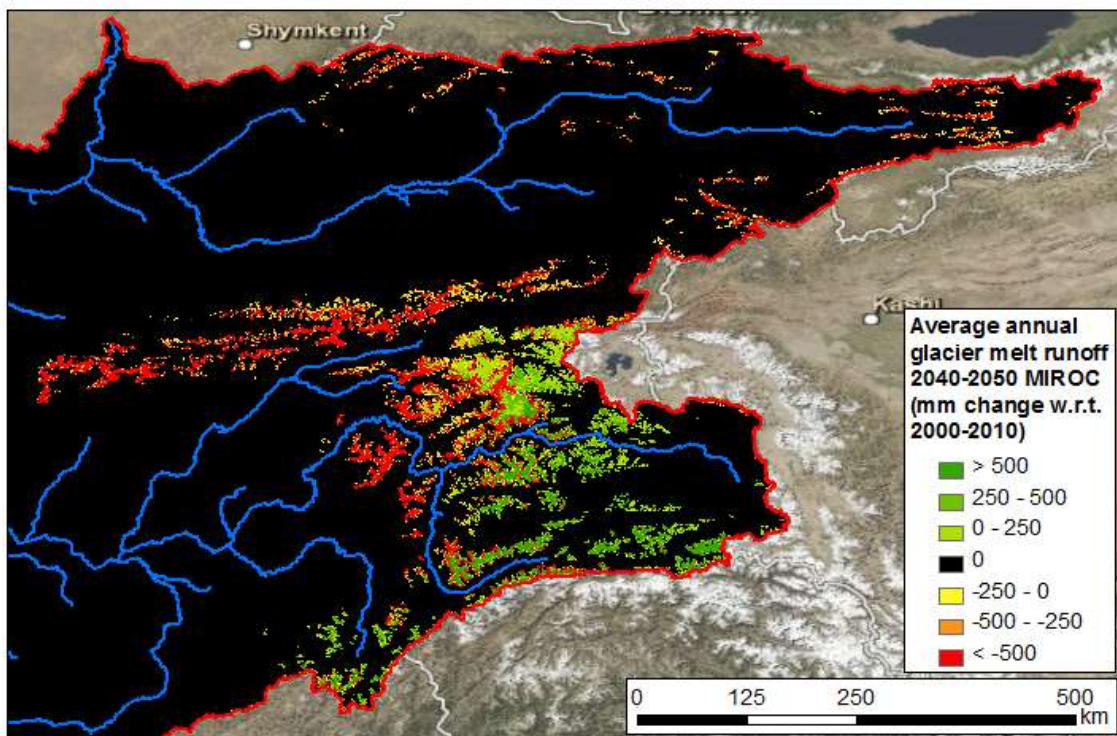
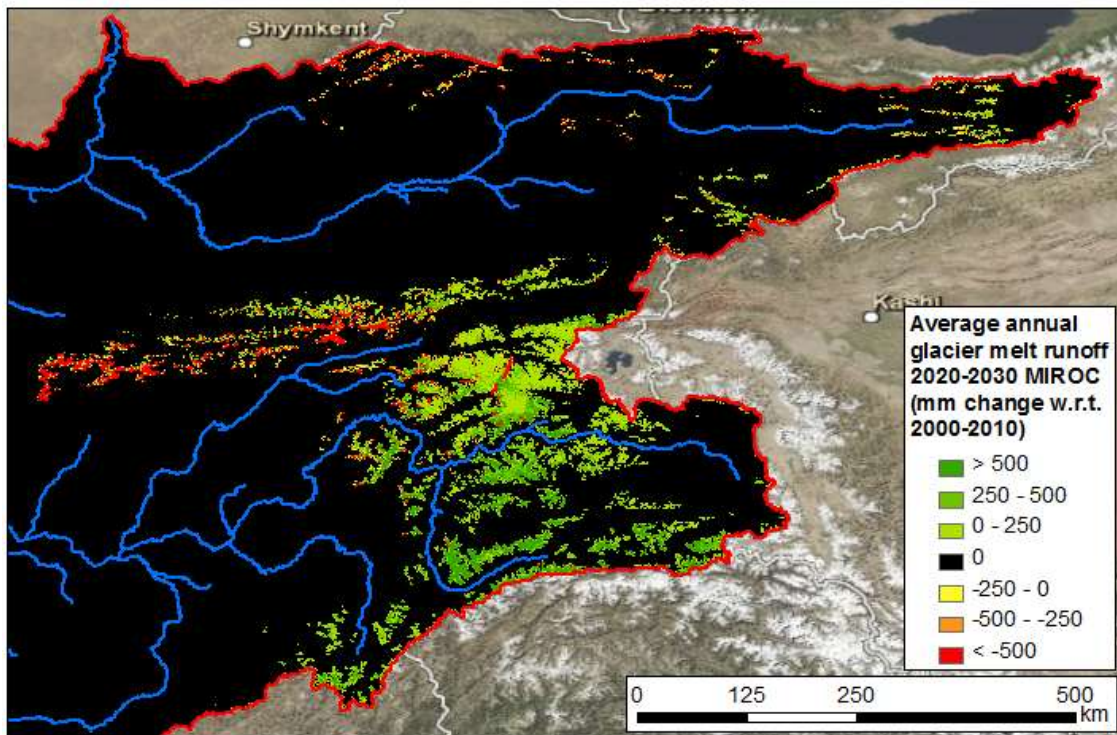


Figure 6-15: Change in average annual runoff generation from glacier melt per grid cell (mm change with respect to reference period) for 2021-2030 and 2041-2050. Output for model forced with MIROC GCM.



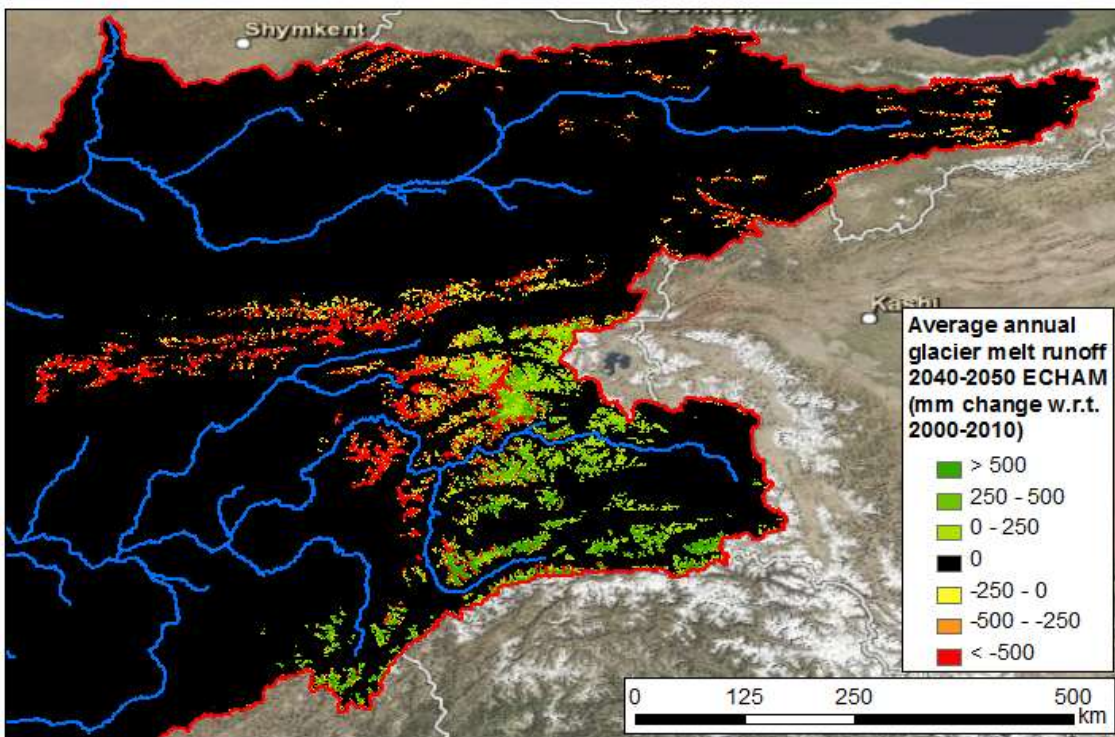
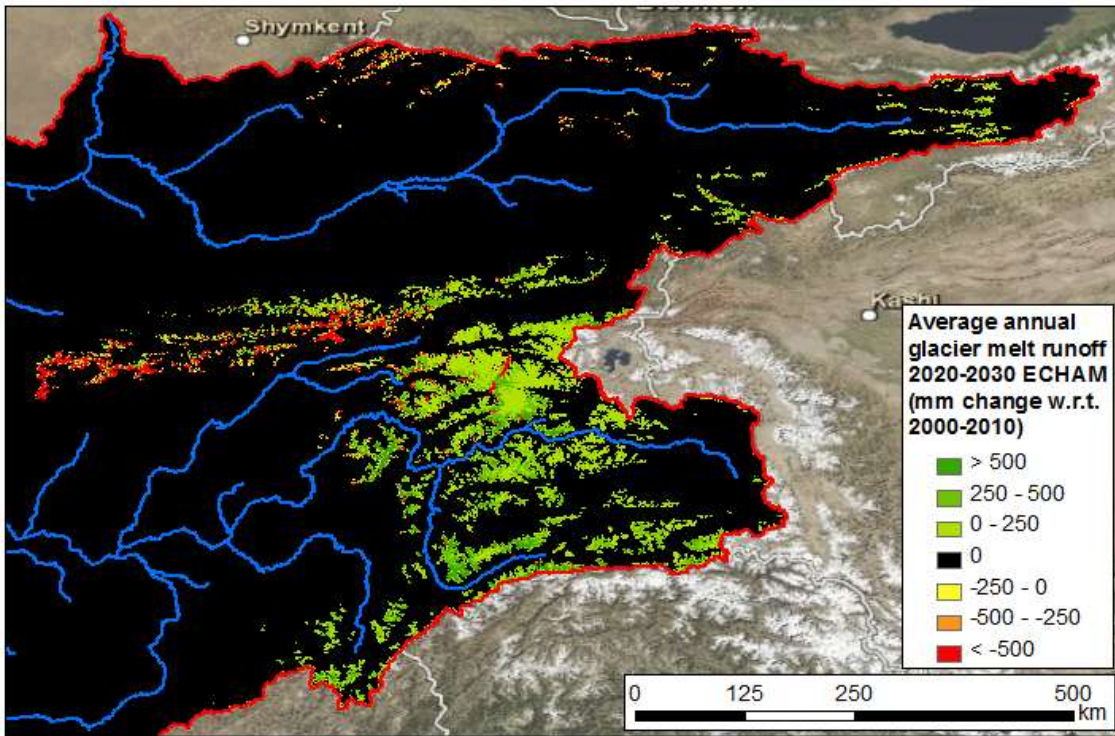


Figure 6-16: Change in average annual runoff generation from glacier melt per grid cell (mm change with respect to reference period) for 2021-2030 and 2041-2050. Output for model forced with ECHAM GCM.

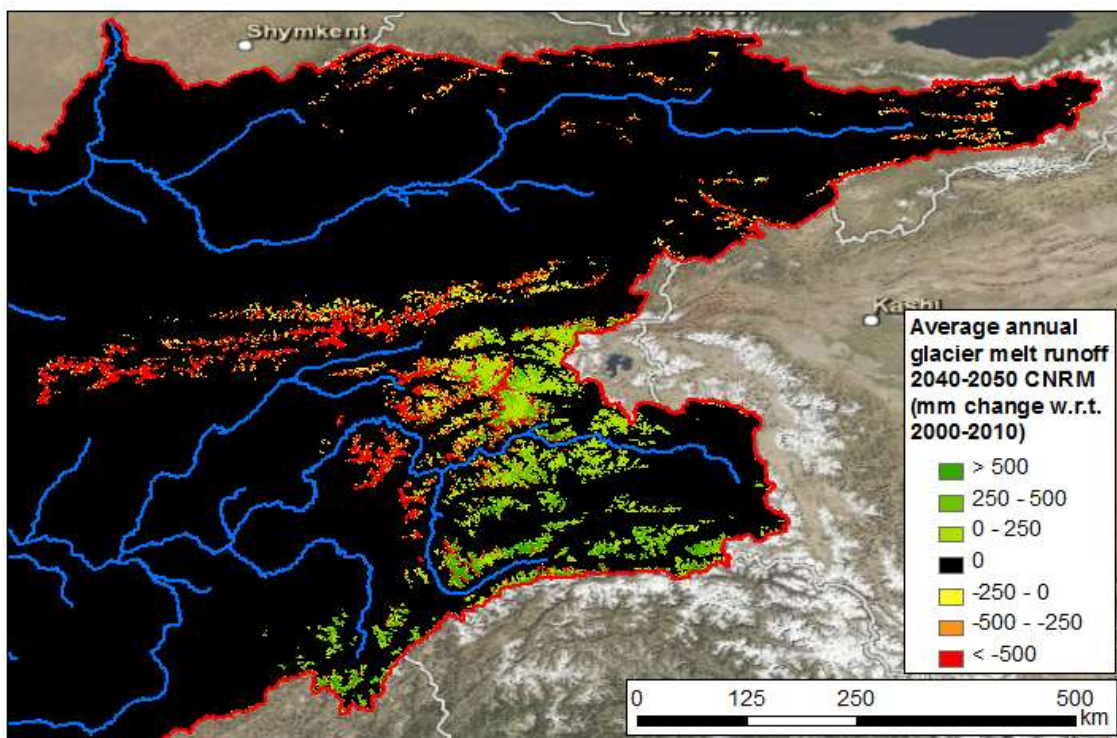
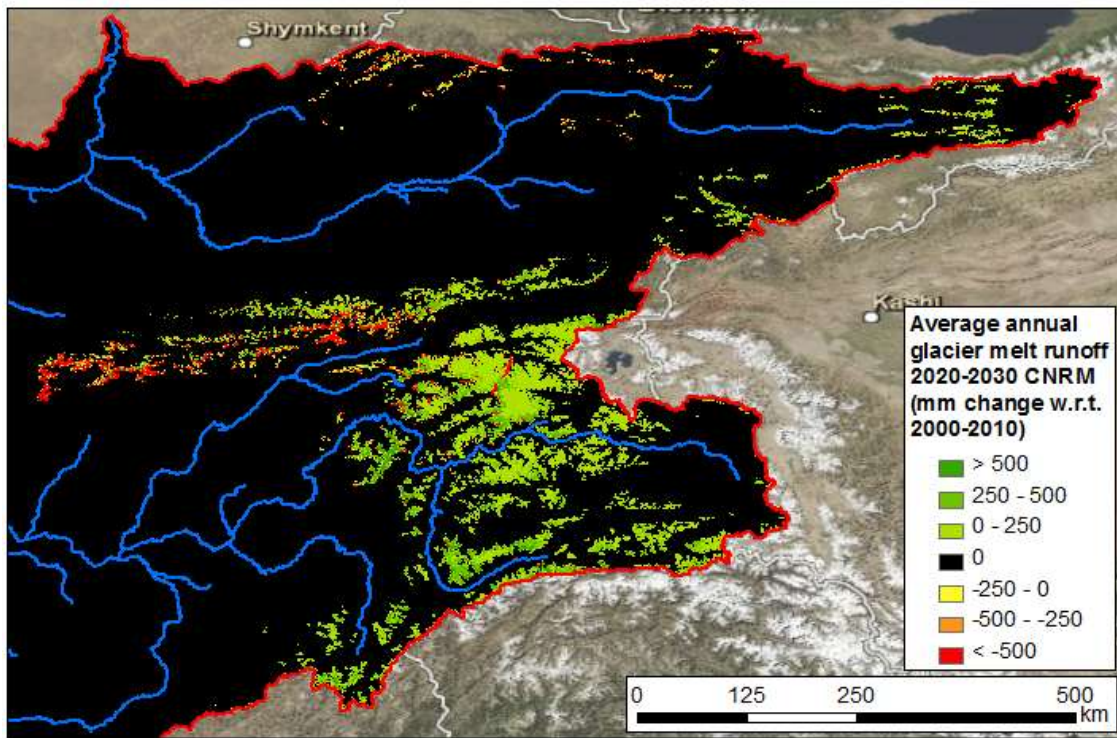


Figure 6-17: Change in average annual runoff generation from glacier melt per grid cell (mm change with respect to reference period) for 2021-2030 and 2041-2050. Output for model forced with CNRM GCM.



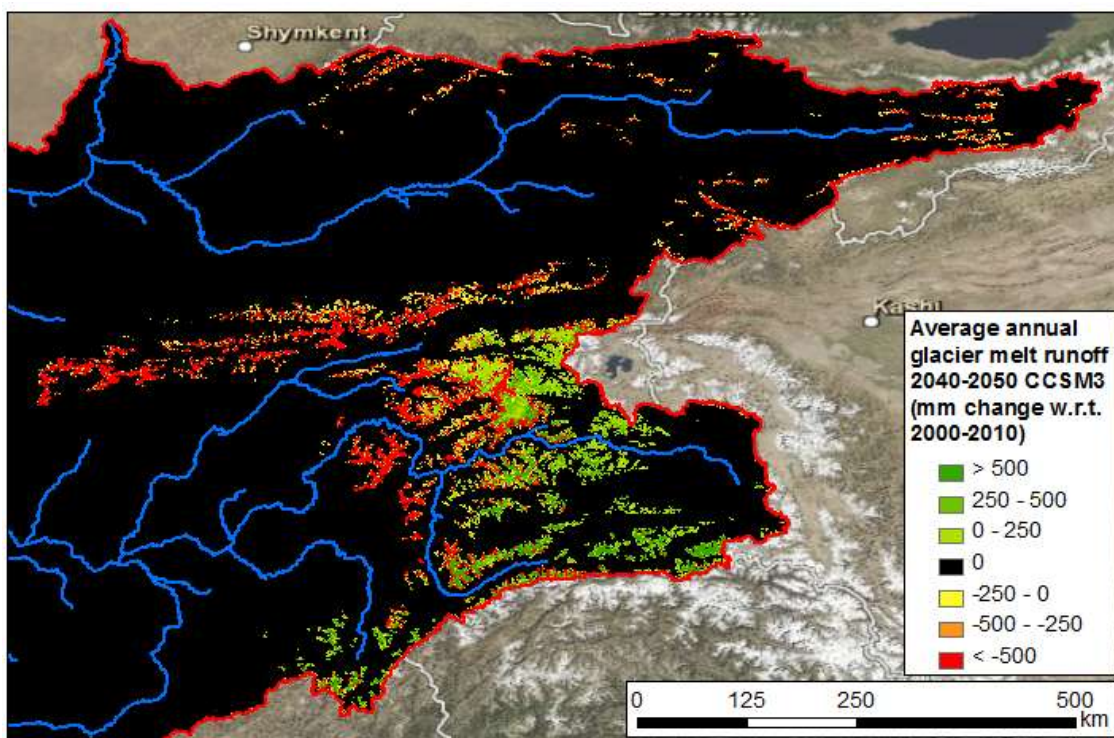
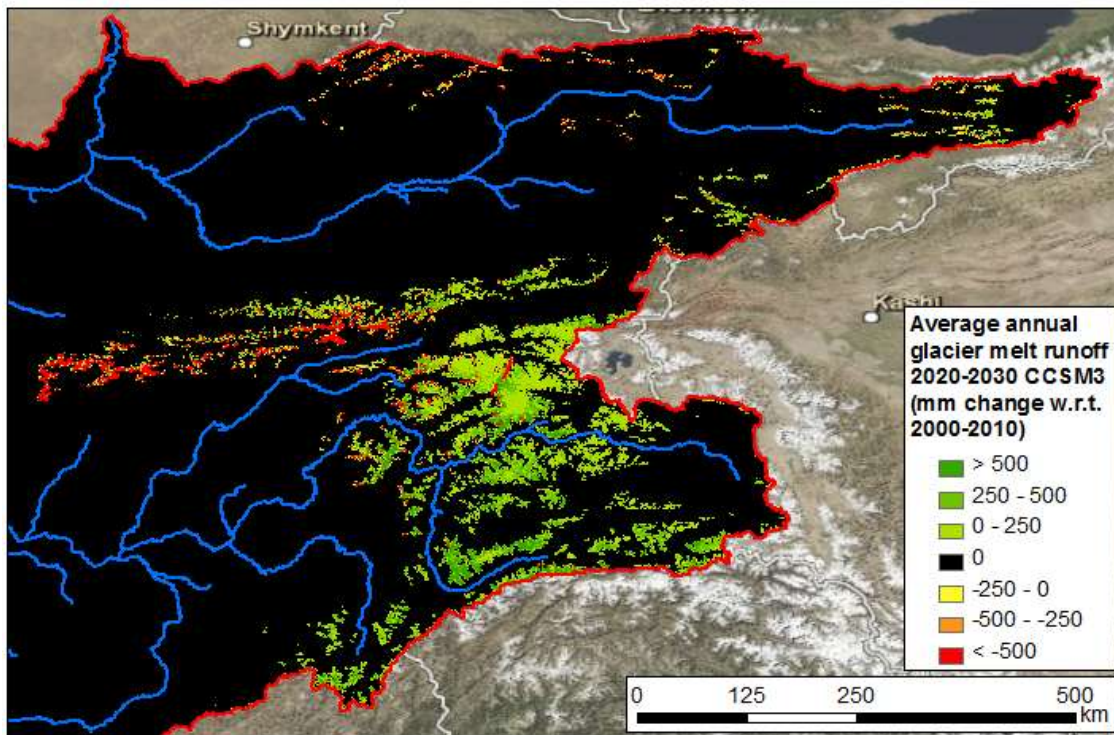


Figure 6-18: Change in average annual runoff generation from glacier melt per grid cell (mm change with respect to reference period) for 2021-2030 and 2041-2050. Output for model forced with CCSM3 GCM.

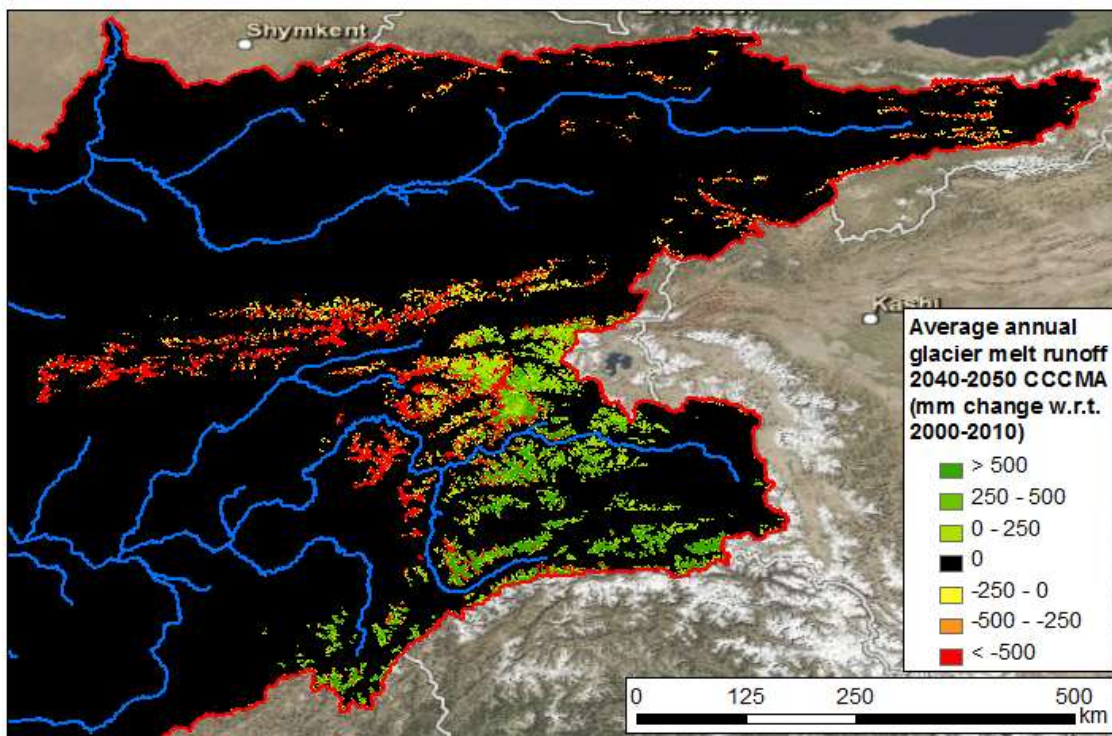
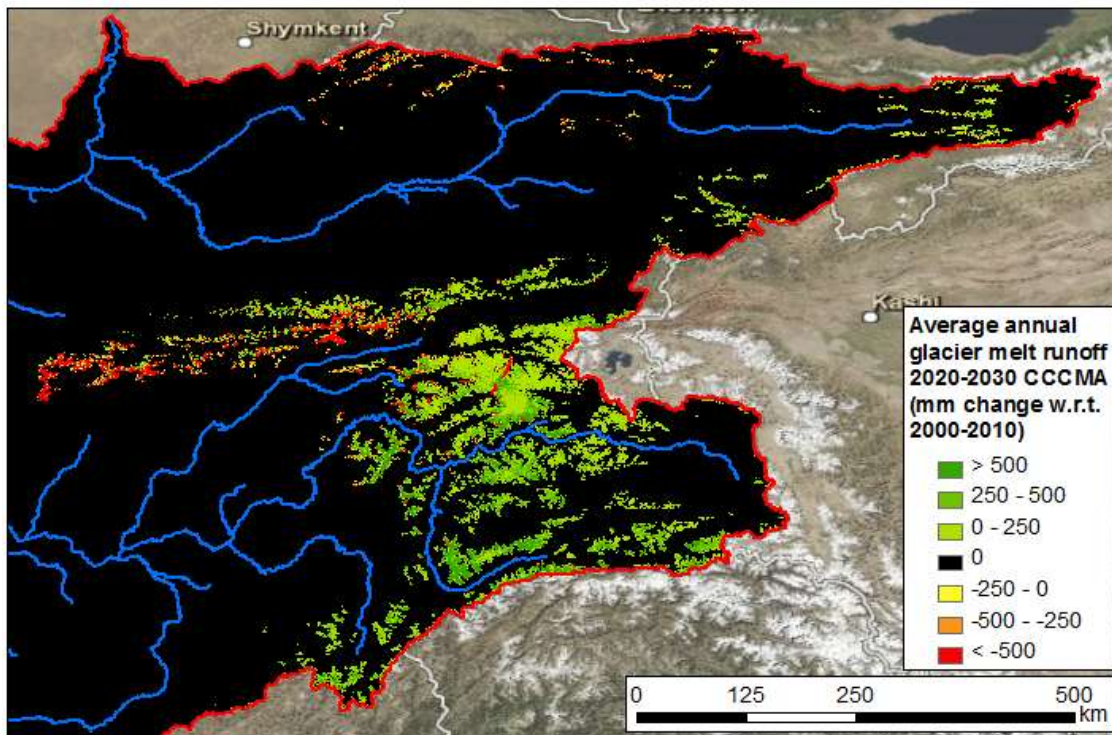


Figure 6-19: Change in average annual runoff generation from glacier melt per grid cell (mm change with respect to reference period) for 2021-2030 and 2041-2050. Output for model forced with CCCMA GCM.

Runoff generation from glacier melt decreases for the grid cells where the glacierized fraction decreases. The persisting glacierized areas on the other hand, show increasing runoff generation. This is due to increasing temperatures and precipitation, which lead to more melt. Especially the glaciers which persist at relatively low altitude show strong increases in melt



water generation. The glacierized area generates more glacier melt runoff in the future, but the glacierized are decreases, leading to an overall reduction in glacier melt water.

6.3.2 Changes in snow melt

Figure 6-20 shows the mean change in average annual runoff generation from snow melt per grid cell for 2021-2030 and 2041-2050 with respect to the reference period (2001-2010). Changes are given in millimeters per year. Figure 6-21 to Figure 6-25 show the changes in runoff generation from snow melt when the model is forced by the five different GCMs, also in millimeters per year.

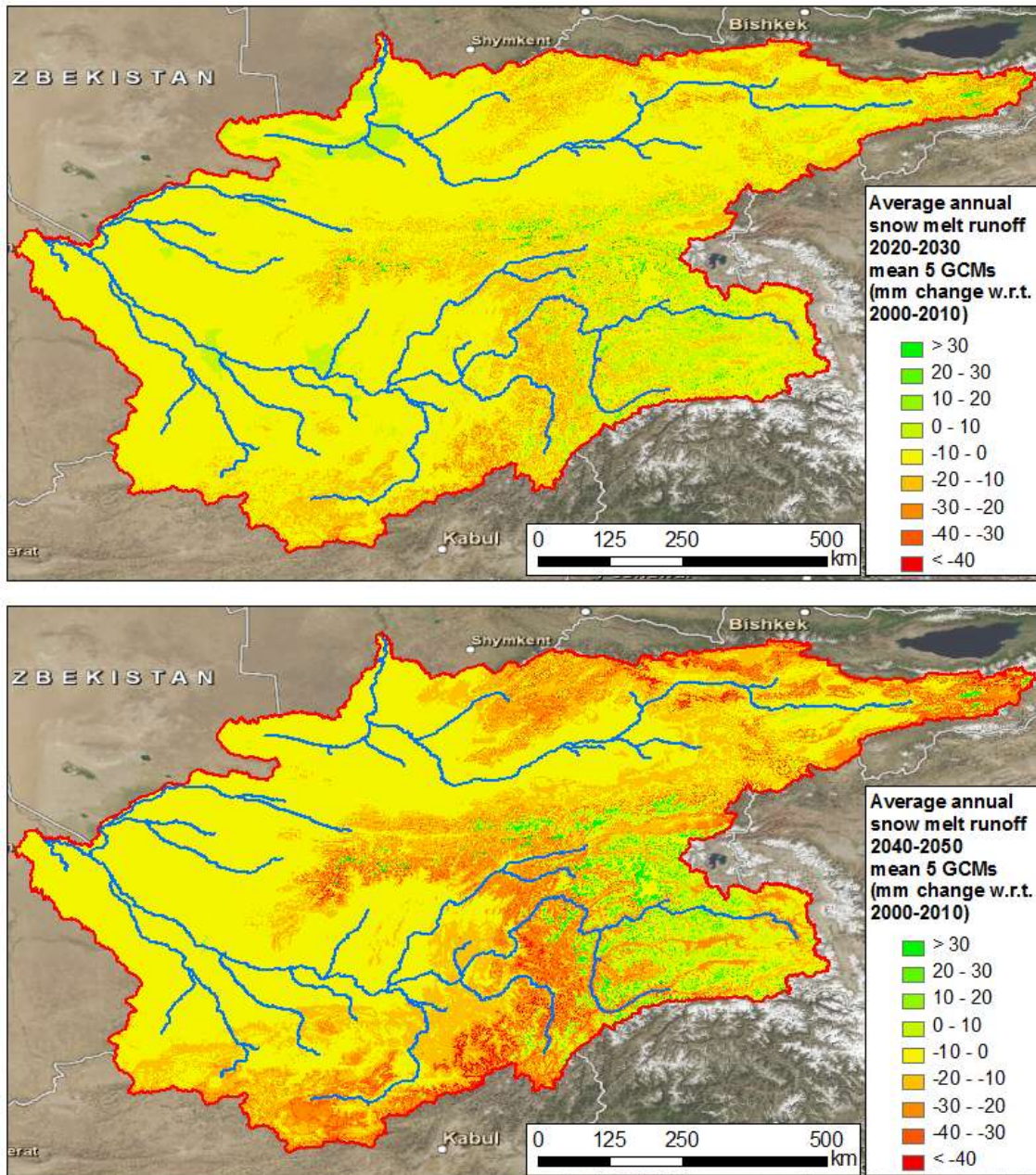


Figure 6-20: Change in average annual runoff generation from snow melt per grid cell (mm change with respect to reference period) for 2021-2030 and 2041-2050. Mean of output after forcing model with 5 GCMs.



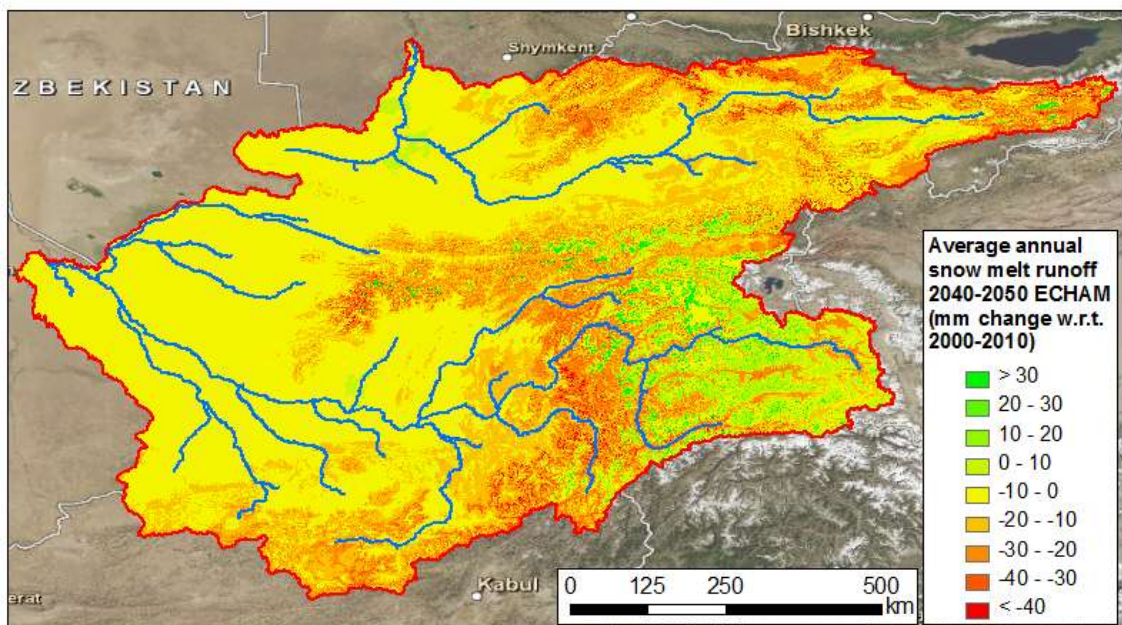
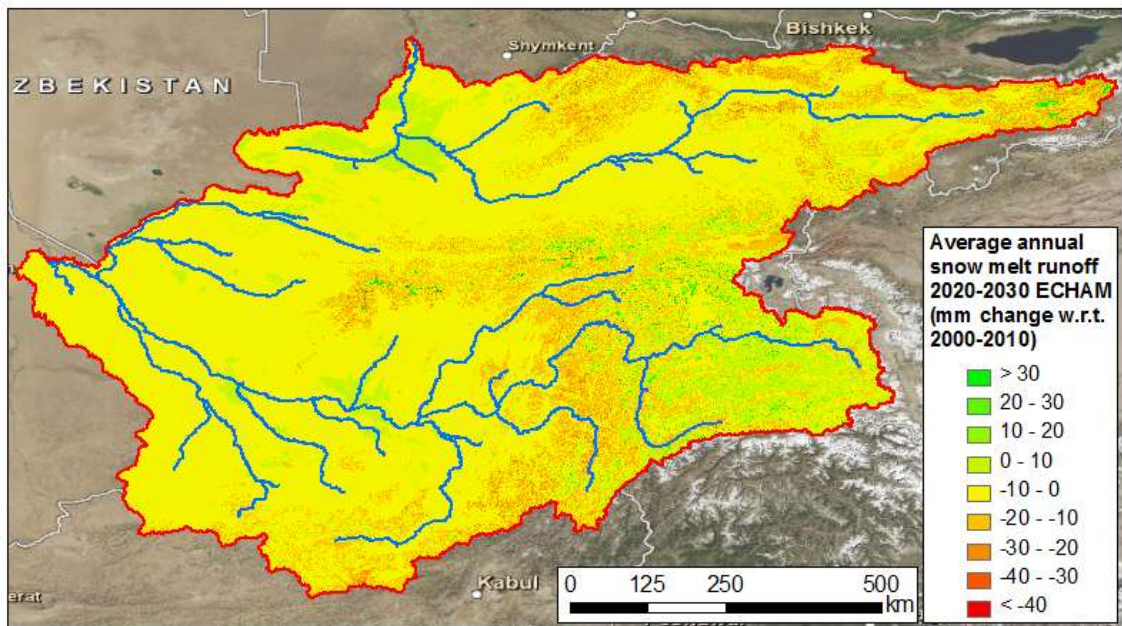


Figure 6-21: Change in average annual runoff generation from snow melt per grid cell (mm change with respect to reference period) for 2021-2030 and 2041-2050. Output for model forced with ECHAM GCM.



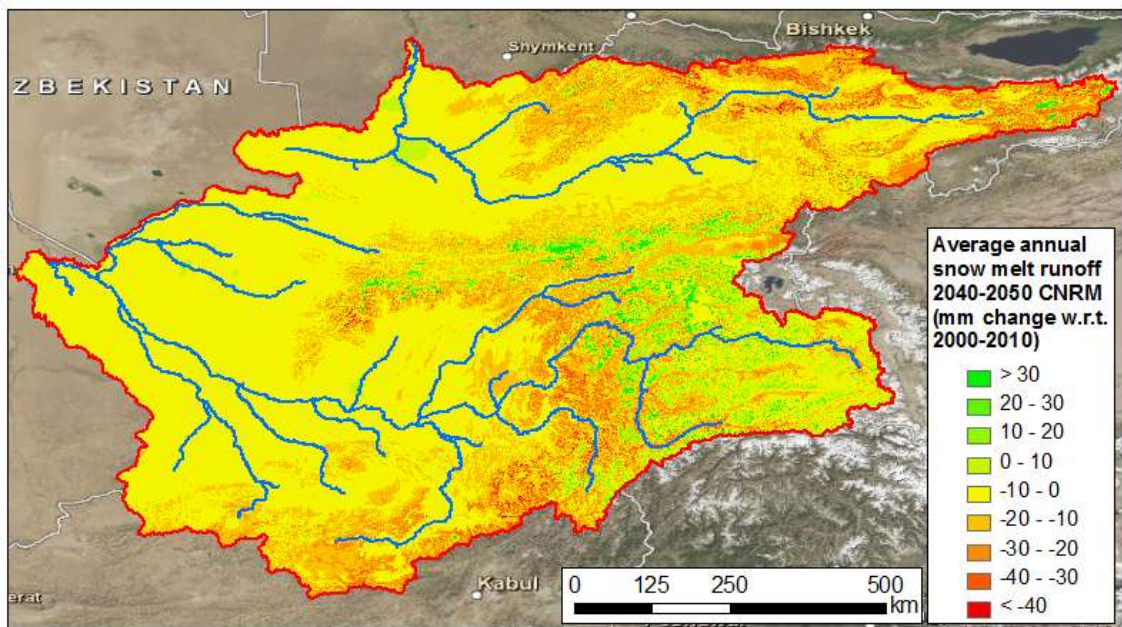
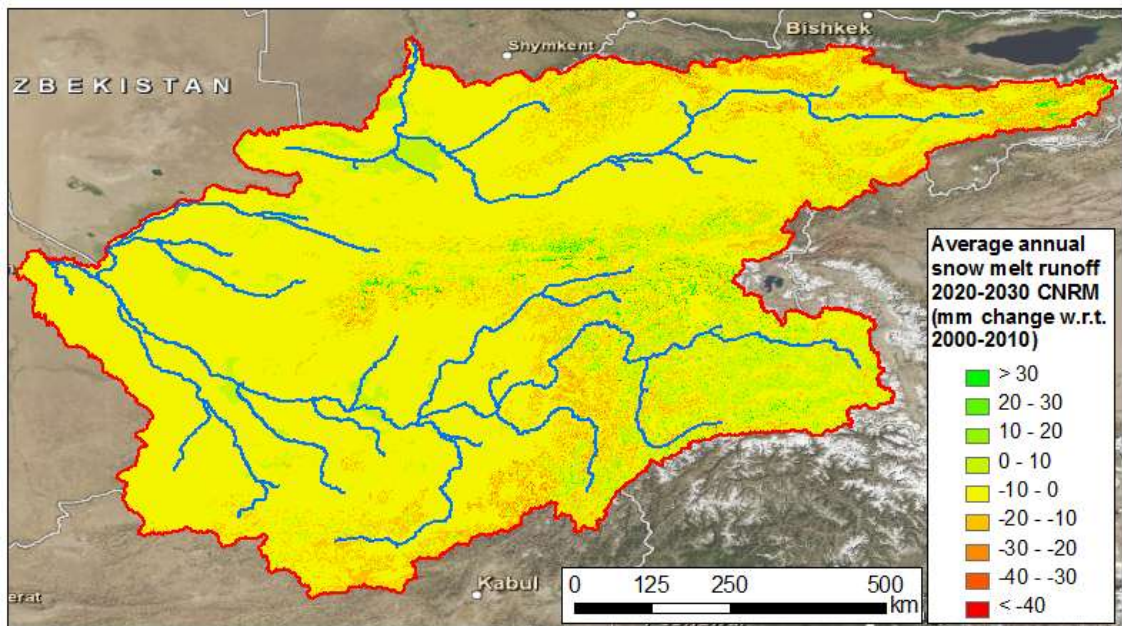


Figure 6-22: Change in average annual runoff generation from snow melt per grid cell (mm change with respect to reference period) for 2021-2030 and 2041-2050. Output for model forced with CNRM GCM.

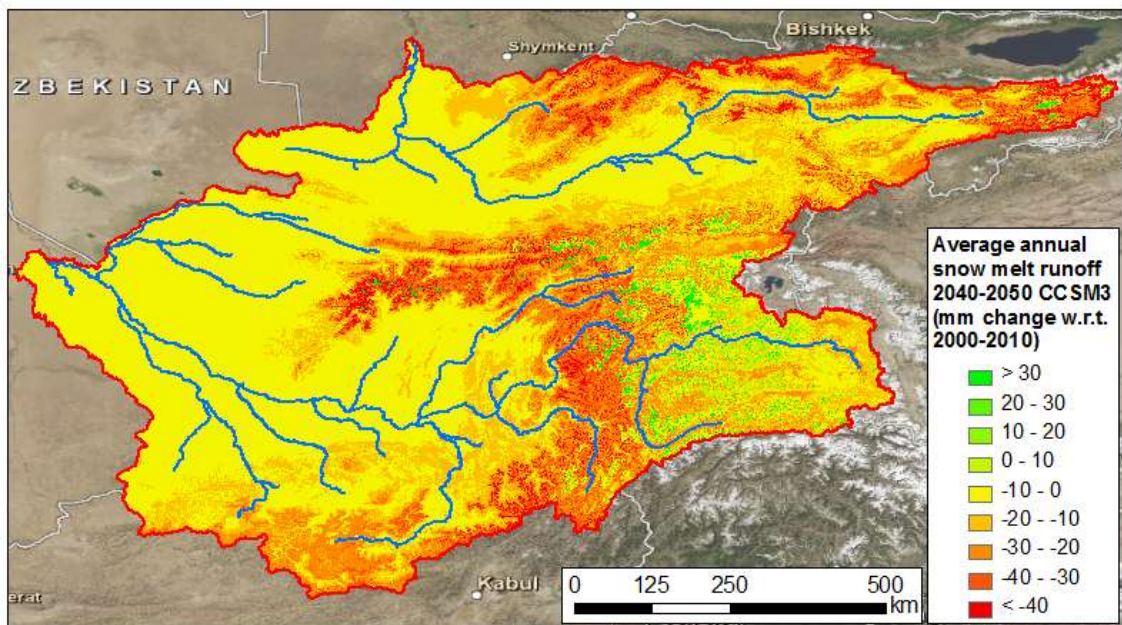
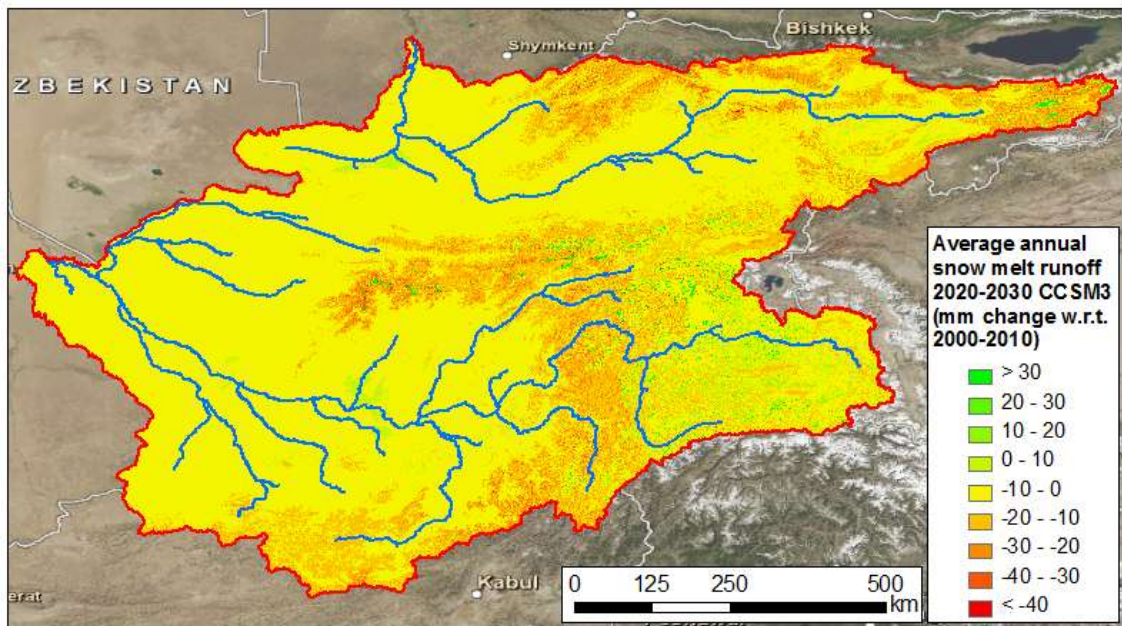


Figure 6-23: Change in average annual runoff generation from snow melt per grid cell (mm change with respect to reference period) for 2021-2030 and 2041-2050. Output for model forced with CCSM3 GCM.



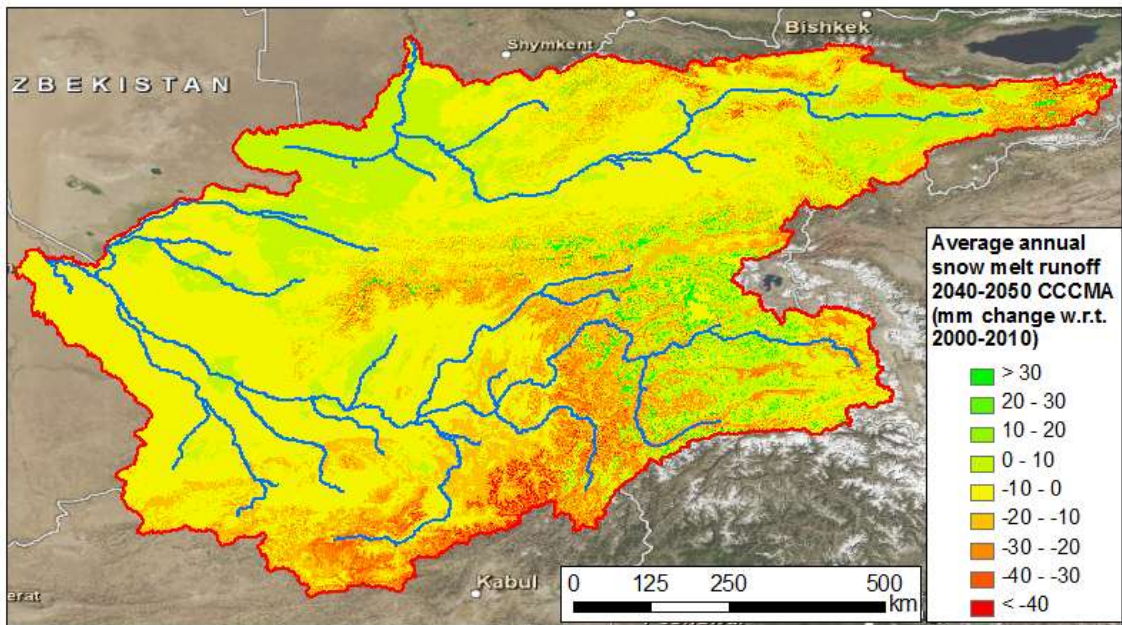
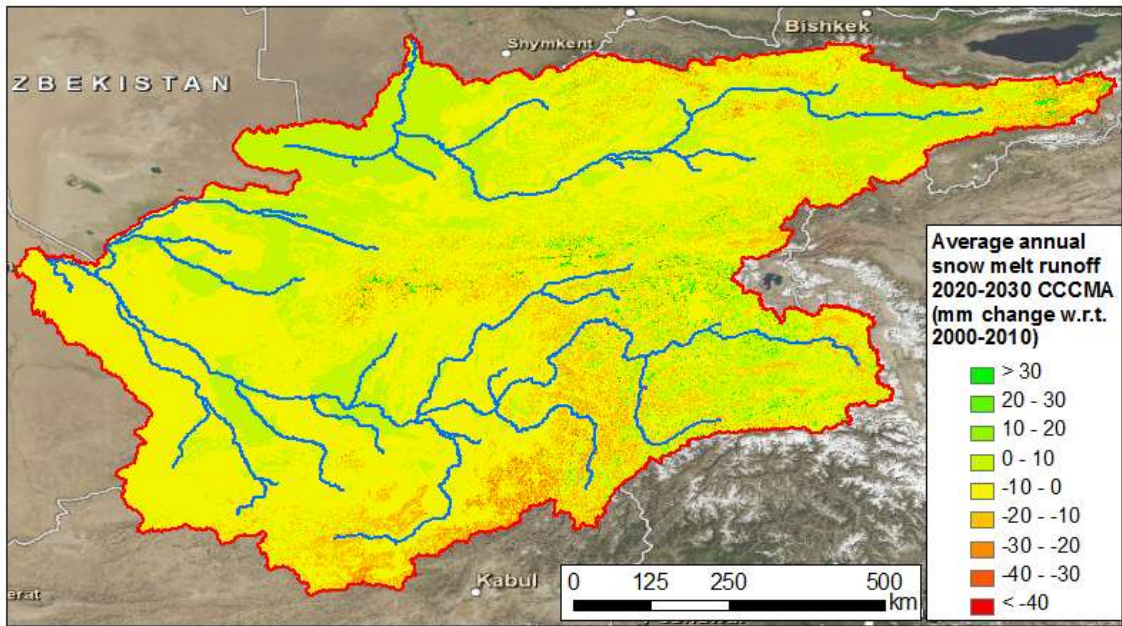


Figure 6-24: Change in average annual runoff generation from snow melt per grid cell (mm change with respect to reference period) for 2021-2030 and 2041-2050. Output for model forced with CCCMA GCM.



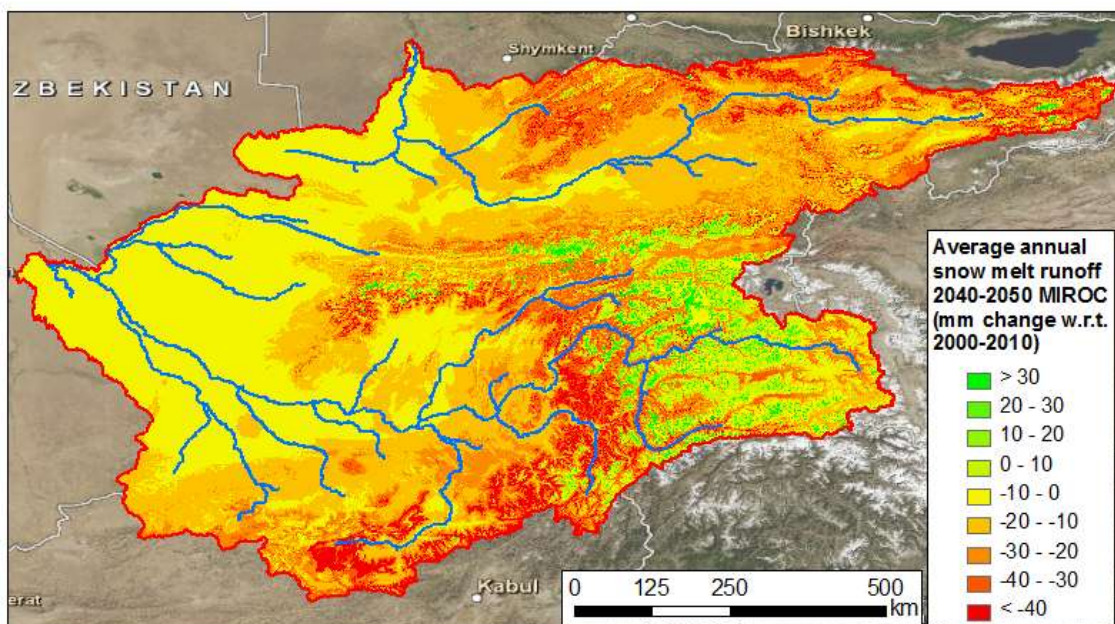
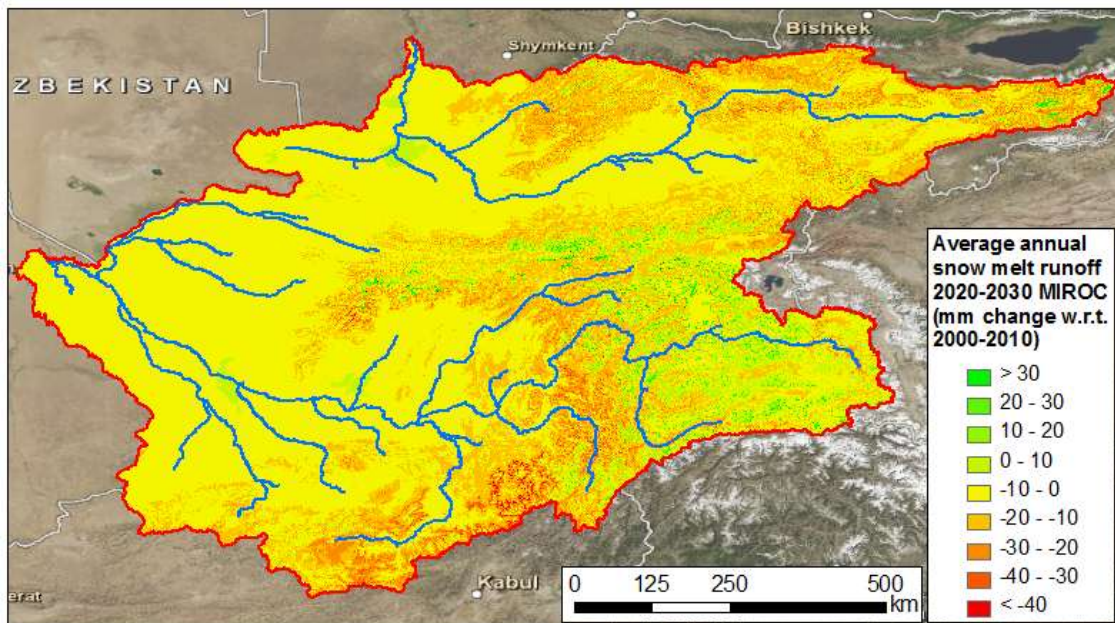


Figure 6-25: Change in average annual runoff generation from snow melt per grid cell (mm change with respect to reference period) for 2021-2030 and 2041-2050. Output for model forced with MIROC GCM.

For changes in runoff originating from snow melt a strong correlation with altitude is observed. Due to increases in temperature, the snow line is shifting to higher altitude. Therefore, strongest reductions in the generation of snow melt are occurring in the lower mountain ranges, where less precipitation will fall as snow, and more precipitation will fall as rain. Areas where the glacierized fraction has reduced show an increase in the snow melt in the model, since areas with 100% fractional glacier cover are only contributing to glacier melt and not to snow melt. Snow falling on a glacier is considered as 'glacier' in the model.



6.3.3 Changes in rain runoff

Figure 6-26 shows the mean change in average annual runoff generation from rain per grid cell for 2021-2030 and 2041-2050 with respect to the reference period (2001-2010). Changes are given in millimeters per year. Figure 6-27 to Figure 6-31 show the changes in runoff generation from rain when the model is forced by the five different GCMs, also in millimeters per year.

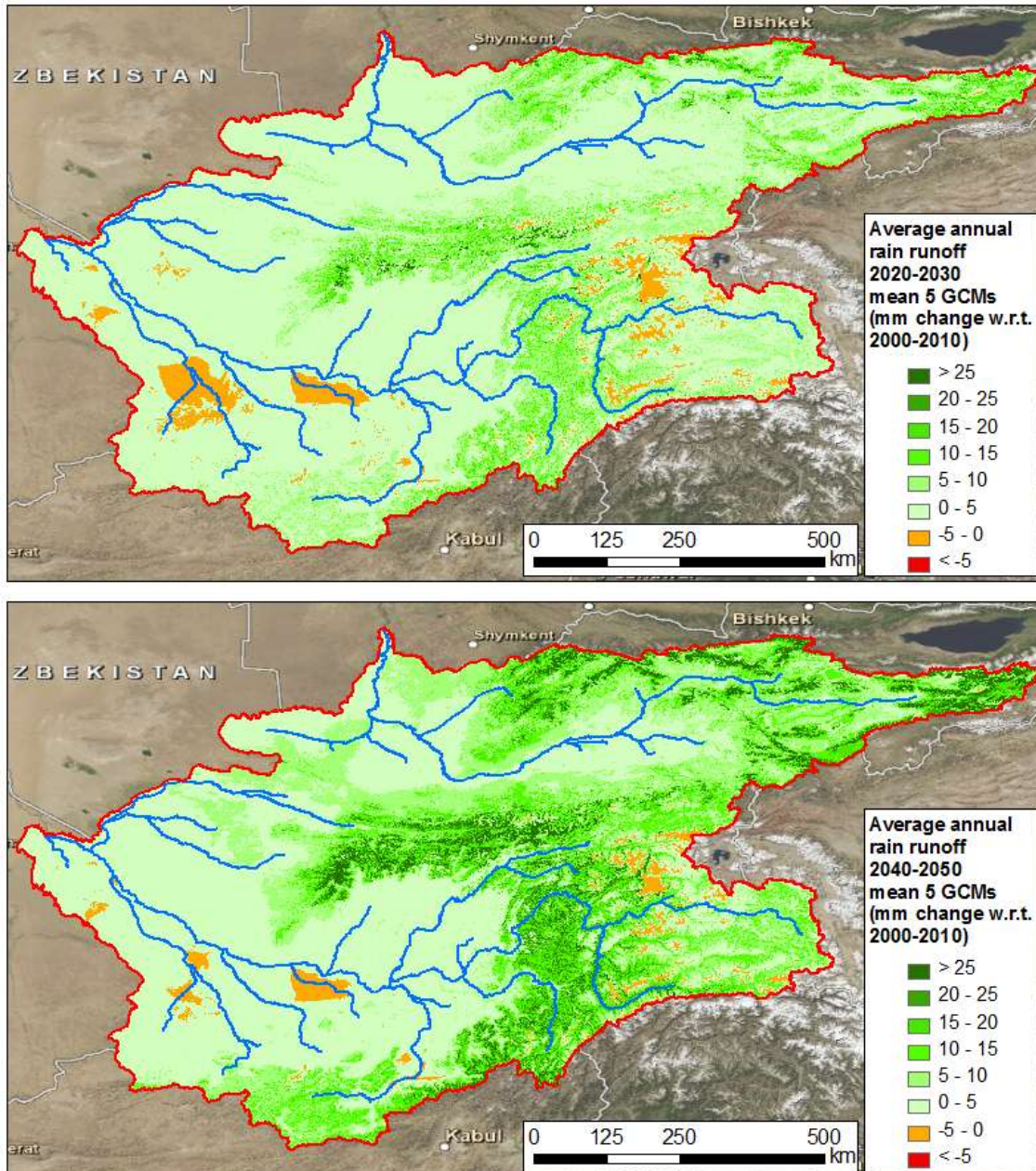


Figure 6-26: Change in average annual runoff generation from rain per grid cell (mm change with respect to reference period) for 2021-2030 and 2041-2050. Mean of output after forcing model with 5 GCMs.



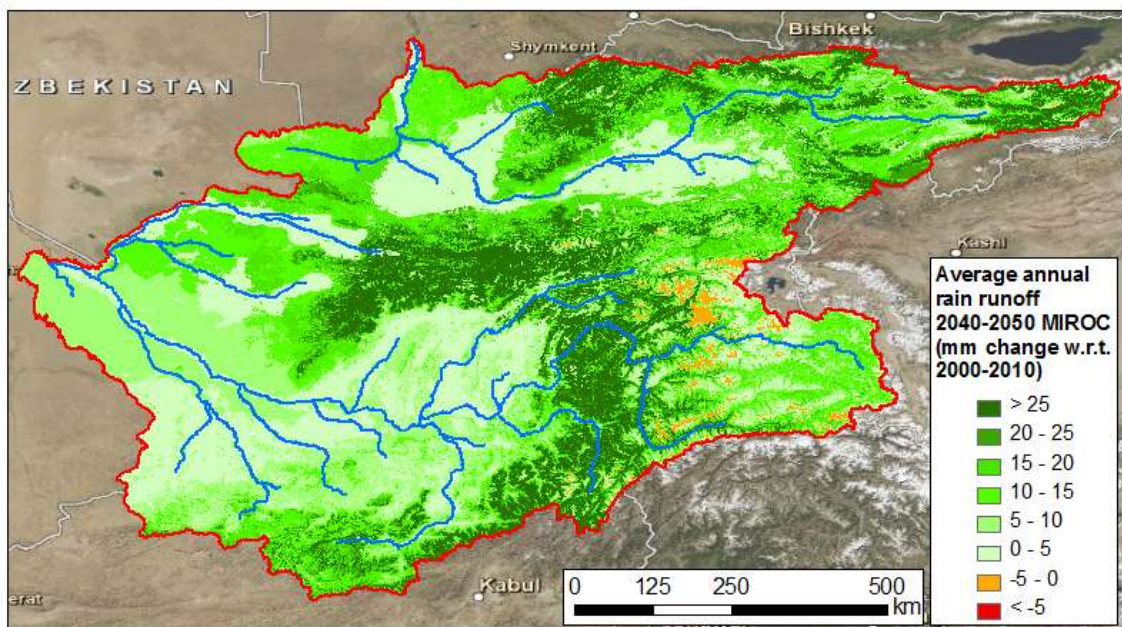
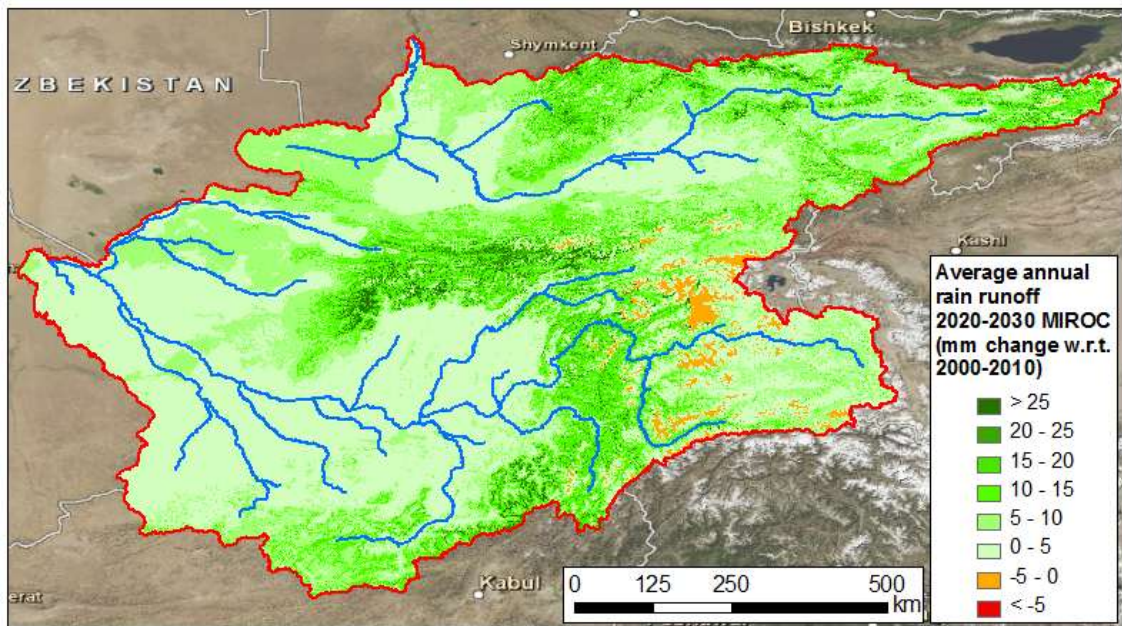


Figure 6-27: Change in average annual runoff generation from rain per grid cell (mm change with respect to reference period) for 2021-2030 and 2041-2050. Output for model forced with MIROC GCM.



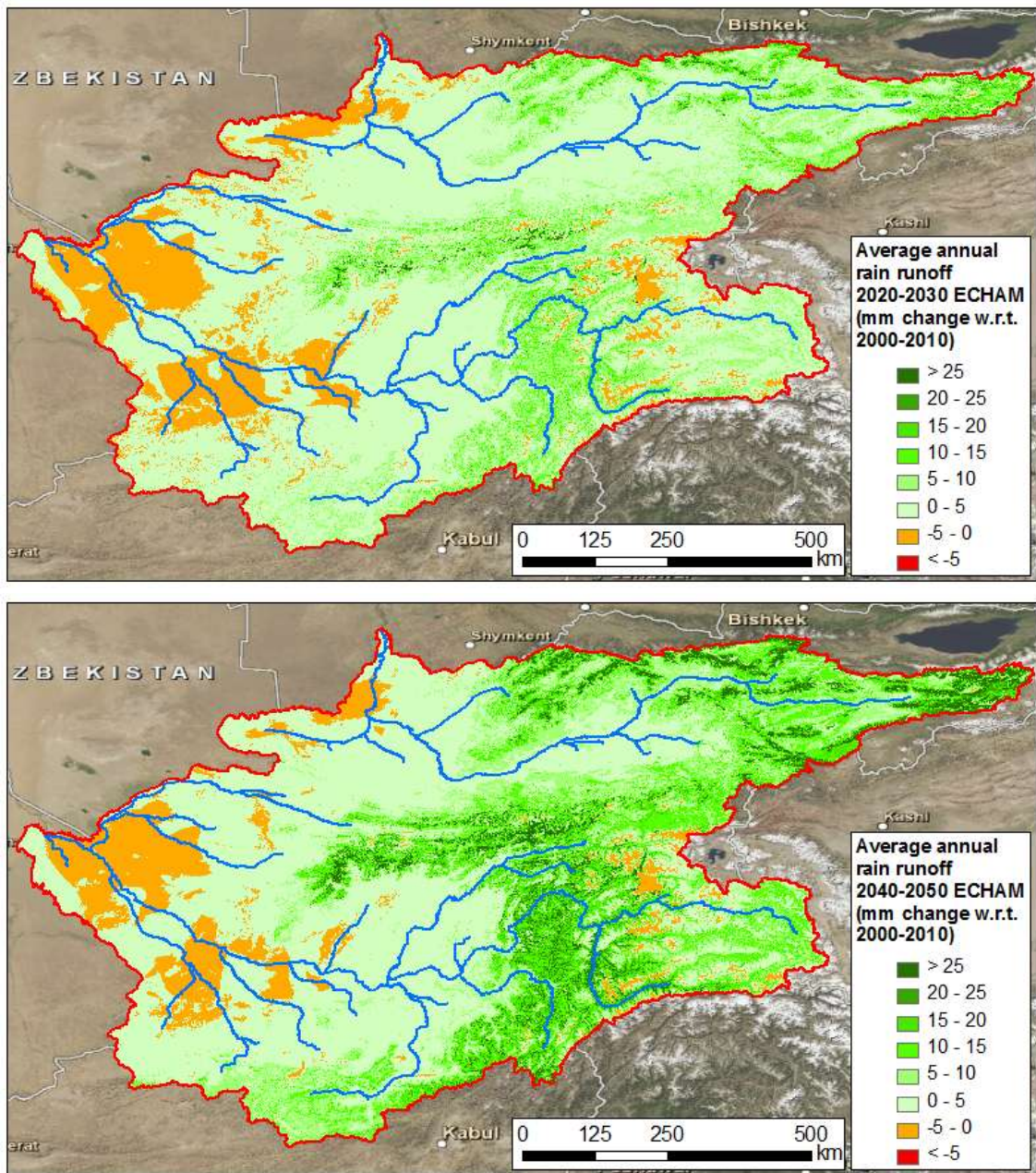


Figure 6-28: Change in average annual runoff generation from rain per grid cell (mm change with respect to reference period) for 2021-2030 and 2041-2050. Output for model forced with ECHAM GCM.

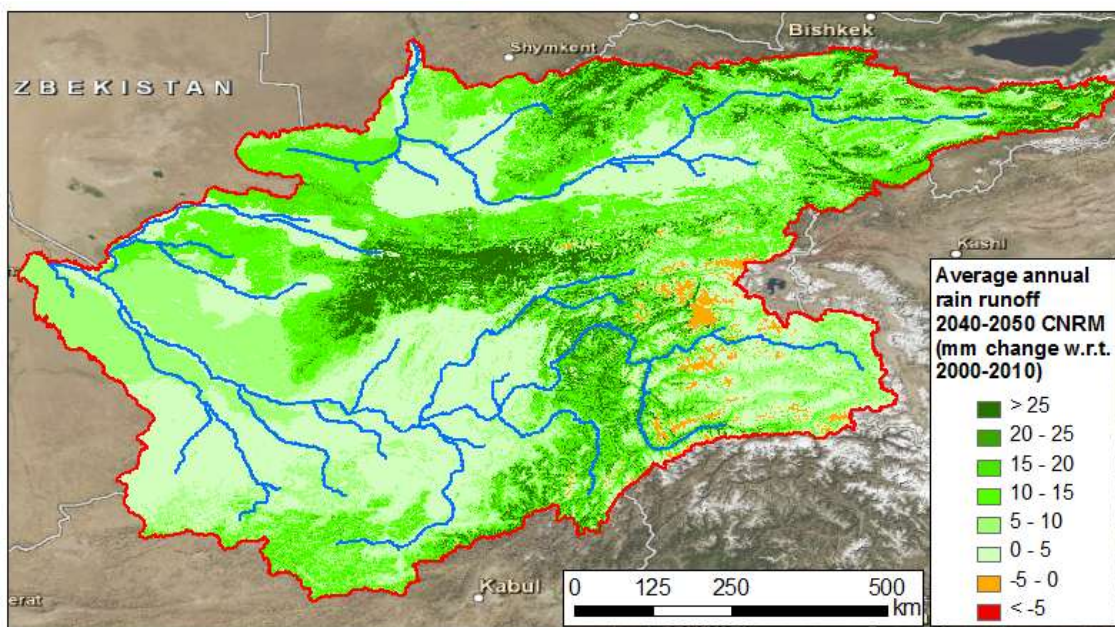
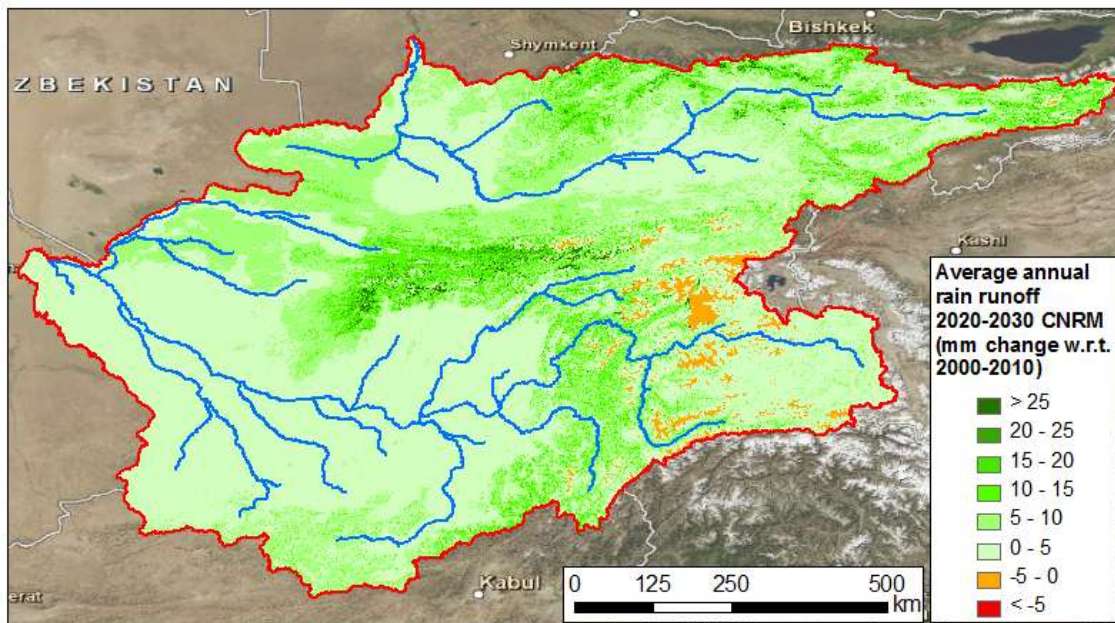


Figure 6-29: Change in average annual runoff generation from rain per grid cell (mm change with respect to reference period) for 2021-2030 and 2041-2050. Output for model forced with CNRM GCM.



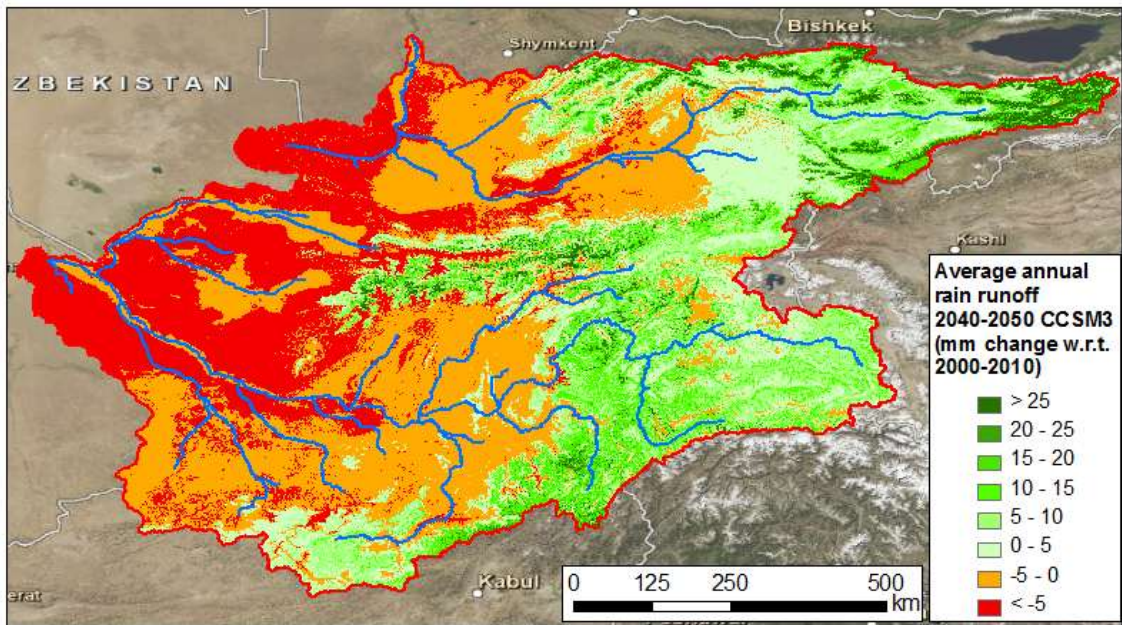
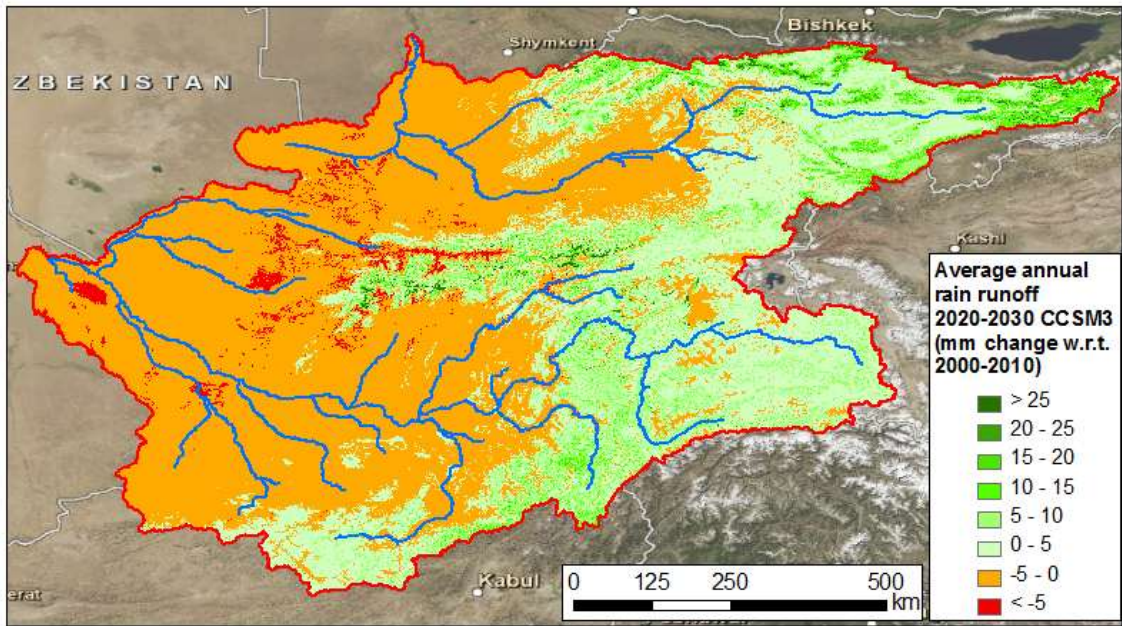


Figure 6-30: Change in average annual runoff generation from rain per grid cell (mm change with respect to reference period) for 2021-2030 and 2041-2050. Output for model forced with CCSM3 GCM.

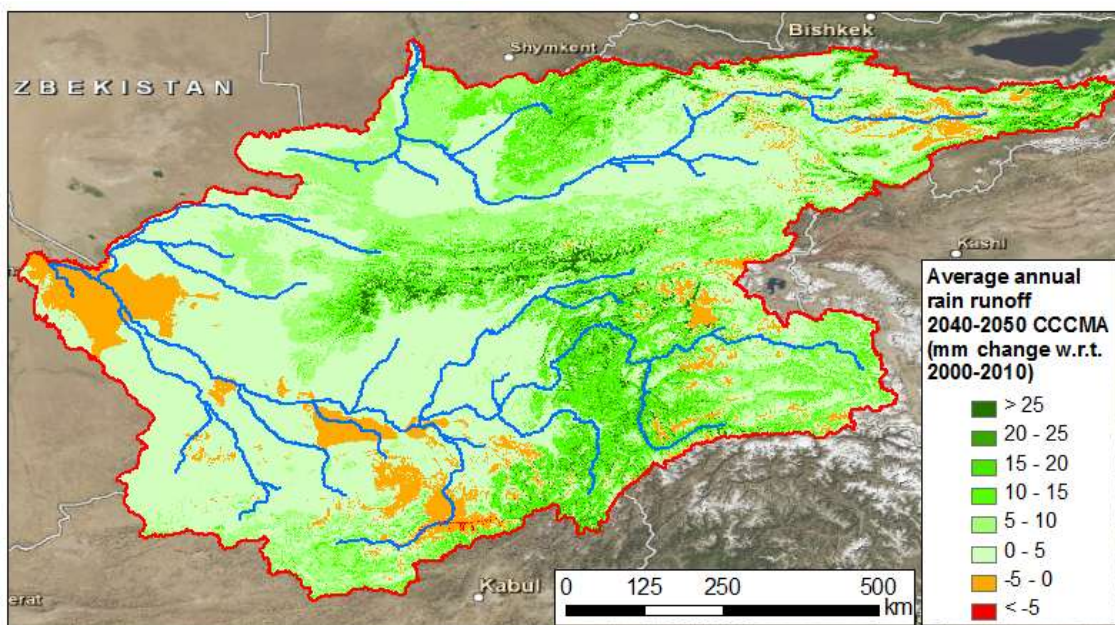
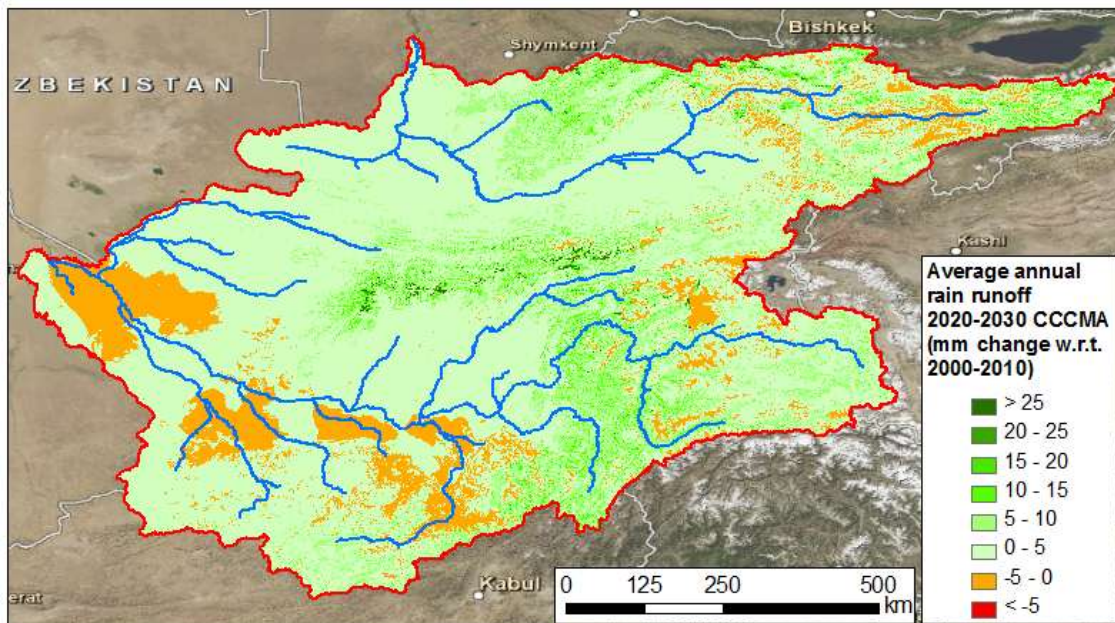


Figure 6-31: Change in average annual runoff generation from rain per grid cell (mm change with respect to reference period) for 2021-2030 and 2041-2050. Output for model forced with CCCMA GCM.

For most GCMs (except for CCSM3), the overall runoff originating from rainfall increases. There are two reasons for this development. First, the amount of precipitation to fall as rain increases while the amount of precipitation to fall as snow decreases, because the snowline is getting higher, as a result of higher temperatures. Second, the amount of precipitation is increasing for the MIROC, ECHAM, CNRM and CCCMA GCMs. The CCSM3 GCM projects decreasing precipitation, leading to decreased runoff from rain. The grid cells with 100% glaciated fraction don't generate runoff from rain in the model for the reference situation as well as for the future situations.



6.3.4 Changes in base flow

Figure 6-32 shows the mean change in average annual base flow generation per grid cell for 2021-2030 and 2041-2050 with respect to the reference period (2001-2010). Changes are given in millimeters per year. Figure 6-33 to Figure 6-37 show the changes in base flow generation when the model is forced by the five different GCMs, also in millimeters per year.

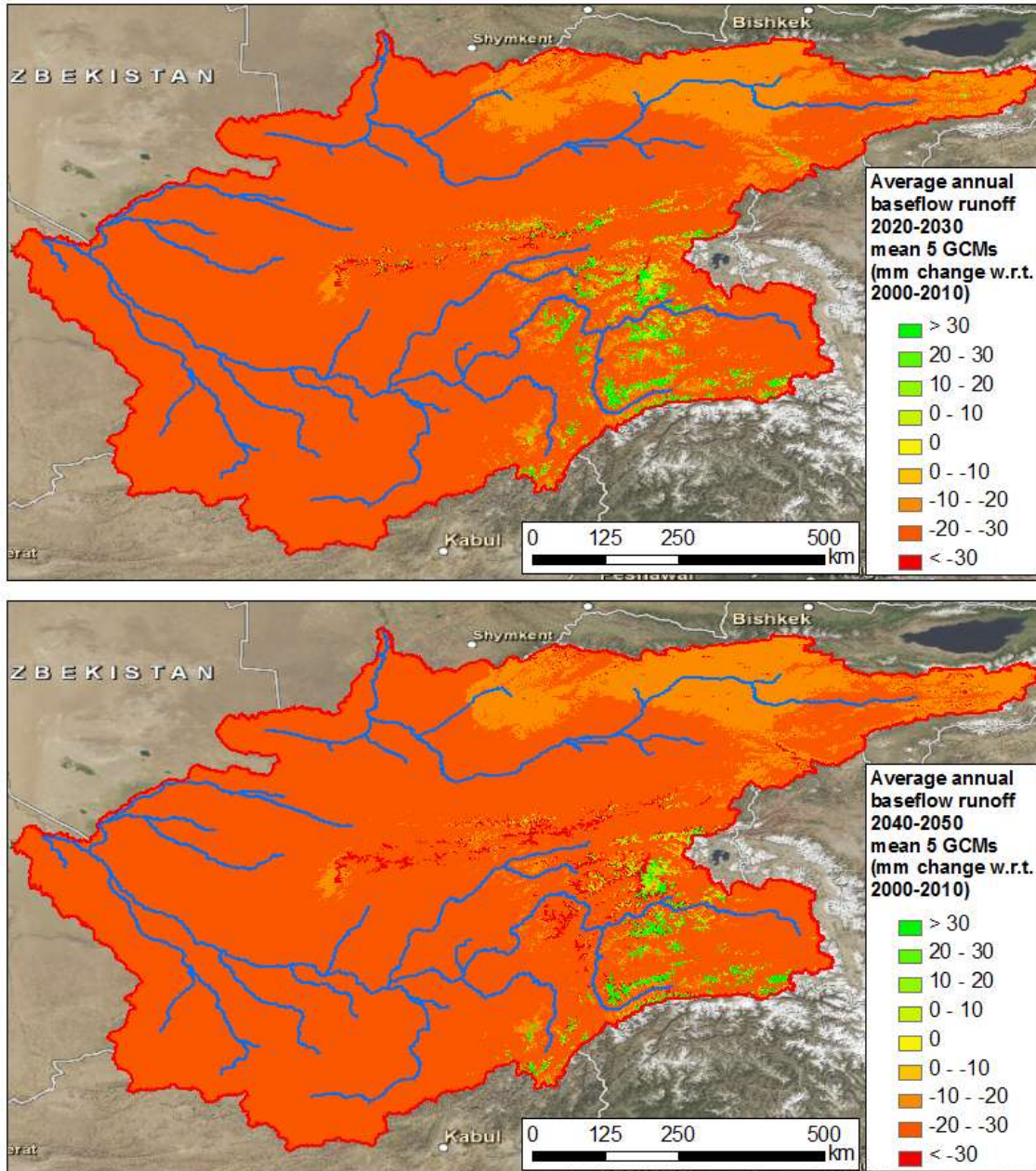


Figure 6-32: Change in average annual base flow generation per grid cell (mm change with respect to reference period) for 2021-2030 and 2041-2050. Mean of output after forcing model with 5 GCMs.



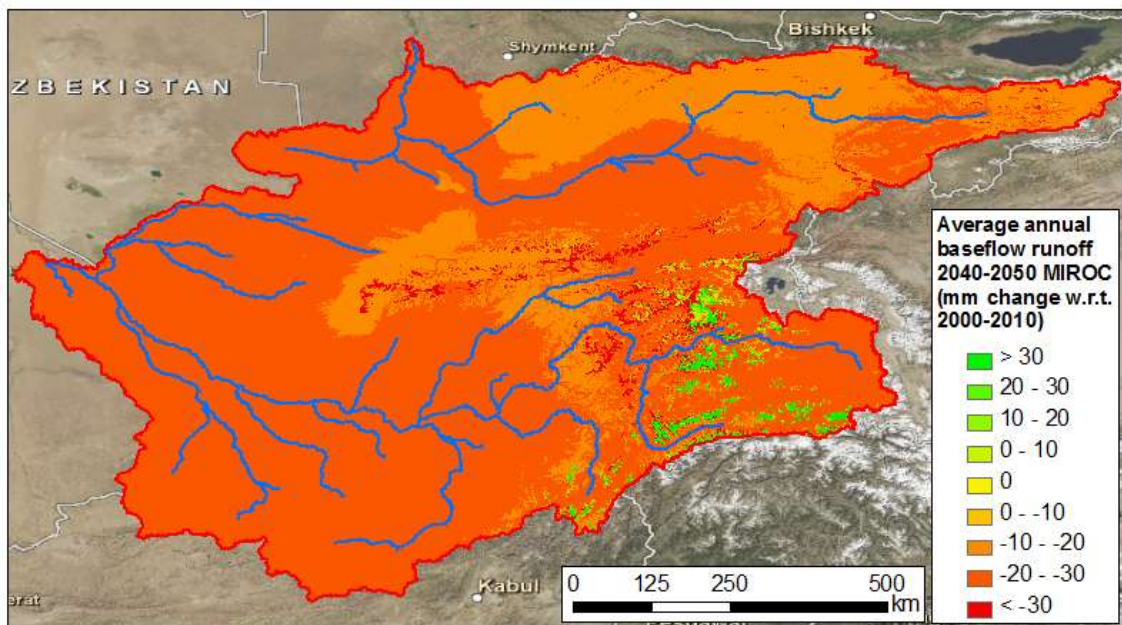
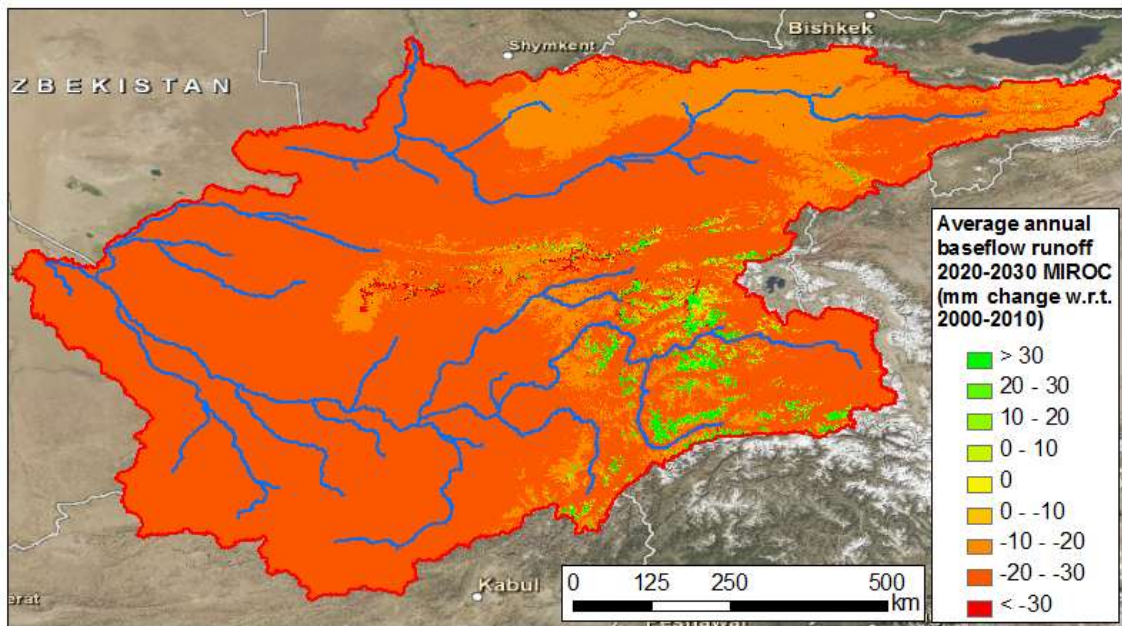


Figure 6-33: Change in average annual base flow generation per grid cell (mm change with respect to reference period) for 2021-2030 and 2041-2050. Output for model forced with MIROC GCM.



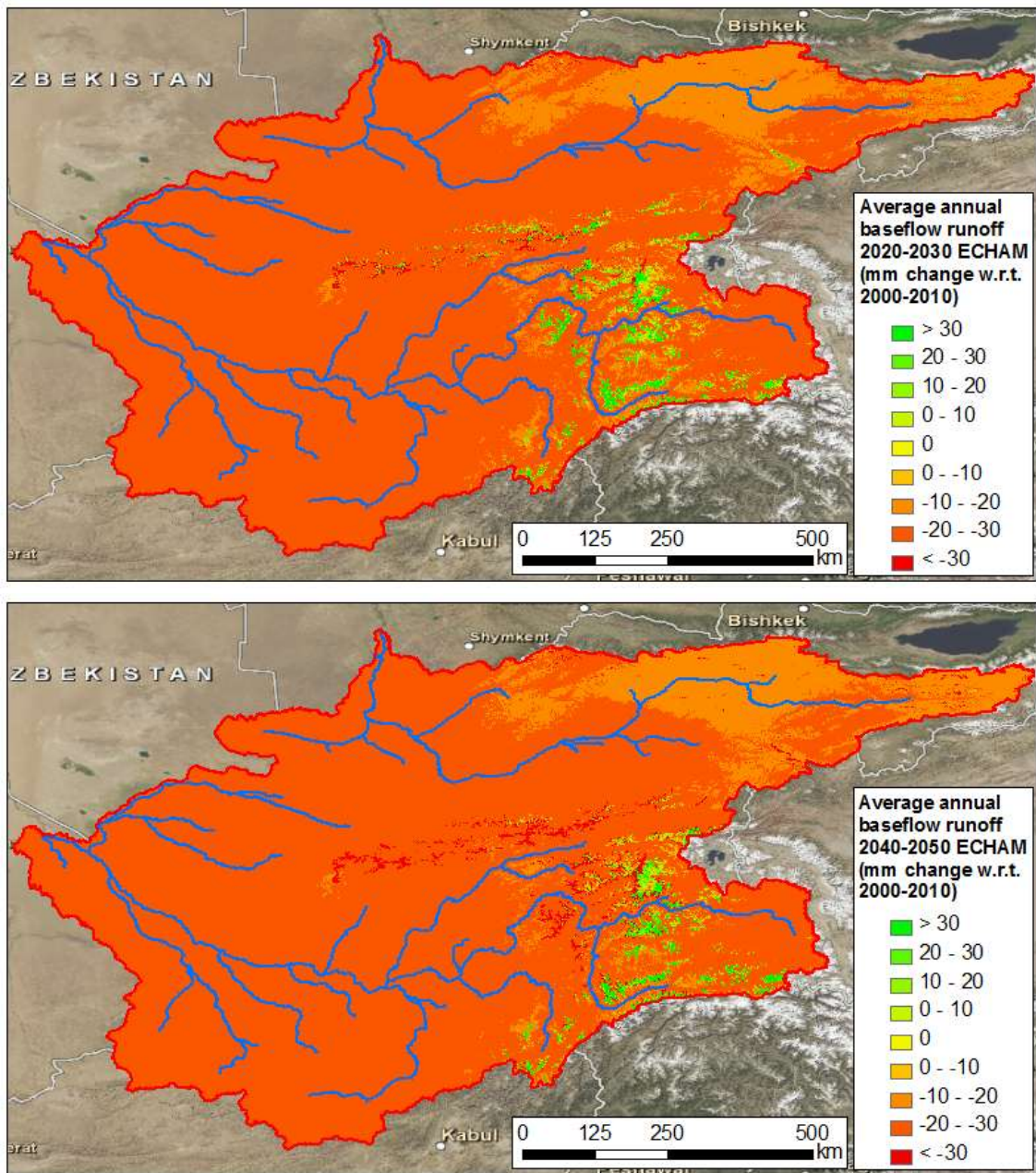


Figure 6-34: Change in average annual base flow generation per grid cell (mm change with respect to reference period) for 2021-2030 and 2041-2050. Output for model forced with ECHAM GCM.

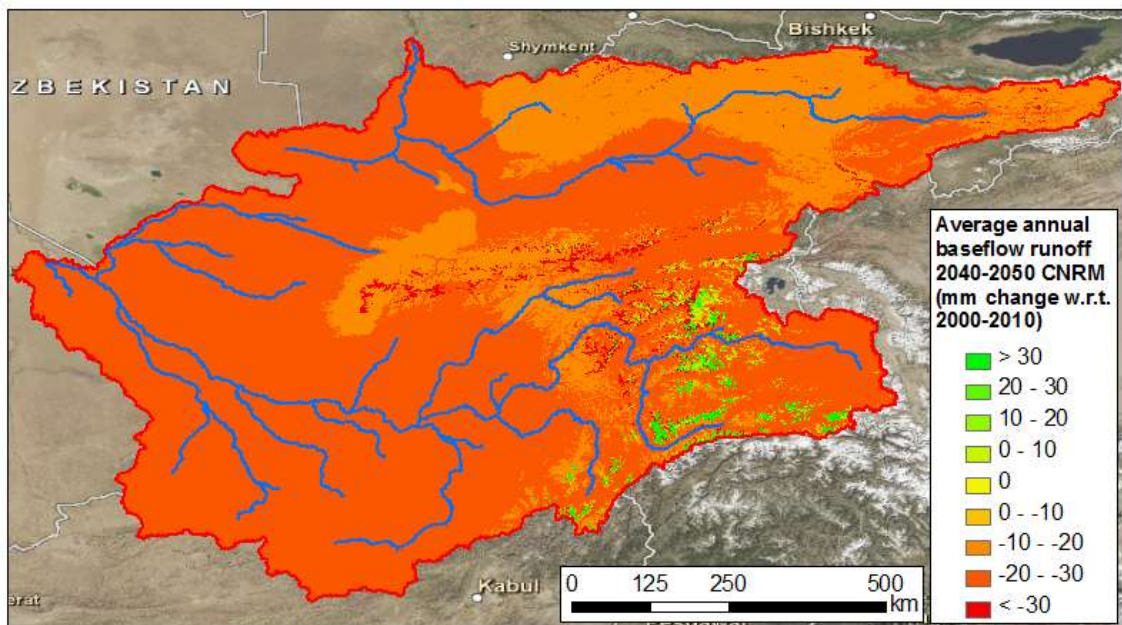
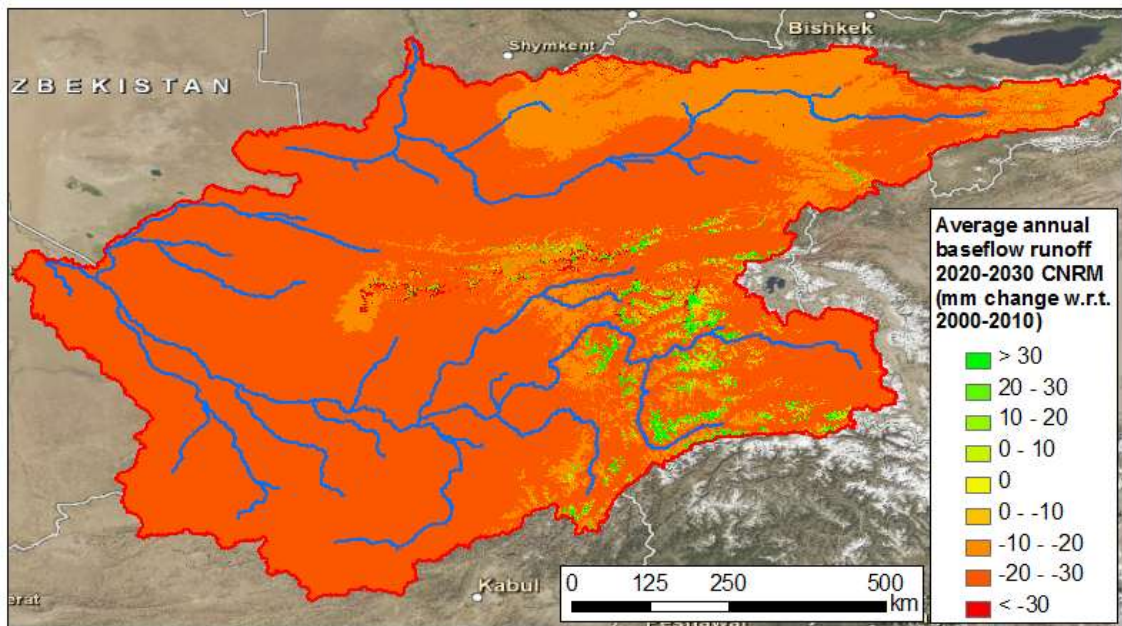


Figure 6-35: Change in average annual base flow generation per grid cell (mm change with respect to reference period) for 2021-2030 and 2041-2050. Output for model forced with CNRM GCM.



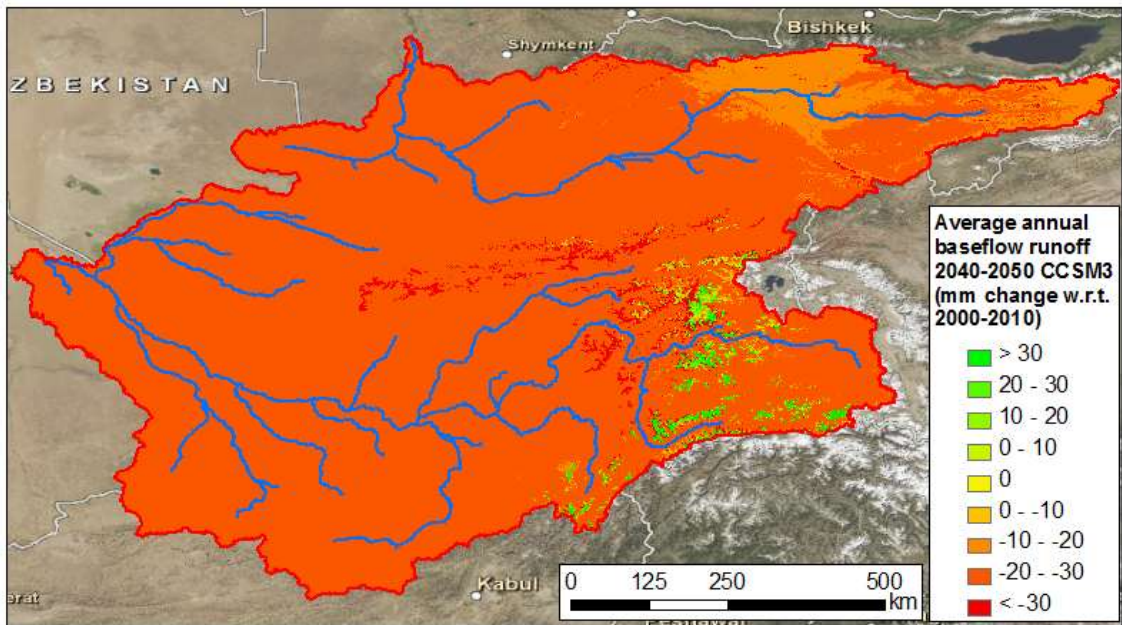
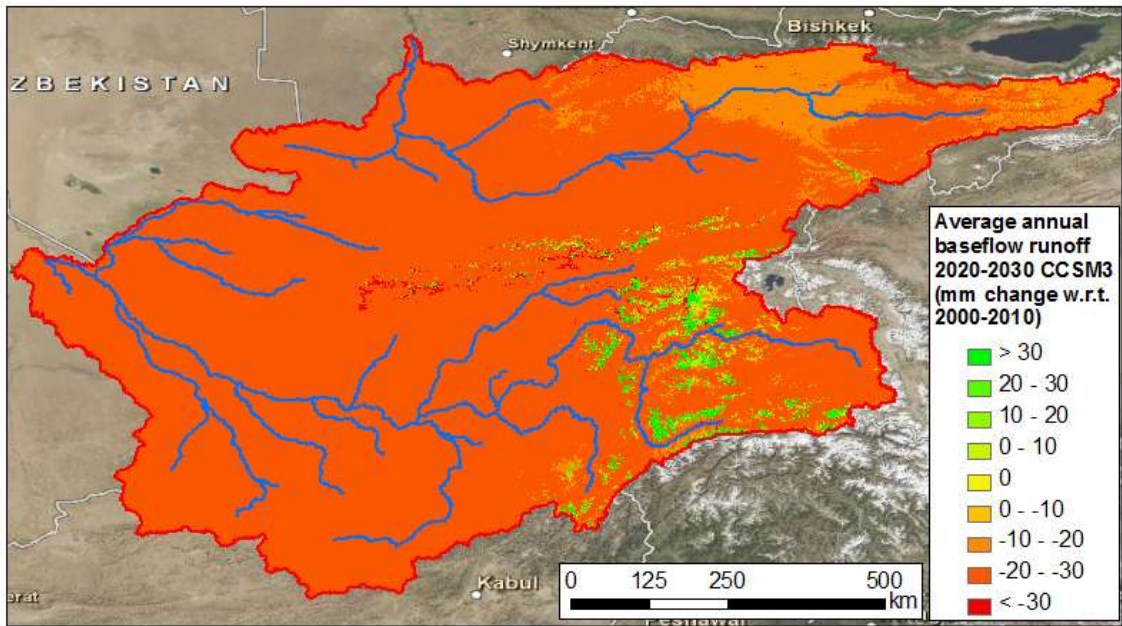


Figure 6-36: Change in average annual base flow generation per grid cell (mm change with respect to reference period) for 2021-2030 and 2041-2050. Output for model forced with CCSM3 GCM.



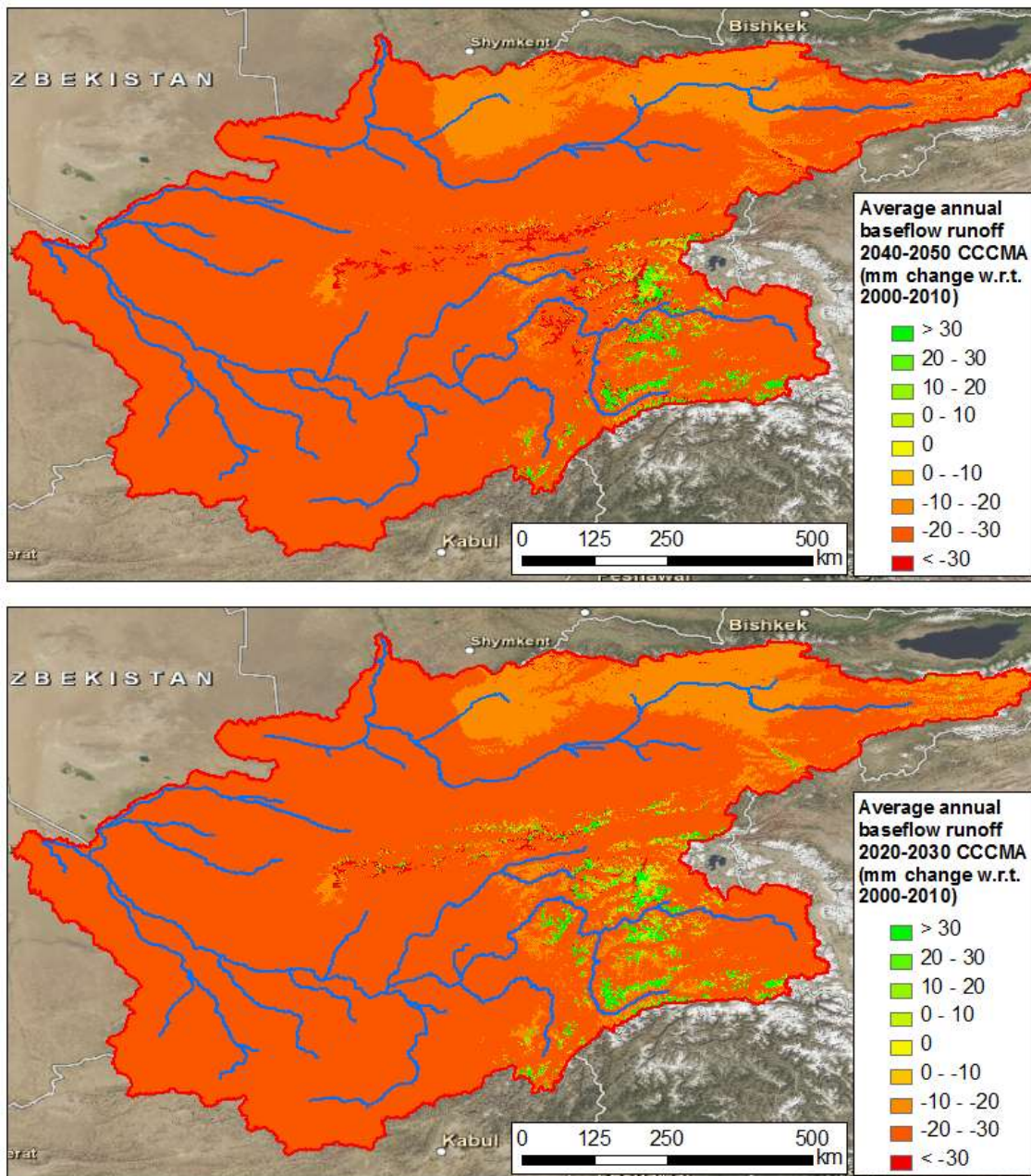


Figure 6-37: Change in average annual base flow generation per grid cell (mm change with respect to reference period) for 2021-2030 and 2041-2050. Output for model forced with CCCMA GCM.

The base flow in the model is related to the total runoff generated by the three other components (glacier melt, snow melt and rain). Therefore, the spatial patterns of changes in base flow generation resemble the spatial patterns of the changes in total runoff generation (Figure 6-8 to Figure 6-13).

6.3.5 Changes in runoff composition

The relative contribution of melt water to the total runoff differs strongly in space as demonstrated in paragraph 5.2 (Figure 5-12 to Figure 5-14 and Figure 5-4 to Figure 5-6). For the Amu Darya, glacial and snow melt are much more important compared to the Syr Darya.



Besides, glacier and snow melt have higher relative contributions in more upstream areas compared to more downstream areas. This also means that the impact of climate change on runoff generation is more severe for the Amu Darya than for the Syr Darya. This is easily illustrated when comparing the development of inflow into Toktogul reservoir in the Syr Darya basin (Figure 6-38) and Nurek reservoir in the Amu Darya basin (Figure 6-39). See Figure 4-12 for the locations of the mentioned reservoirs.

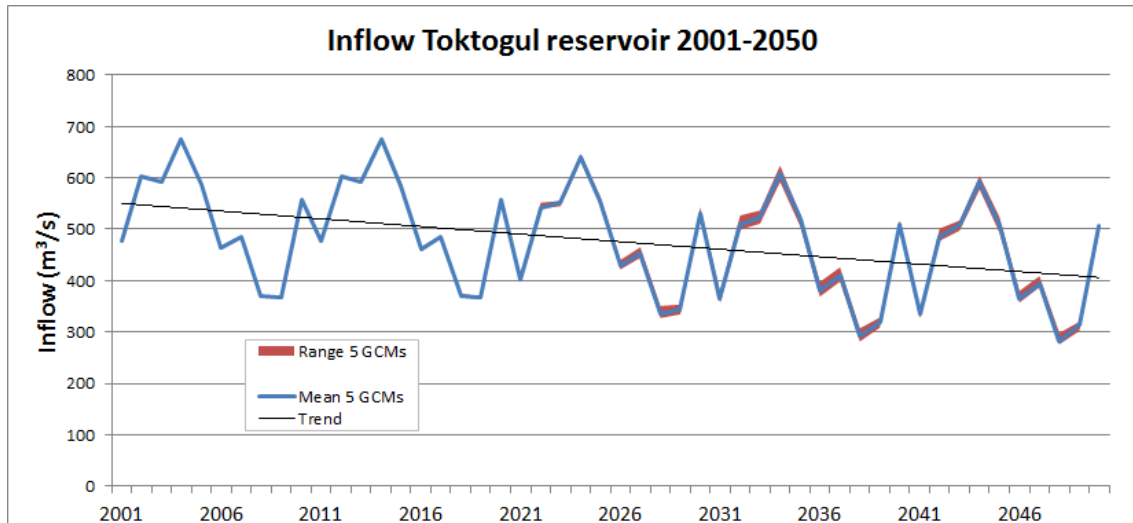


Figure 6-38: Projected average annual inflow Toktogul reservoir 2001-2050. Figure shows mean of model output when forced with 5 GCMs and the range of projections when forced by 5 GCMs.

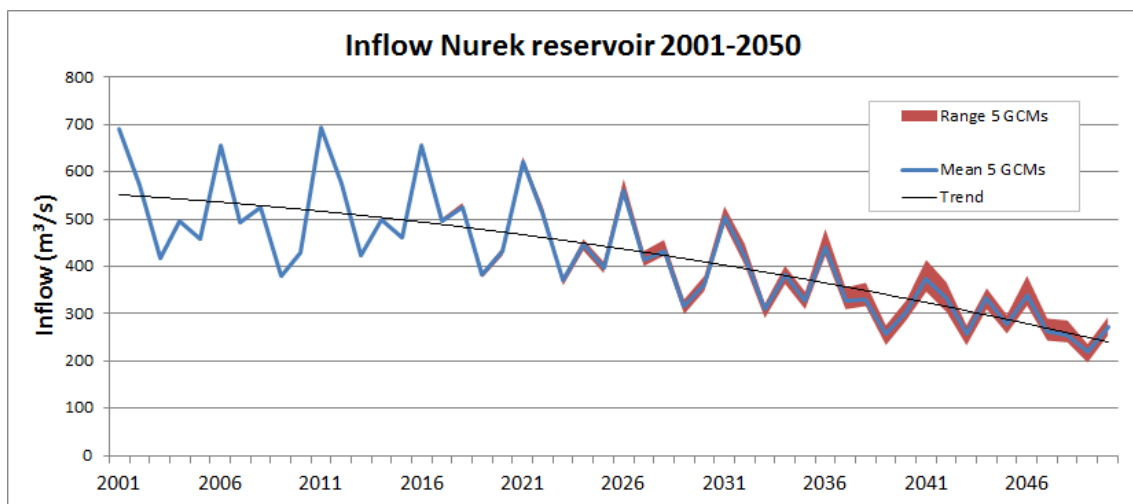


Figure 6-39: Projected average annual inflow Nurek reservoir 2001-2050. Figure shows mean of model output when forced with 5 GCMs and the range of projections when forced by 5 GCMs.

When looking at the trends for the changes in inflow into the reservoirs a decrease for both reservoirs is observed. However, this decrease is much stronger for Nurek reservoir in the Amu Darya and also more accelerated towards the end of the time interval. By looking at the contributions of the different runoff components (glacier melt, snow melt, rain and baseflow) this can be explained (Figure 6-40, Figure 6-41).

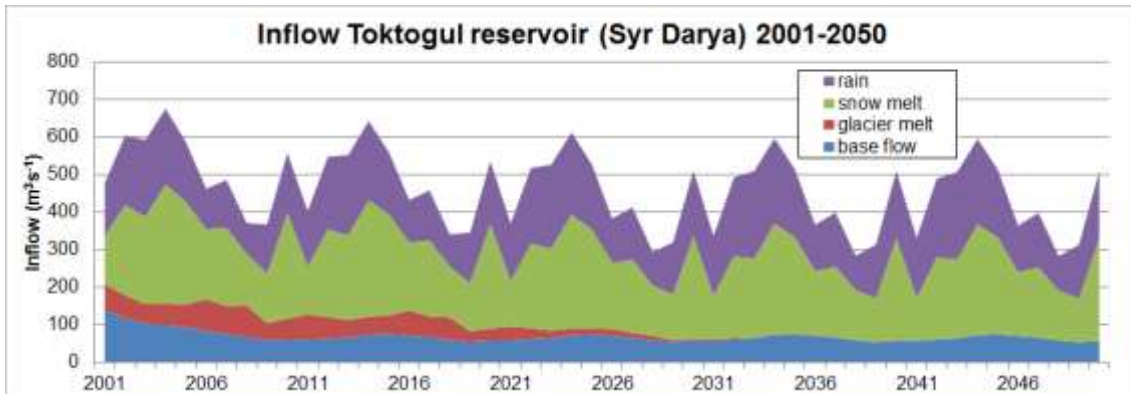


Figure 6-40: Projected average annual inflow Toktogul reservoir 2001-2050 per runoff component. Figure shows mean of model output when forced with 5 GCMs.

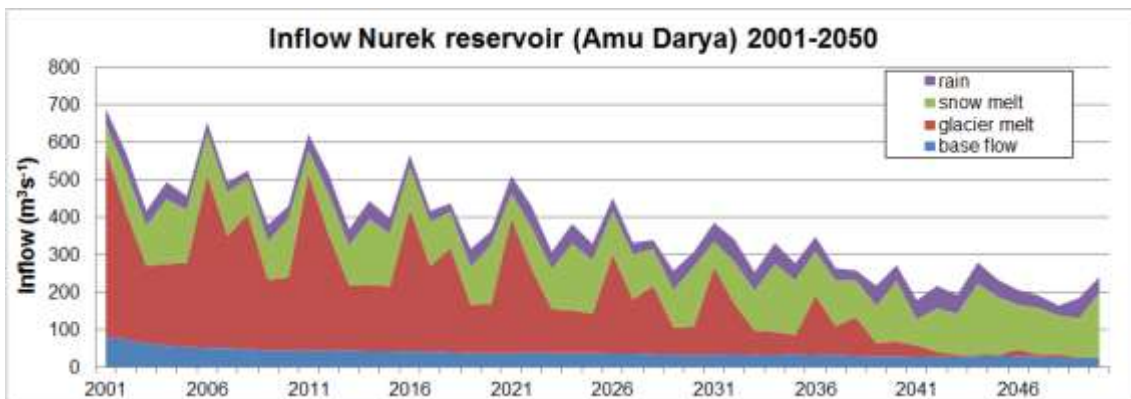


Figure 6-41: Projected average annual inflow Nurek reservoir 2001-2050 per runoff component. Figure shows mean of model output when forced with 5 GCMs.

The glacier melt plays a much larger role for the total runoff for the inflow into Nurek reservoir than for the inflow into Toktogul reservoir. As the contribution of glacier melt decreases dramatically until 2050, the inflow into Nurek reservoir also decreases very significantly. This effect is much smaller for Toktogul reservoir, although the contribution of glacier melt becomes zero, meaning all glaciers in this catchment have disappeared.

6.4 Simulated inflow to downstream areas

The runoff generated in the upstream parts of the basins is routed to the downstream parts of the basins. Figure 6-42 shows the division in upstream areas for which the runoff generation is modeled. The runoff flowing into the downstream areas from these areas is modeled and used as input in different locations for the downstream model. The simulated inflow from the mountainous regions into the reservoirs and downstream agricultural areas changes significantly. Especially the inflow from glacier melt decreases significantly in the future. Figure 6-43 to Figure 6-48 show the simulated projected change in inflow at the boundary between the upstream AralMountain model and the downstream WEAP-model for the reference situation (2001-2010) and future situations (2021-2030, 2041-2050). The graphs show the range of projections when the model is forced by the five mentioned GCMs. The AralMountain model output at these locations is used as input for the downstream WEAP-model.



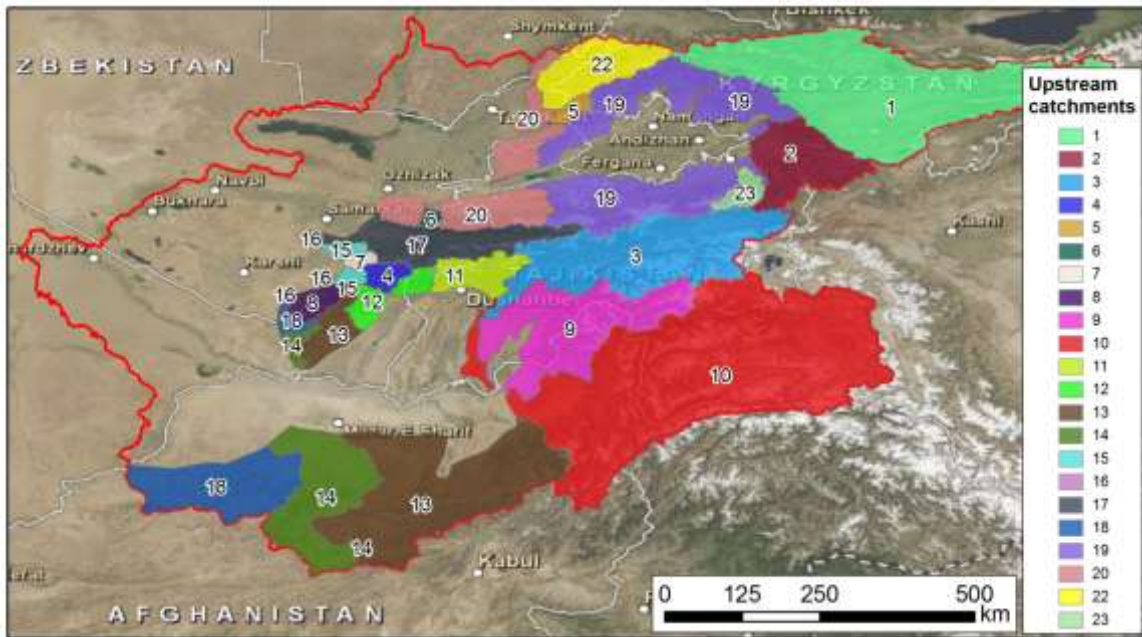


Figure 6-42: Upstream catchments used to calculate inflow from upstream to downstream areas. See Table 10 for corresponding catchment names.

Table 10: Catchment names Figure 6-42.

Catchment no.	Catchment name
1	Toktogul reservoir
2	Andijan reservoir
3	Nurek reservoir
4	Tupalangskoe reservoir
5	Akhangaran reservoir
6	Zaamin reservoir
7	Gissarak reservoir
8	Pachkamar reservoir
9	Kulyab catchment
10	Kurgantube catchment
11	Dushanbe catchment
12	Surkhandarya upstream catchment
13	Surkhandarya downstream catchment
14	Karukum kanal catchment
15	Kashkadarya upstream catchment
16	Kashkadarya downstream catchment
17	Zeravshan Valley catchment
18	Lebap upstream catchment
19	Fergana Valley catchment
20	Syrdaryo, Tashkent, Jizakh catchment
21	South Kazakhstan upstream catchment
22	Charvak reservoir
23	Papan reservoir

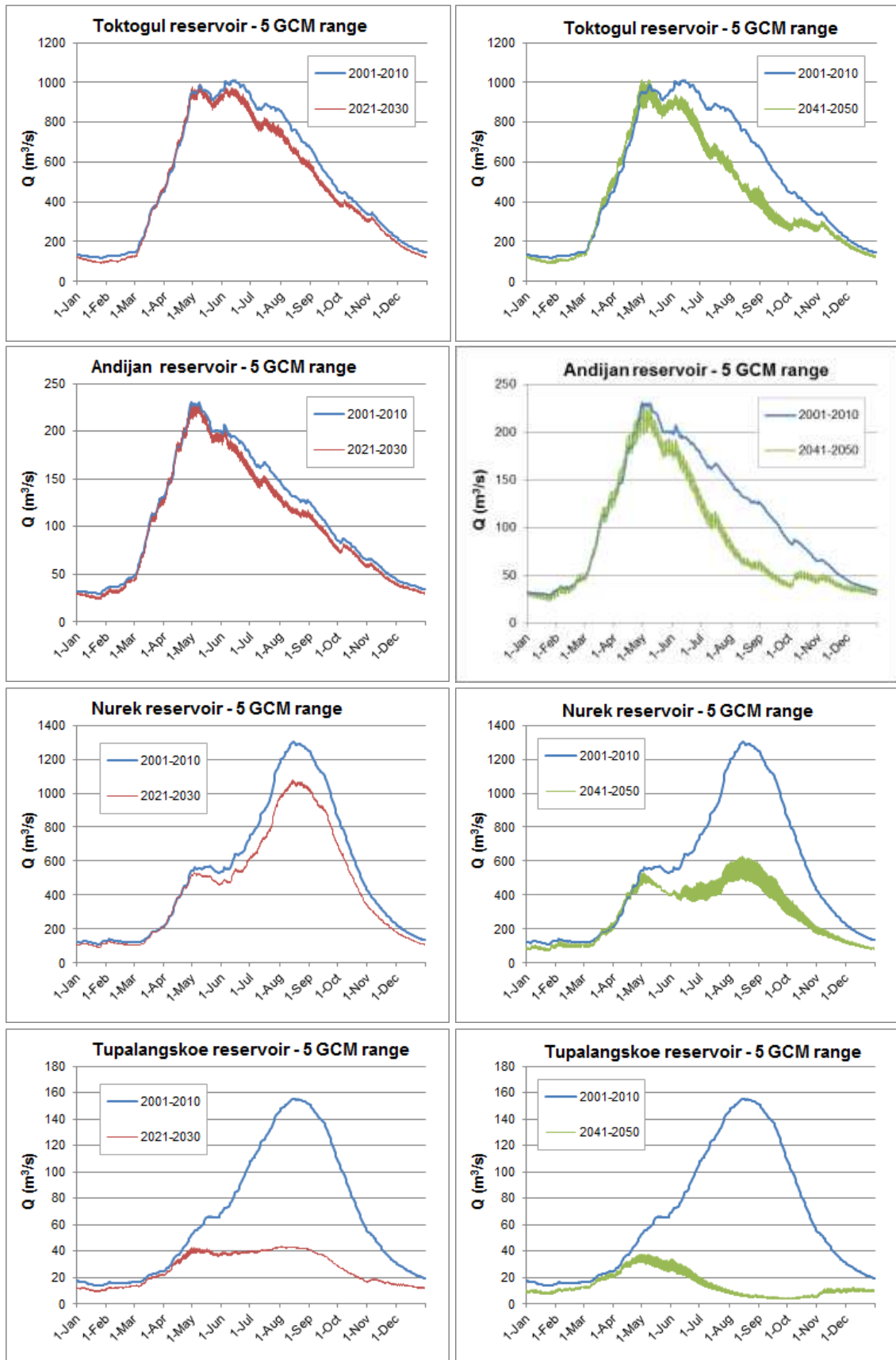


Figure 6-43: Hydrographs for inflow from upstream into downstream areas showing future projections (2021-2030, 2041-2050) compared to reference period (2001-2010). The range of outputs for the model forced by five GCMs is shown.



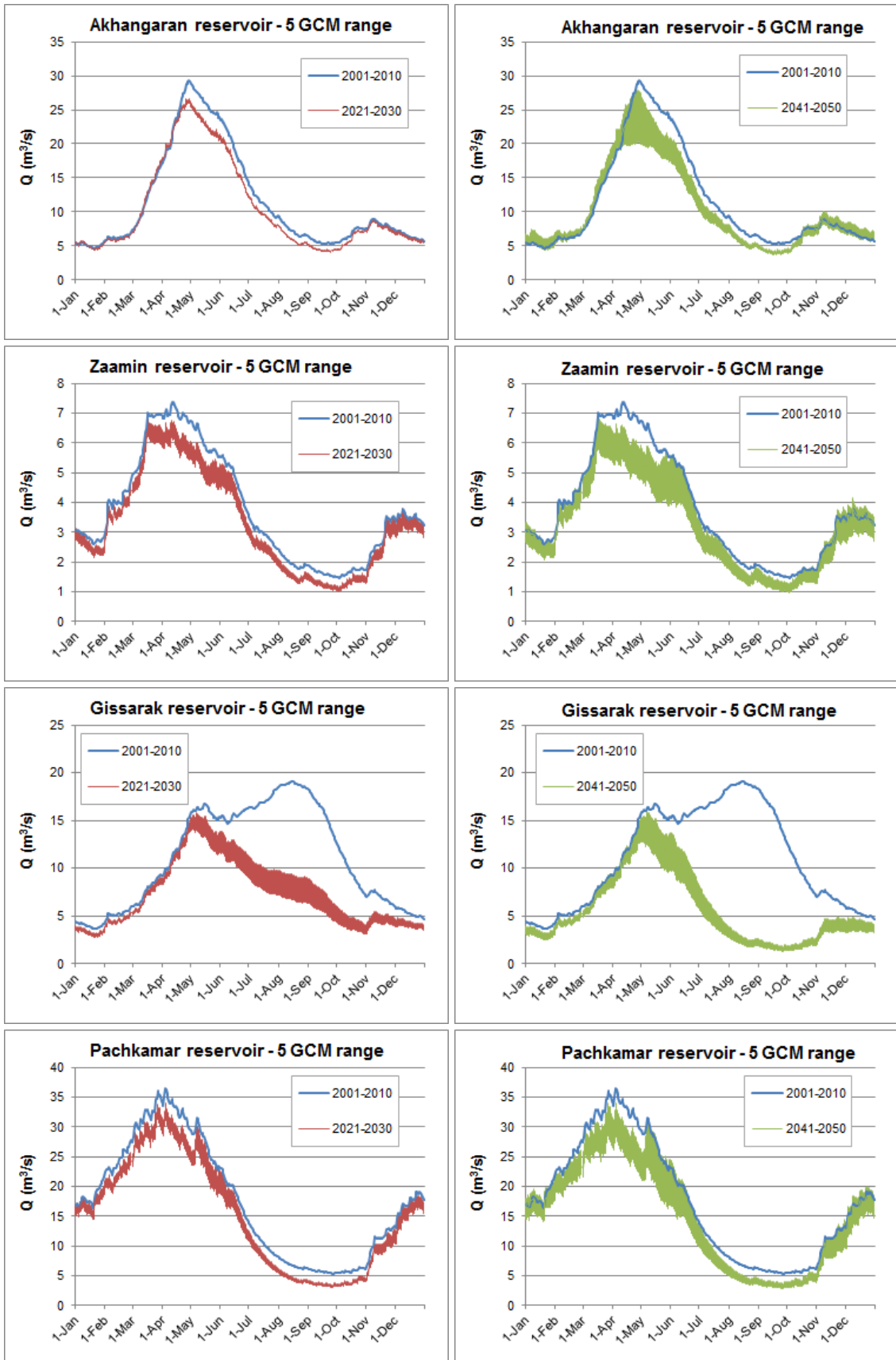


Figure 6-44: Hydrographs for inflow from upstream into downstream areas showing future projections (2021-2030, 2041-2050) compared to reference period (2001-2010). The range of outputs for the model forced by five GCMs is shown.



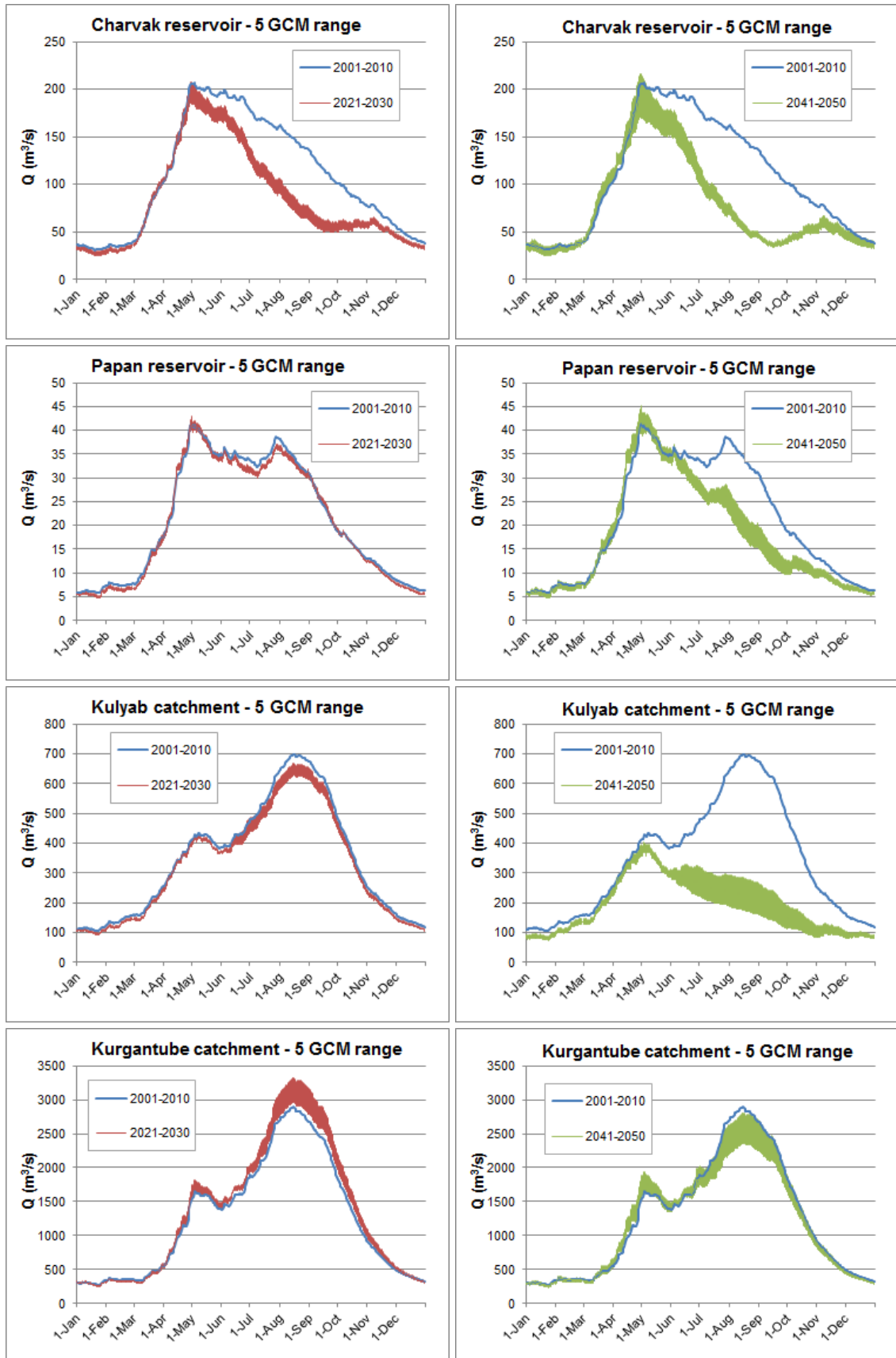


Figure 6-45: Hydrographs for inflow from upstream into downstream areas showing future projections (2021-2030, 2041-2050) compared to reference period (2001-2010). The range of outputs for the model forced by five GCMs is shown.



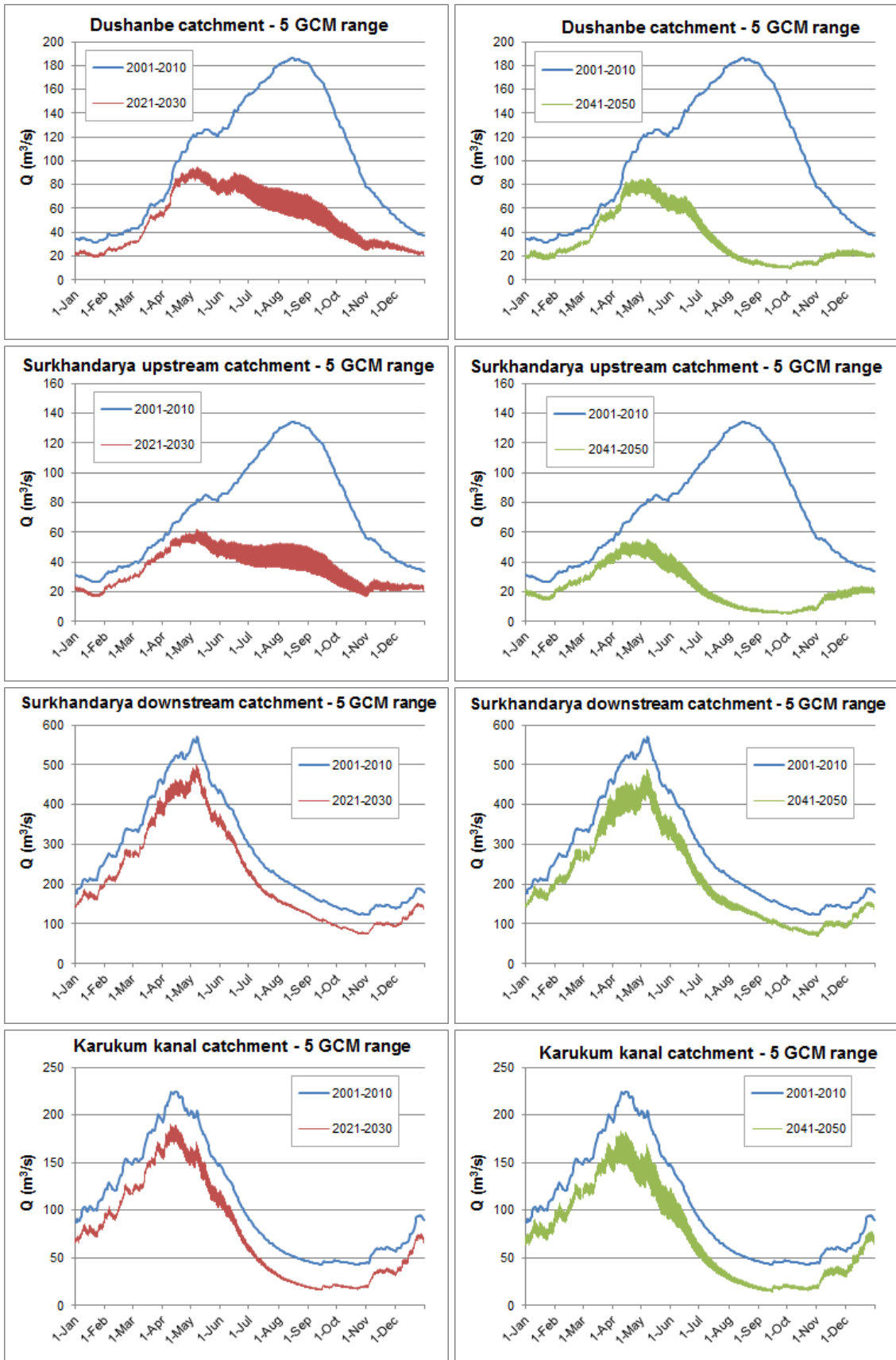


Figure 6-46: Hydrographs for inflow from upstream into downstream areas showing future projections (2021-2030, 2041-2050) compared to reference period (2001-2010). The range of outputs for the model forced by five GCMs is shown.



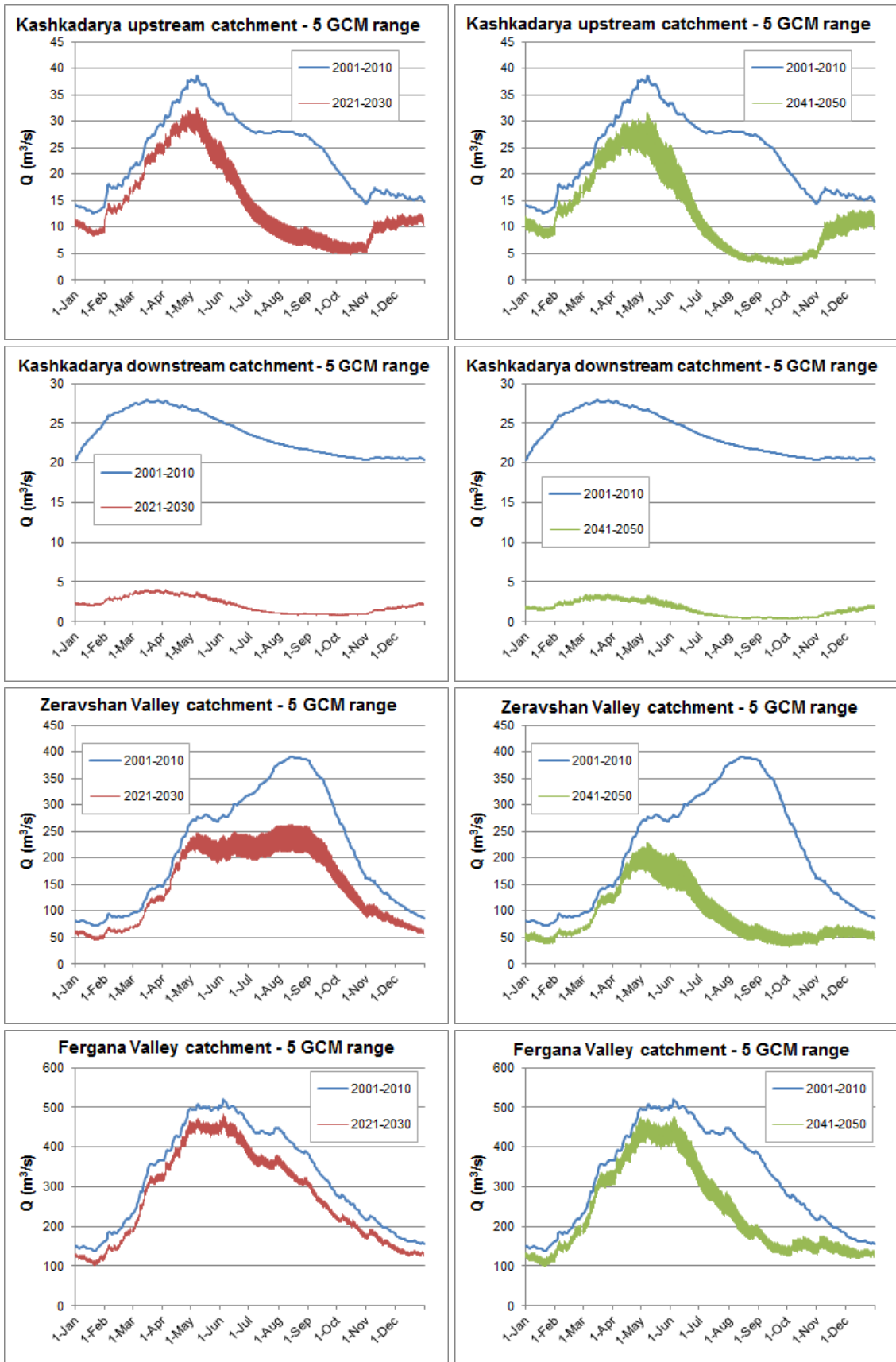


Figure 6-47: Hydrographs for inflow from upstream into downstream areas showing future projections (2021-2030, 2041-2050) compared to reference period (2001-2010). The range of outputs for the model forced by five GCMs is shown.



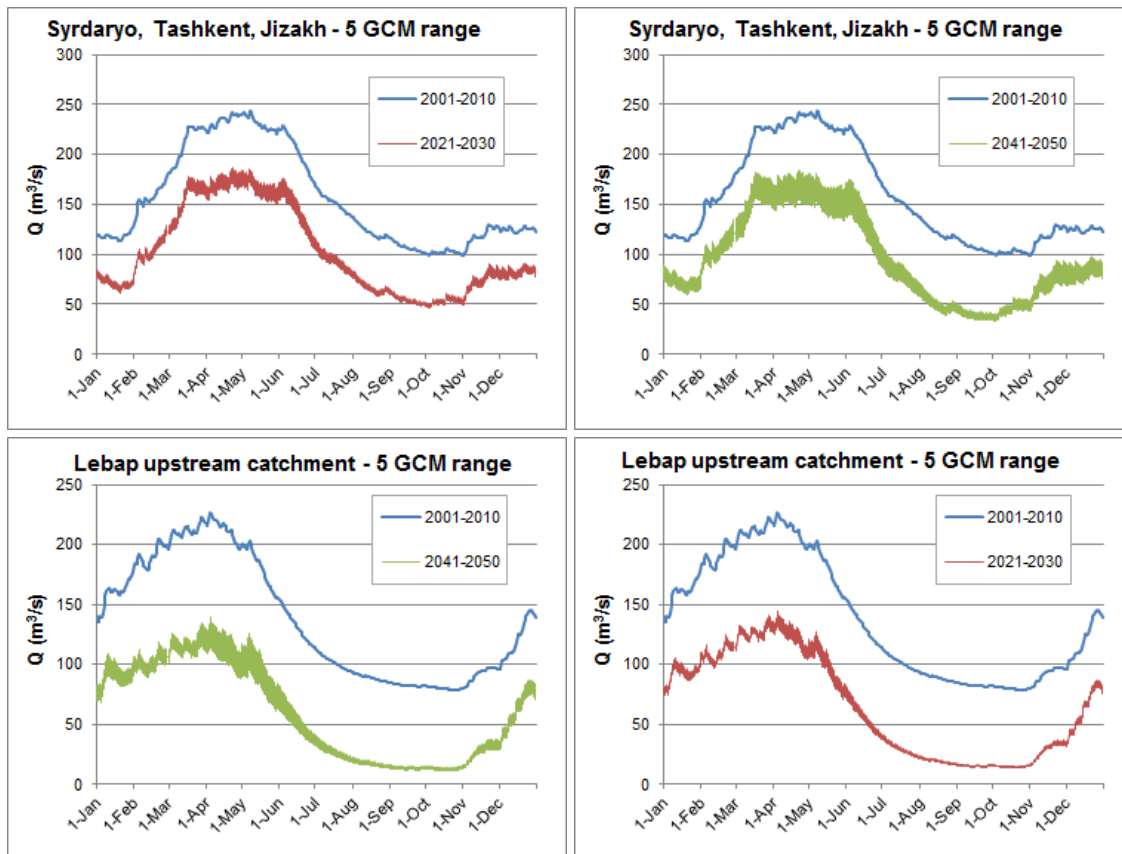


Figure 6-48: Hydrographs for inflow from upstream into downstream areas showing future projections (2021-2030, 2041-2050) compared to reference period (2001-2010). The range of outputs for the model forced by 5 GCMs is shown.

The modeled runoff projections show that the impact of climate change for river runoff is highly variable in the region. Most of the hydrographs show a decrease in runoff. For the highly glacierized Kurgantube catchment, the model projects increased runoff generation for 2021-2030, which turns into a decrease by 2041-2050. As this area is highly glacierized, a temperature increase will lead to initial increases in runoff originating from glacier melt, but ultimately cause a decrease in runoff generation because the glacierized surface decreases.

From the reported changes in water inflow into downstream users (in fact the runoff at the boundary locations between the upstream model and the downstream model) it also becomes clear that the Amu Darya basin is more vulnerable to climate change than the Syr Darya basin, because of the decreasing glacierized area. A typical example is the decreases in runoff for Dushanbe catchment, Gissarak reservoir, Nurek reservoir, Tupalangskoe reservoir, Kashkhadarya upstream and downstream catchments, the Zeravshan Valley catchment, Surkhandarya upstream catchment and Kulyab catchment in Figure 6-43 to Figure 6-48. All of these catchments have glaciers in their catchments. The runoff peaks in early summer for some of them remain quite high, but last much shorter, especially in 2041-2050. The climate change impact is less strong for catchments where runoff is dominated by rain and snow, although also in these areas the climate change impact for runoff generation is significant. See for example the Fergana Valley catchment, Toktogul reservoir, Papan reservoir, and Andijan reservoir. The impact of climate change is less significant for the lower, more downstream parts like Surkhandarya downstream catchment, and Karakum kanal catchment. The absolute changes in runoff at the boundary locations is listed in Table 11.

Table 12 lists the relative changes in runoff at the boundary locations including the range of projected changes when the model is forced with the five mentioned GCMs.

Table 11: Simulated average annual inflow into downstream areas (Mm³) for reference period (2001-2010) and future situations (2021-2030, 2041-2050). Values are mean values for the five GCM outputs.

	Toktogul reservoir	Andijan reservoir	Nurek reservoir	Tupalangskoe reservoir	Akhangaran reservoir	Zaamin reservoir
2001-2010	16424	3481	16772	2107	362	119
2021-2030	15144	3235	14099	849	333	105
2041-2050	13576	2717	9430	456	328	104

	Gissarak reservoir	Pachkamar reservoir	Kulyab catchment	Kurgantube catchment	Dushanbe catchment	Surkhandarya upstream catchment
2001-2010	353	552	10960	39500	3203	2322
2021-2030	233	480	10402	42245	1614	1142
2041-2050	180	477	6087	38593	1088	737

	Surkhandarya downstream catchment	Karakum kanal catchment	Kashkadarya upstream catchment	Kashkadarya downstream catchment	Zeravshan Valley catchment	Lebap upstream catchment
2001-2010	8718	3309	754	743	6855	4335
2021-2030	6882	2389	458	66	4772	2049
2041-2050	6619	2298	408	51	2918	1924

	Fergana Valley catchment	Syrdaryo, Tashkent, Jizakh catchment	Charvak reservoir	Papan reservoir
2001-2010	10212	4947	3464	674
2021-2030	8645	3245	2698	655
2041-2050	7492	3031	2489	562



Table 12: Changes in inflow into downstream areas for future projections (2021-2030, 2041-2050). Ranges indicate maximum and minimum availability change as projected by the five GCMs.

	Toktogul reservoir	Andijan reservoir	Nurek reservoir	Tupalangskoe reservoir	Akhangaran reservoir	Zaamin reservoir
2021-2030	-6.8 – -9.1%	-5.6 – -8.9%	-13.8 – -18.8%	-54.1 – -65.6%	-5.8 – -12.0%	-8.8 – -17.4%
2041-2050	-16.4 – -18.8%	-19.1 – -25.2%	-40.4 – -49.1%	-76.5 – -81.1%	-4.8 – -16.7%	-6.3 – -23.4%

	Gissarak reservoir	Pachkamar reservoir	Kulyab catchment	Kurgantube catchment	Dushanbe catchment	Surkhandarya upstream catchment
2021-2030	-28.5 – -40.6%	-10 – -18.5%	-3.3 – -8.1%	12.4 – 2.9%	-45.2 – -54.4%	-45.6 – -56.6%
2041-2050	-44.2 – -56.4%	-7.6 – -24.5%	-38.6 – -51.3%	3.0 – -9.4%	-63.8 – -69.2%	-65.9 – -72.1%

	Surkhandarya downstream catchment	Karukum kanal catchment	Kashkadarya upstream catchment	Kashkadarya downstream catchment	Zeravshan Valley catchment	Lebap upstream catchment 1
2021-2030	-19.5 – -22.6%	-25.6 – -31.0%	-34.9 – -44.9%	-90.8 – -91.5%	-25.1 – -36.7%	-51.4 – -54.9%
2041-2050	-20.3 – -28.1%	-26.0 – -37.0%	-41.4 – -53.3%	-92.7 – -94.1%	-52.2 – -64.0%	-53 – -59.8%

	Fergana Valley catchment	Syrdaryo, Tashkent, Jizakh catchment	Charvak reservoir	Papan reservoir
2021-2030	-13.7 – -17.9%	-32.8 – -37.5%	-19 – -26.4%	-2.2 – -3.6%
2041-2050	-23 – -32%	-35.7 – -44.7%	-25.1 – -34%	-12.3 – -21.4%

Summarizing for the two river basins a substantial decrease in water availability for downstream users has been calculated (Table 13). For the Syr Darya basin it is projected that average inflow into downstream areas decreases by 15% for 2021-2030 and 25% for 2041-2050, with respect to the reference situation (2001-2010). For the Amu Darya expected decreases are 13% (2021-2030) and 31% (2041-2050). The results in the table show the range of values for the model when forced with the five mentioned GCMs.

Moreover, changes in water availability are not distributed homogeneously throughout the year. The decrease is strongest in the late summer / start of autumn, when water shortage is already at its peak. In August, September and October water availability decreases by 45% for the Syr Darya and 42% for the Amu Darya in 2050.



Table 13: Projected average changes in water availability for downstream users Range for five GCMs is shown.

	Syr Darya	Amu Darya
2021-2030	-13% – -17%	-11% – -15%
2041-2050	-22% – -28%	-26% – -35%

Note that Syr Darya runoff decreases linearly in time, while the decrease in runoff for the Amu Darya decreases slower until 2021-2030, but is likely to be accelerated towards 2041-2050.

As seen in Figure 6-43 to Figure 6-48, the decrease in runoff is not uniform throughout the year. The decrease in runoff is strongest in the late summer / start of autumn for both river basins, as is visualized in Figure 6-49 and Figure 6-50. In August, September and October strongest runoff decreases are observed with runoff decreasing up to 47-52% for the Syr Darya in September and 36-47% for the Amu Darya in August, September and October in 2041-2050. The lowest decreases in runoff are observed in spring (March, April, May) for both river basins. Note that the difference between the minimum and maximum prediction based on the five GCMs is higher for the Amu Darya basin.

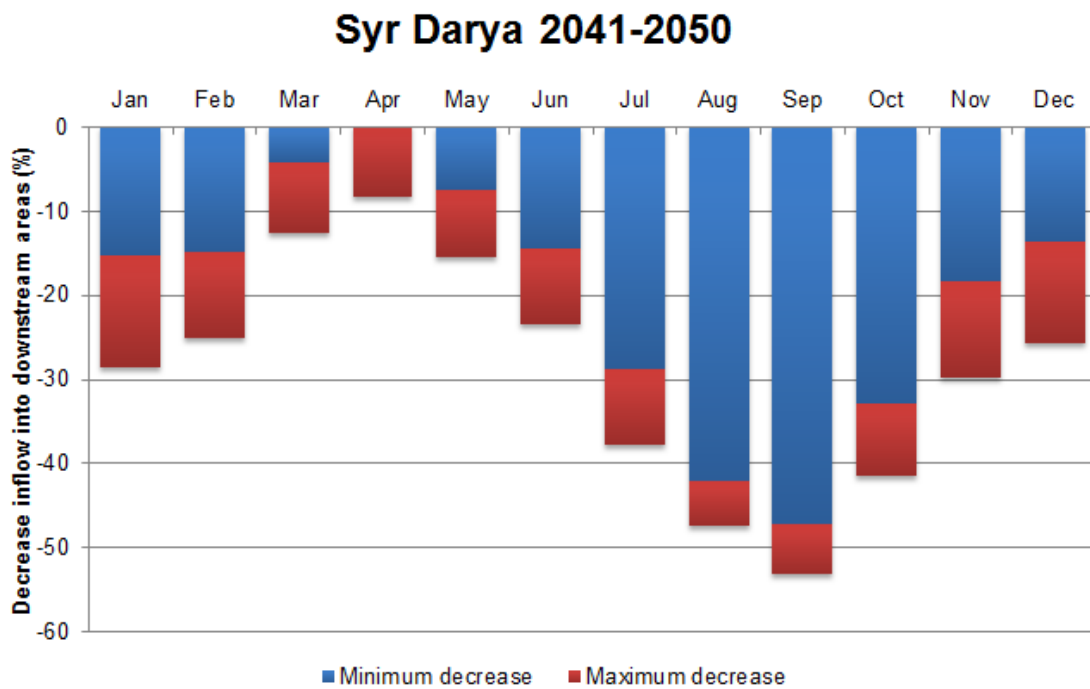


Figure 6-49: Average change in monthly inflow into downstream areas for Syr Darya basin in 2041-2050. Range for model forced with five GCMs is shown.



Amu Darya 2041-2050

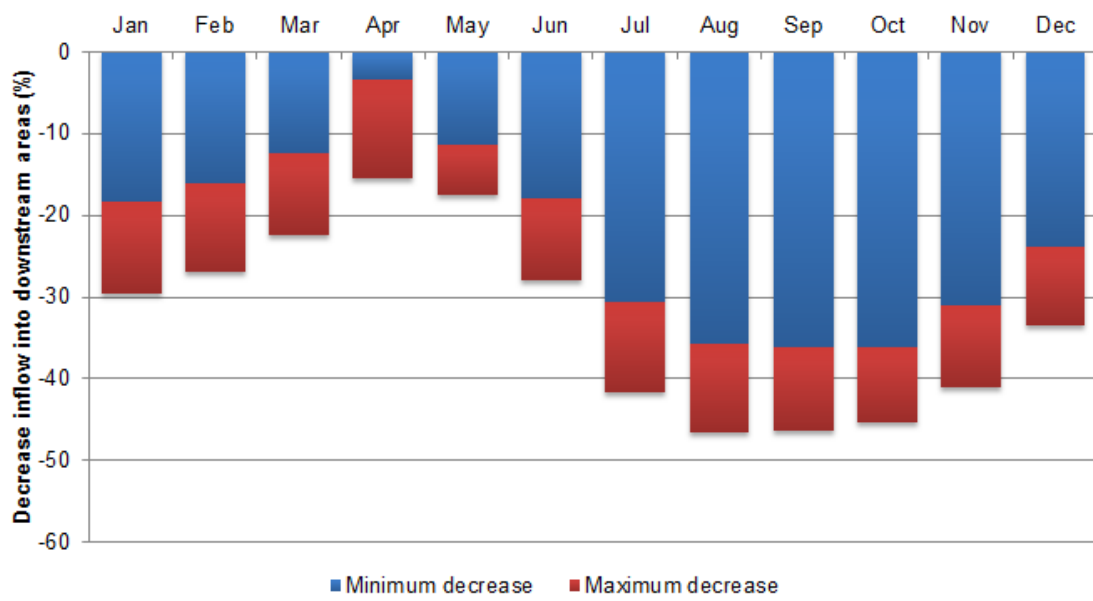


Figure 6-50: Average change in monthly inflow into downstream areas for Amu Darya basin in 2041-2050. Range for model forced with five GCMs is shown.



7 Conclusions

Climate change might have a big impact on water resources in the Central Asia region, but a rigorous analysis of these impacts is so far missing as the hydrological regimes of the two major rivers in the region (Syr Darya and the Amu Darya) are complex. Only recently, by the advent of advanced computer modeling combined with remotely sensed data and scientific progress, options occur to better understand processes and impact related to climate change.

The work described in this report is a first contribution to a larger study initiated by the Asian Development Bank to better understand and to explore adaptation strategies in the Aral Sea Basin. The ultimate objective of this project is to develop national capacity in each of the participating countries (Kyrgyz Republic, Tajikistan, Kazakhstan, Turkmenistan, Uzbekistan) to use the models, tools, data and results to prepare climate impact scenarios and develop adaptation strategies. This will then result in improved national strategies for climate change adaptation.

This report describes the analysis focusing on the upstream parts of the Amu Darya and Syr Darya river basins. Based on local and public domain datasets and hydro-meteorological observations a spatially distributed glacio-hydrological model has been developed for the upstream parts of the two rivers. This is one of the first models that covers the entire upstream parts of these basins and includes all processes related to glacier and snow melt, rain runoff and base flow.

Some of the key messages resulting from the study are:

- The developed model is able to mimic observed streamflows and can be used to explore the impact of climate change on the hydrological cycle.
- There are large differences in the role that melt water plays in runoff generation in the Amu Darya and Syr Darya river basins. Melt water has a higher contribution to runoff in the Amu Darya basin compared to the Syr Darya river basin.
- It is very likely that glacier extent in the Pamir and Tien Shan mountain ranges will decrease by 45 to 60% by the year 2050.
- The composition of the four components of stream flow (rainfall-runoff, snow melt, glacier melt, base flow) is very likely to change in the future. This will have major impacts on total runoff, but especially on seasonal shifts in runoff. The runoff peak will shift from summer to spring and decrease in magnitude. Model output when forced with climate projections generated with five Global Circulation Models shows decreasing runoff generation in the upstream parts of the two basins until 2050. The changes differ strongly spatially. The runoff generation decreases most significantly in upstream areas of glacier retreat.
- Total annual runoff into the downstream areas is expected to decrease by 22-28% for the Syr Darya and 26-35% for the Amu Darya by 2050.
- Strongest decreases in stream flow are expected for the late summer months (August, September, October), where inflow into downstream areas decreases around 45% for both river basins.

Output of the upstream model as presented in this report will be used as input for a downstream water allocation model to investigate the impact of climate change for water resources in the entire basins until 2050 and to explore possible adaptation measures.



8 References

- Aizen, V. B., V. a. Kuzmichenok, A. B. Surazakov, and E. M. Aizen (2007), Glacier changes in the Tien Shan as determined from topographic and remotely sensed data, *Global and Planetary Change*, 56(3-4), 328-340, doi:10.1016/j.gloplacha.2006.07.016. [online] Available from: <http://linkinghub.elsevier.com/retrieve/pii/S0921818106001913> (Accessed 14 September 2011)
- Aizen, V. B., P. a. Mayewski, E. M. Aizen, D. R. Joswiak, A. B. Surazakov, S. Kaspari, B. Grigholm, M. Krachler, M. Handley, and A. Finaev (2009), Stable-isotope and trace element time series from Fedchenko glacier (Pamirs) snow/firn cores, *Journal of Glaciology*, 55(190), 275-291, doi:10.3189/002214309788608787. [online] Available from: <http://openurl.ingenta.com/content/xref?genre=article&issn=0022-1430&volume=55&issue=190&page=275>
- Arnell, N. W. (1999), Climate change and global water resources, *Global Environmental Change*, 9, S31-S49.
- Barnett, T. P., J. C. Adam, and D. P. Lettenmaier (2005), Potential impacts of a warming climate on water availability in snow-dominated regions., *Nature*, 438(7066), 303-309, doi:10.1038/nature04141. [online] Available from: <http://www.ncbi.nlm.nih.gov/pubmed/16292301> (Accessed 10 June 2011)
- Bates, B. C., Z. W. Kundzewicz, S. Wu, and J. P. Palutikof (2008), *Climate Change and Water. Technical Paper of the Intergovernmental Panel on Climate Change*, IPCC, Geneva.
- Cruz, R. V., H. Harasawa, M. Lal, S. Wu, Y. Anokhin, B. Punsalmaa, Y. Honda, M. Jafari, C. Li, and N. Huu Ninh (2007), Coordinating Lead Authors : Lead Authors : Contributing Authors : Review Editors :, in *Asia. Climate Change 2007: Impacts, Adaptation and Vulnerability. Contribution of Working Group II to the Fourth Assessment Report of the Intergovernmental Panel on Climate Change*, pp. 469-506, Cambridge University Press, Cambridge.
- Defourny, P., C. Vancutsem, P. Bicheron, C. Brockmann, F. Nino, L. Schouten, and M. Leroy (2007), GLOBCOVER : A 300 m global land cover product for 2005 using ENVISAT MERIS time series, in *Proceedings of ISPRS Commission VII Mid-Term Symposium: Remote Sensing: from Pixels to Processes, Enschede (NL) 8-11 May 2006*, pp. 8-11.
- Droogers, P., A. V. Loon, and W. W. Immerzeel (2008), Quantifying the impact of model inaccuracy in climate change impact assessment studies using an agro-hydrological model, *Hydrology and Earth System Sciences*, (2004), 669-678.
- Hock, R. (2005), Glacier melt: a review of processes and their modelling, *Progress in Physical Geography*, 29(3), 362-391, doi:10.1191/0309133305pp453ra. [online] Available from: <http://ppg.sagepub.com/cgi/doi/10.1191/0309133305pp453ra> (Accessed 30 July 2011)
- Hsu, K.-lin, and S. Sorooshian (2009), Satellite-Based Precipitation Measurement Using PERSIANN System, in *Hydrological Modelling and the Water Cycle*, pp. 27-48.
- Ibatulin, S., A. Yasinsky, and A. Mironenkov (2009), *The Impact of Climate Change on Water Resources in Central Asia. Sector report no. 6*.
- Immerzeel, W. W., L. P. . Van Beek, and M. F. P. Bierkens (2010a), Climate change will affect the Asian water towers., *Science*, 328(5984), 1382-5, doi:10.1126/science.1183188.



- Immerzeel, W. W., L. P. H. van Beek, M. Konz, A. B. Shrestha, and M. F. P. Bierkens (2011), Hydrological response to climate change in a glacierized catchment in the Himalayas, *Climatic Change*, doi:10.1007/s10584-011-0143-4. [online] Available from: <http://www.springerlink.com/index/10.1007/s10584-011-0143-4> (Accessed 2 August 2011)
- Immerzeel, W. W., L. P. H. van Beek, and M. F. P. Bierkens (2010b), Climate change will affect the Asian water towers., *Science*, 328(5984), 1382-1385, doi:10.1126/science.1183188. [online] Available from: <http://www.ncbi.nlm.nih.gov/pubmed/20538947> (Accessed 20 July 2011)
- Karssenberg, D., P. Burrough, R. Sluiter, and K. de Jong (2001), The PCRASTER software and course materials for teaching numerical modelling in the environmental sciences, *Transactions in GIS*, 5, 99-110, doi:10.1111/1467-9671.00070. [online] Available from: <http://doi.wiley.com/10.1111/1467-9671.00070>
- Kaser, G., J. G. Cogley, M. B. Dyurgerov, M. F. Meier, and a. Ohmura (2006), Mass balance of glaciers and ice caps: Consensus estimates for 1961–2004, *Geophysical Research Letters*, 33(19), 1-5, doi:10.1029/2006GL027511. [online] Available from: <http://www.agu.org/pubs/crossref/2006/2006GL027511.shtml> (Accessed 14 July 2011)
- Kaser, G., M. Grosshauser, and B. Marzeion (2010), Contribution potential of glaciers to water availability in different climate regimes., *Proceedings of the National Academy of Sciences of the United States of America*, 107(47), 20223-7, doi:10.1073/pnas.1008162107. [online] Available from: <http://www.pubmedcentral.nih.gov/articlerender.fcgi?artid=2996705&tool=pmcentrez&rendertype=abstract> (Accessed 21 June 2011)
- Khromova, T. E., M. B. Dyurgerov, and R. G. Barry (2003), Late-twentieth century changes in glacier extent in the Ak-shirak Range, Central Asia, determined from historical data and ASTER imagery, *Geophysical Research Letters*, 30(16), 3-7, doi:10.1029/2003GL017233. [online] Available from: <http://www.agu.org/pubs/crossref/2003/2003GL017233.shtml> (Accessed 30 July 2011)
- Khromova, T. E., G. B. Osipova, D. G. Tsvetkov, M. B. Dyurgerov, and R. G. Barry (2006), Changes in glacier extent in the eastern Pamir, Central Asia, determined from historical data and ASTER imagery, *Remote Sensing of Environment*, 102(1-2), 24-32, doi:10.1016/j.rse.2006.01.019. [online] Available from: <http://linkinghub.elsevier.com/retrieve/pii/S0034425706000484> (Accessed 30 July 2011)
- Niederer, P., V. Bilenko, N. Ershova, H. Hurni, S. Yerokhin, and D. Maselli (2007), Tracing glacier wastage in the Northern Tien Shan (Kyrgyzstan/Central Asia) over the last 40 years, *Climatic Change*, 86(1-2), 227-234, doi:10.1007/s10584-007-9288-6. [online] Available from: <http://www.springerlink.com/index/10.1007/s10584-007-9288-6> (Accessed 30 September 2011)
- Rees, H. G., and D. N. Collins (2006), Regional differences in response of flow in glacier-fed Himalayan rivers to climatic warming, *Hydrological Processes*, 20, 2157- 2169, doi:10.1002/hyp.
- Siegfried, T., T. Bernauer, R. Guennet, S. Sellars, A. W. Robertson, J. Mankin, P. Bauer-Gottwein, and A. Yakovlev (2011), Will climate change exacerbate water stress in Central Asia?, *Climatic Change*, doi:10.1007/s10584-011-0253-z. [online] Available from: <http://www.springerlink.com/index/10.1007/s10584-011-0253-z> (Accessed 14 October 2011)
- Siegfried, T., S. Sellars, T. Bernauer, R. Guennet, J. Mankin, A. W. Robertson, and P. B. Gottwein (2010), Coping With International Water Conflict in Central Asia : Implications of Climate Change and Melting Ice in the Syr Darya Catchment, *International Studies*, 1-36.



Singh, P., and L. Bengtsson (2004), Hydrological sensitivity of a large Himalayan basin to climate change, *Hydrological Processes*, 18, 2363-2385, doi:10.1002/hyp.1468. [online] Available from: <http://doi.wiley.com/10.1002/hyp.1468> (Accessed 5 August 2011)

Solomina, O., R. Barry, and M. Bodnya (2004), The retreat of Tien Shan glaciers (Kyrgyzstan) since the Little Ice Age estimated from aerial photographs, lichenometric and historical data, *Geografiska Annaler, Series A: Physical Geography*, 86(2), 205-215, doi:10.1111/j.0435-3676.2004.00225.x. [online] Available from: <http://doi.wiley.com/10.1111/j.0435-3676.2004.00225.x>

Viviroli, D. et al. (2011), Climate change and mountain water resources: overview and recommendations for research, management and policy, *Hydrology and Earth System Sciences*, 15(2), 471-504, doi:10.5194/hess-15-471-2011. [online] Available from: <http://www.hydrol-earth-syst-sci.net/15/471/2011/> (Accessed 19 July 2011)

